Towards the Development of a Medium-Throughput Assay to Investigate the Kinetics of β-Haematin Formation in the Presence of Diverse Inhibitors

by
Sharné-Maré Fitzroy

Thesis presented in partial fulfilment of the requirements for the degree of Master of Science in the Faculty of Chemistry and Polymer Science at Stellenbosch University

Supervisor: Dr Katherine A. de Villiers

December 2015

Declaration

By submitting this thesis electronically, I, Sharné-Maré Fitzroy, declare that the entirety of the work contained therein is my own, original work, that I am the sole author thereof (save to the extent explicitly otherwise stated), that reproduction and publication thereof by Stellenbosch University will not infringe any third party rights and that I have not previously in its entirety or in part submitted it for obtaining any qualification.

December 2015

Abstract

A new, improved-throughput lipid-water interface assay was developed in which the inhibition of β-haematin formation by diverse inhibitors was investigated. Monopalmitoyl-*rac*-glycerol was used as a model lipid, and following the introduction of the inhibitors into the aqueous buffer layer, β-haematin inhibitory activity was investigated under biologically-relevant conditions. Clinically-relevant antimalarial drugs, namely chloroquine, amodiaquine, quinidine, quinine and mefloquine were used in order to validate the newly-optimized assay as a means of assaying drug activity. Having developed this more efficient assay, a larger set of compounds, including short-chain chloroquine analogues and a series of benzamide non-quinoline inhibitors, were successfully introduced into the system. The IC_{50} values determined for the inhibition of β-haematin formation through this newly-optimized assay show good correlations with previously-determined IC_{50} values, also determined in the lipid-mediated system, as well as biological activities determined against chloroquine-sensitive strains of *Plasmodium falciparum*.

Furthermore, the effect of each antimalarial drug, short-chain chloroquine analogue and benzamide non-quinoline compound on the kinetics of β-haematin formation was investigated in the lipid-mediated system. A theoretical kinetic model, which is based on the Avrami equation and the Langmuir isotherm, was used to analyse the experimental data. Importantly, it has been possible to extract equilibrium adsorption constants (K_{ads}) for each compound, which provides a quantitative measure of the strength of interaction between an inhibitor and the surface of growing β-haematin. Thus, the experimental data support a mechanism of inhibitor action *via* adsorption for both quinoline- and non-quinoline inhibitors. An important observation made during this study suggests that both K_{ads} and the rate of the proposed precipitation of an inhibitor-Fe(III)PPIX complex (k_2) have an effect on the IC_{50} value of an inhibitor. While the latter process was not investigated in the current work, the interplay between the two parameters appears to be of uttermost importance in determining the overall activity of a family of β-haematin inhibitors.

Finally, the direct adsorption of an inhibitor to preformed β-haematin crystals was investigated in independent studies in order to support the conclusions drawn from the kinetics studies. A decrease in the absorbance of a solution was observed in all cases when preformed β-haematin was added, which was attributed to the physical adsorption of the inhibitor to the crystals. From these studies an adsorption constant was extracted which indicated a good correlation with the inhibitory activity and K_{ads} values determined in the kinetics experiments.

The work in this research project provides important insight into the possible mode of β-haematin inhibition by diverse inhibitors. If the interactions that aid the adsorption of compounds to surface binding sites are identified, the insight will be invaluable in the rational design of novel haemozoin inhibitors.

Uittreksel

'n Nuwe, verbeterde-deurset lipied-water tussenfase toets is ontwikkel waarin die inhibisie van β-haematien vorming deur verskillende inhibeerders ondersoek was. Monopalmitiengliserol was gebruik as 'n model-lipied, en deur die inhibeerders in die waterige buffer laag in te sluit, was dit moontlik om die β-haematien inhiberende aktiwiteit onder biologies-relevante kondisies the ondersoek. Klinies-relevante antimalaria-middels, naamlik chlorokien, amodiakien, kinidien, kinien en meflokien was gebruik om die nuwe geoptimaliserende toets te evalueer as 'n middel van toetsing van inhiberende aktiwiteit. Deur die ontwikkeling van hierdie meer doeltreffende toets, was dit moontlik om 'n groter hoeveelheid verbindings, insluitend kort-ketting chlorokien analoë en 'n reeks bensamied nie-kinolien inhibeerders, in die sisteem te inkorporeer. Die IC_{50} waardes bepaal vir die inhibisie van β-haematien vorming deur hierdie nuwe geoptimaliserende toets, dui op goeie korrelasies met voorheen bepaalde IC_{50} waardes, óók bepaal in die lipied-beheerde sisteem, asook die biologiese aktiwiteite bepaal teen chlorokien-sensitiewe stamme van *Plasmodium falciparum*.

Verder is die effek van elke antimalarial-middel, kort-ketting chlorokien analoog en bensamied nie-kinoline inhibeerder op die kinetika van β-haematien vorming ondersoek in die lipied-beheerde sisteem. 'n Teoretiese kinetiese model wat gebaseer is op die Avrami-vergelyking en die Langmuir-isoterm was gebruik om die eksperimentele data te analiseer. Dit was moontlik om 'n ewewigs-adsorpsiekonstante (K_{ads}) vir elke inhibeerder te bepaal. Die K_{ads} waarde is 'n kwantitatiewe meting van die sterkte van die interaksie tussen 'n inhibeerder en die oppervlakte van groeiende β-haematien. Dus ondersteun die eksperimentele data 'n meganisme van inhibeerder aksie deur adsorpsie deur beide die kinolien en nie-kinolien inhibeerders. 'n Belangrike waarneming tydens die studie dui daarop dat beide K_{ads} en die koers van die voorgestelde neerslagreaksie van 'n inhibeerder-Fe(III)PPIX kompleks (k_2) 'n effek op die IC_{50} waarde van 'n inhibeerder het. Terwyl die laasgenoemde proses nie ondersoek was in die huidige studie nie, blyk dit dat die wisselwerking tussen hierdie twee parameters die algehele aktiwiteit van 'n familie van inhibeerders bepaal.

Die direkte adsorpsie van 'n inhibeerder aan reeds-gevormde β-haematien kristalle was ondersoek in onafhanklike studies om die gevolgtrekkings van die kinetika studies te ondersteun. 'n Daling in die absorbansie van 'n oplossing was waargeneem in alle gevalle wanneer reeds-gevormde β-haematien daarby gevoeg was. Hierdie waarneming is toegeskryf aan die fisiese adsorpsie van die inhibeerder aan die kristalle. Vanuit hierdie studies was 'n adsorpsiekonstante bepaal wat goeie korrelasies met die inhiberende aktiwiteit en K_{ads} waardes, verkry in die kinetika eksperimente, aandui.

Die werk in hierdie navorsings projek verleen belangrike insig in die moontlike manier van β-haematien inhibisie deur verskillende inhibeerders. As die interaksies wat bydra tot die adsorpie van verbindings aan die oppervlak-bindings punte geïdentifiseer word, sal die insig van hierdie werk belangrik wees in die ontwikkeling van nuwe haemasoïen inhibeerders.

Dedication

To my Parents,

Eddie and Riana Fitzroy

Acknowledgements

This thesis would not be possible without the grace and love from the King of all kings and the saviour of my soul. Thank You Lord for giving me this great opportunity to do my masters and to complete this thesis. Thank you for carrying me when I needed you the most. All praise goes to You.

Thank you **Dr Katherine de Villiers** for being the best supervisor ever. You are a great mentor, leader, teacher, friend, "go-to-person" and woman of God. Your kindness, support, positive heart and willingness to help will always be remembered. You are inspiring to work with and I am greatly privileged to have worked with you over these few years.

None of this would even be remotely possible without my parents, **Eddie** and **Riana Fitzroy**. Thank you for your love, understanding, emotional and financial support and for always being there for me. I appreciate your patience with me throughout this whole process and for giving me the opportunity to study for such a long period of time. I love you.

Thank you to everyone in my research group. **Ronel Müller, Dr David Kuter** and **Chandré Sammy**. Your help, ideas and input over these two years are greatly appreciated. My days in the office and laboratory would not have been so much fun if it was not for all your laughs and great hearts.

Professor Timothy Egan, you are such an inspiration in this field of work and I am so privileged to have worked with you. Thank you for sharing all of your knowledge and having an input on several aspects of this work. It was great working with you and the **UCT haem group**.

Thank you **Francois Louw** for your support and love throughout my season of writing up my thesis. I would not have enjoyed it half as much if it was not for your positive encouragement, Godly advice and special treats throughout. Thank you for believing in me in times when I struggled to believe in myself and for being proud of me.

My life as a student at Stellenbosch University is incomplete without the amazing friends I made throughout this season of my life. **Carla, Jani, Elaine, Tanica, Lisa, Alet, Megan, Gerstin, Ilze, Leané, Dalene, Natasha, Candice** and **Anja** – your friendship means the world to me. Also, I special thank you to **Andrea** and **Tanya**.

Conference Proceedings

1. SACI Young Chemists' Symposium, **2014**, University of Cape Town, Cape Town, RSA
   Oral Presentation: <u>Sharné Fitzroy</u> and Dr Katherine A. de Villiers, Development towards a High-Throughput Screen for Kinetic Inhibition of β-Haematin Formation *via* Adsorption.

2. SACI Inorganic Chemistry Conference **2015**, Rhodes University, Grahamstown, RSA
   Poster Presentation: <u>Sharné Fitzroy</u> and Dr Katherine A. de Villiers, Development towards a High-Throughput Screen for Kinetic Inhibition of β-Haematin Formation *via* Adsorption.

List of Abbreviations

ACN	acetonitrile
ATR-IR	attenuated total reflection infrared
AQ	amodiaquine
AtQ	atovaquone
$BHIA_{50}$	β-haematin inhibitory activities
CQ	chloroquine
CQ_{fb}	free base chloroquine
CQR	chloroquine-resistant strain
CQS	chloroquine-sensitive strain
Cl-Fe(III)PPIX	haemin
DMSO	dimethyl sulfoxide
DV	digestive vacuole
EQD	9-epiquinidine
EQN	9-epiquinine
EXAFS	extended X-ray adsorption fine structure
Fe(II)PPIX	iron (II) protoporphyrin IX, haem
Fe(III)PPIX	iron (III) protoporphyrin IX, haematin
FT-IR	Fourier-transform infrared
Hb	haemoglobin
HDP	haem detoxification protein
HEPES	N-2-[hydroxyethyl]piperizine-N'-[2-ethanesulfonic acid]
Hf	halofantrine
HRP	histidine-rich protein
IC_{50}	concentration required of to inhibit 50% of β-haematin formation
K_{ads}	adsorption equilibrium constant
k_2	rate constant of the proposed precipitation of an inhibitor-haematin complex
MMG	monomyristoylglycerol
MOG	monooleoylglycerol
MPG	monopalmitoylglycerol

MSG	monostearoylglycerol
MQ	mefloquine
n	Avrami constant
NaOH	sodium hydroxide
NLBs	neutral lipid bodies
NP40	Nonidet P-40
Pf	*Plasmodium falciparum*
*Pf*CRT	*P. falciparum* CQ-resistance transporter
Pgh1	P-glycoprotein homologue 1
Phiβ	pyridine hemichrome inhibition of β-haematin
PXRD	powder X-ray diffraction
RBCs	red blood cells
SEM	scanning electron microscopy
SCD	single crystal X-ray diffraction
TEM	transmission electron microscopy
QD	quinidine
QN	quinine
z	rate constant in the absence of an inhibitor
z_{obs}	observed rate constant

Table of Contents

Chapter 3. The Effect of Quinoline Inhibitors on the Formation of β-Haematin at the Lipid-Water Interface

Chapter 4. The Effect of Non-quinoline Inhibitors on the Formation of β-Haematin at the Lipid-Water Interface

Chapter 5. Independent Adsorption Studies

Chapter 1. Literature Review

1.1 Introduction

Malaria is one of the most deadly parasitic human diseases known worldwide and is responsible for over hundreds of thousands of deaths per year, especially among young children in Africa.[1] It is, however, endemic in several nations, affecting millions of people annually, and is notably a contributor to economic underdevelopment in some of these countries. Malaria is one of few diseases which can be viewed as both a cause and a consequence of poverty, owing to its highest distribution in underprivileged regions and billions of US dollars spent annually on malaria control and elimination.[1] The malaria parasite, *Plasmodium falciparum*, which is the primary causative agent of human malaria, has over the years started to demonstrate increasing resistance towards antimalarial drugs.[1] Consequently, the development of novel chemotherapeutic agents has become of high importance, since malaria remains a great global health problem. Unfortunately, the mechanism of action of the majority of clinically-relevant antimalarial drugs is still not fully understood and this has motivated research in this area.

1.2 Malaria Overview

1.2.1   History and Discovery of Malaria

Malaria is an ancient disease which dates as far back as early 2700 BC.[2] In about 400 BC, Hippocrates was aware of the poor health, enlarged spleens and fevers amongst local populations living in marshy places, and was the first to make a connection between these symptoms.[3] Owing to the relationship between these observed symptoms and marshy environments, the word malaria was derived from the Italian word "mal'aria", meaning "bad air".[4]

This idea that malaria fevers were caused by miasmas rising from swamps continued for over 2500 years and the search for the cause of malaria intensified over the years after the discovery of bacteria in 1676, and the incrimination of microorganisms as causes of infectious diseases.[3] In 1717, Giovanni Maria Lancisi discovered a brown-black pigment in the blood of patients affected by malaria.[5] The search for the cause of the disease was an ongoing process and increased over the years until the first scientific study by Charles Louis Alphonse Laveran in the 1880s. Lavern discovered the etiological agent of malaria, the malaria parasite, and identified pigments in the body of living parasites in 26 patients.[6,7] The idea that mosquitoes might be associated with malaria was first suggested by the American physician, Albert King,[8] and was studied further by the British scientist, Patrick Manson, who was convinced that mosquitoes were involved in malaria transmission (he based

this on his early findings that mosquitoes could transmit filarial worms responsible for lymphatic filariasis).[9] In 1897, Sir Ronald Ross discovered that the avian malaria parasite, *Plasmodium relictum*, was transmitted by culicine mosquitoes, and suggested that mosquitoes also transmit human malaria parasites.[10] It was, however, during the period 1898-1900, that various Italian scientists, namely Giovanni Battista Grassi, Amico Bignami and Giuseppe Bastianelli, were able to conclusively demonstrate that human malaria parasites were indeed transmitted by female *Anopheles* mosquitoes.[11]

1.2.2 Distribution and Statistics of Malaria

An estimated 3.3 billion people in 97 countries are at risk of being infected with malaria. 198 million cases of malaria infections occurred globally in 2013, of which 584 000 led to death; 78% of these deaths occurred in children aged five years and younger. The disease predominates among the sub-Saharan Africa countries, in which 90% of all malaria deaths occur, however, it is also found in the South American-, Eastern Mediterranean-, European-, South-East Asia- and Western pacific regions (Figure 1.1).[1]

As a result of the distribution of insecticide-treated mosquito bed nets, improvements have been reported for malaria infections and deaths over the last few years,[1] however, regardless of these vast improvements, an overall increase in parasite resistance towards known quinoline-based antimalarial drugs and artemisinin-based combination therapy is evident in *P. falciparum* strains across different regions. This high level of resistance is limiting the use of certain cheap and previously highly effective drugs, such as chloroquine (CQ), in treating malaria in many parts of the world.[1]

Confirmed malaria cases per 1000 population
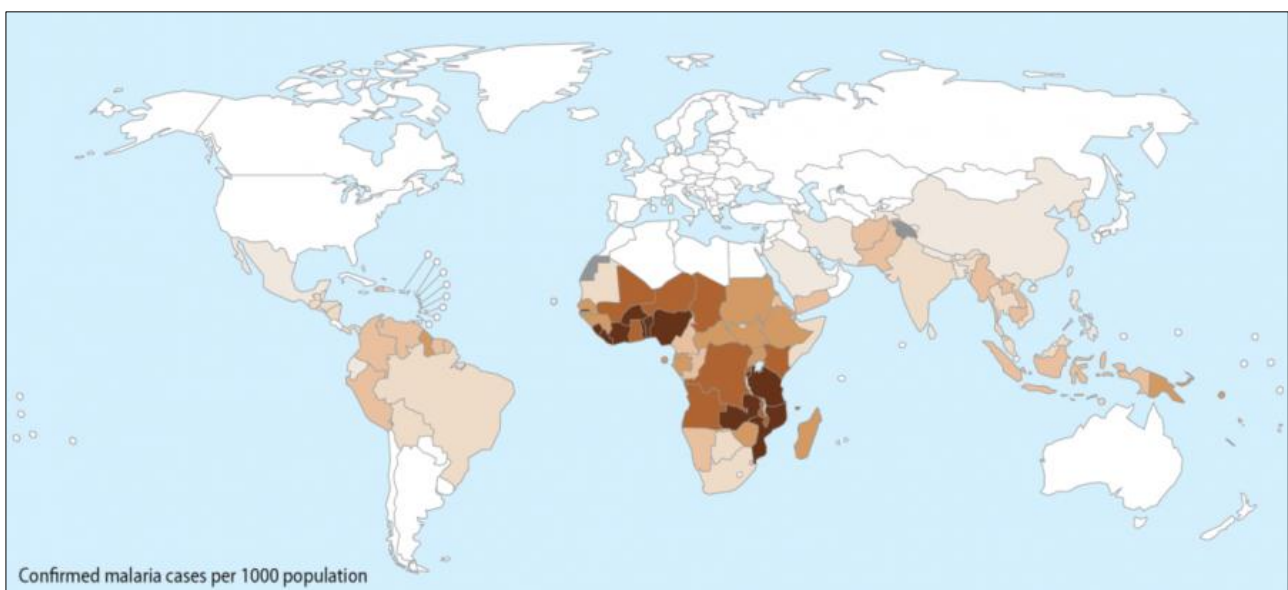
Figure 1.1 Worldwide distribution of malaria. Darker shading indicates countries with the highest ongoing malaria transmission in 2013. Reproduced with permission from reference 1.

1.3 The Malaria Parasite

1.3.1   The Life Cycle of the Malaria Parasite

Malaria is caused by five species of protozoan parasites belonging to the genus *Plasmodium*, of which four of these species are infectious to humans: *P. falciparum*, *P. ovale*, *P. vivax* and *P. malariae*,[12] while the fifth parasite species, *P. knowlesi*, causes malaria mainly among monkeys in certain areas of South-East Asia.[1] Of these species, *P. falciparum* and *P. vivax* are the most virulent, with the former being responsible for the majority of deaths from malaria.[1,13] *P. falciparum* predominates in the African regions, while *P. vivax* has a geographically wider distribution, owing to its ability to survive at lower temperatures and in regions with higher altitudes and cooler climates.[1]

The malaria parasite is transmitted to its vertebrate host *via* the bite of an infected female *Anopheles* mosquito. It has a complicated life cycle, since it requires a vector and a host, and can be described in different stages. Once the human host is bitten by the infected female mosquito, sporozoites are transferred from the saliva of the mosquito into the host's blood (Figure 1.2 (a)) and carried in the bloodstream to the liver cells (Figure 1.2 (b)), where they undergo exoerythrocytic schizogony, a phase of asexual multiplication. In the liver, sporozoites replicate to form uninucleate merozoites (Figure 1.2 (c)) which go on to invade the red blood cells (RBCs) upon release from the liver. This initiates a second asexual multiplication phase known as the blood cycle (Figure 1.2 (d)). While undergoing asexual reproduction in the RBCs, merozoites develop through the ring- and later the trophozoite-stage. The parasite subdivides to produce daughter merozoites in the schizont stage, and these merozoites are released back into the bloodstream and the process is repeated. The intraerythrocytic stage of the parasite's life cycle gives rise to all clinically known symptoms of malaria, and repeats every 48 hours in the *P. falciparum* parasite species. Known symptoms associated with malaria infection include fever, headaches, chills, sweats and fatigue.[14] As part of the blood cycle, some merozoites develop as male and female gametocytes. These are transferred back to a different female *Anopheles* mosquito during its blood meal (Figure 1.2 (e)), after circulating around in the host's bloodstream. The gametocytes mature to gametes that eventually form oocysts that divide to create sporozoites once more. After moving to the salivary glands of the mosquito, an uninfected host becomes infected when bitten (Figure 1.2 (a)) and the cycle of infection starts once more.[3,12,14,15,16]

The malaria parasites are clever organisms for dwelling inside the cells of its host, since this strategy helps them to avoid the host's immune system. The complex lifecycle involves several mechanisms by which the parasite can sustain its chemical composition and obtain the nutrients required for its survival.[12] The blood stage of the parasite's life cycle is, however, of most importance and interest, since it is the stage associated with the symptoms of this infectious disease.
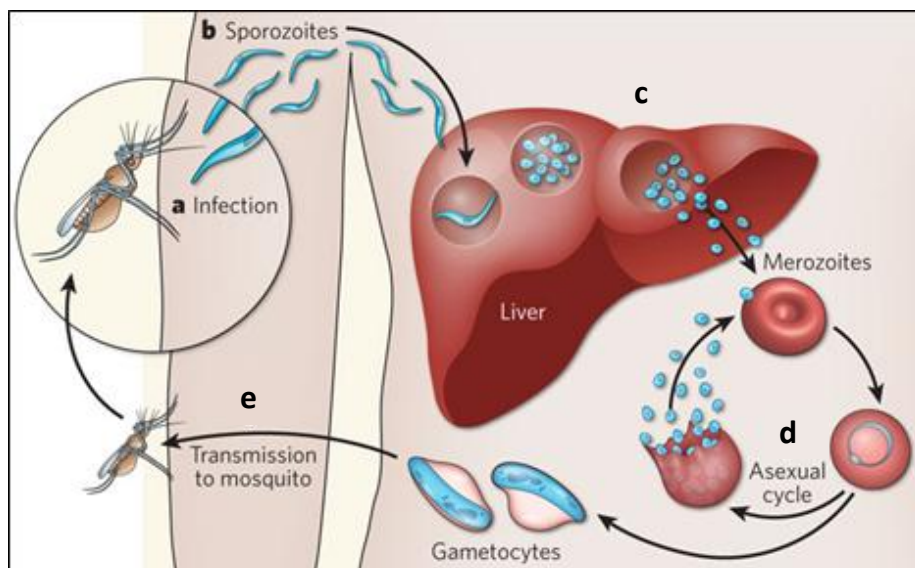
Figure 1.2 The complex life cycle of a malaria parasite, *Plasmodium falciparum*. Reproduced with permission from reference 16.

1.3.2   The Blood Stage of the Parasite's Life Cycle

After entering the RBCs of the host in the blood stage of the parasite's life cycle, the parasite grows and matures while surrounded by cytosol, mainly consisting of haemoglobin (Hb).[17] Hb is a convenient source of amino acids. At least 65% of Hb present in the RBC cytoplasm is degraded to peptide fragments by multiple proteases[18] within an acidic compartment known as the digestive vacuole (DV) within the parasite (pH 4.8).[19] Some of these parasite proteases, important for Hb proteolysis, include different acidic proteases, aspartic proteases, a cysteine protease and a zinc metallo-protease.[17,20,21,22,23] Only a fraction of amino acids derived from Hb proteolysis are needed for the biosynthesis of parasite proteins, which provide a source of nutrition for normal parasite growth and development.[17,18] The rest of the Hb is subsequently degraded to make space for parasite growth.

During Hb degradation, four haem (iron (II) protoporphyrin IX, Fe(II)PPIX) (Figure 1.3 (a)) equivalents per unit of Hb are released into the DV, where the iron centre is rapidly oxidised from the Fe(II) to Fe(III) state.[24] The structure of Fe(III)PPIX is characterized by an iron centred (ferric state) porphyrin with 4 methyl-, 2 vinyl- and 2 propionic acid side chains. The five-coordinate Fe(III) centre also has an axial ligand which is pH-dependent, being either an aqua (H_2O) or a hydroxide (^-OH) group. The resulting Fe(III)PPIX product (Figure 1.3 (b)) is, however, toxic to the parasite, possibly promoting the formation of reactive oxygen species and subsequent membrane damage *via* lipid peroxidation. These processes ultimately result in parasite death.[24]

As a survival mechanism, the parasite detoxifies the harmful Fe(III)PPIX *via* biocrystallisation, by converting at least 95% of it into a highly insoluble, inert crystalline material called haemozoin or malaria pigment.[25] This material consists of centrosymmetric dimers of Fe(III)PPIX (Figure 1.3 (c)).[25,26] Figure 1.4 is a schematic representation summarizing the biological pathway for haemozoin formation in the DV of a parasite within the RBC of a host.[26]
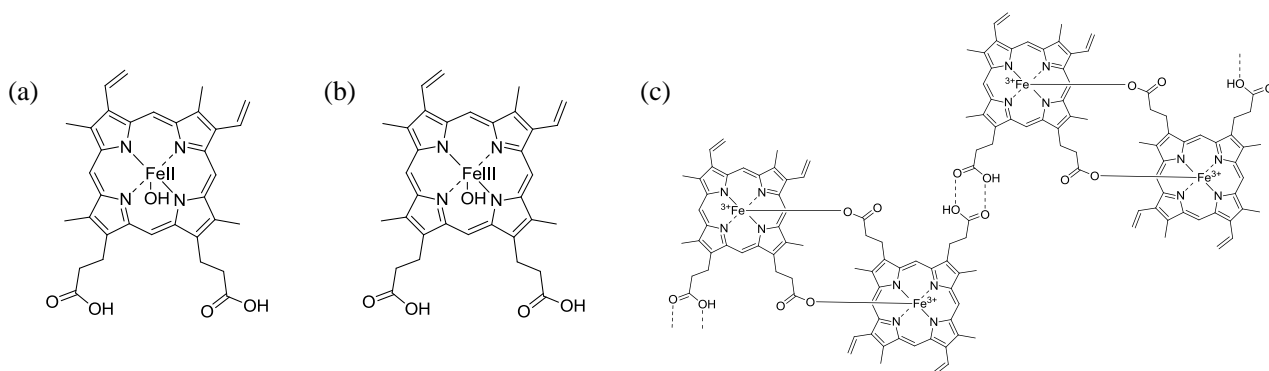
Figure 1.3 The molecular structures of (a) haem (Fe(II)PPIX) and (b) haematin (Fe(III)PPIX), both with a hydroxide axial ligand, and (c) haemozoin (malaria pigment).
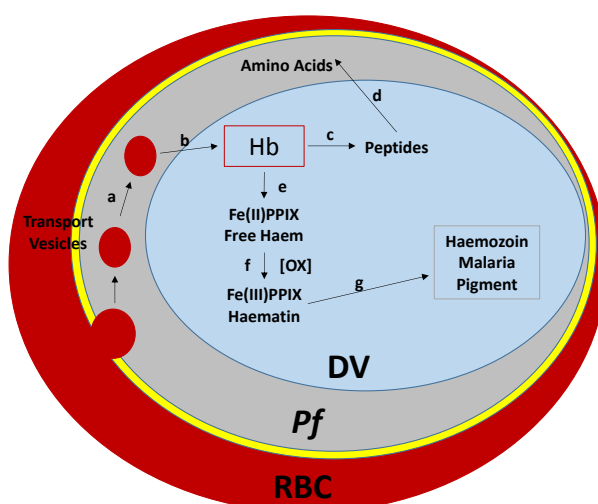
Figure 1.4 Schematic representation of the biological pathway for haemozoin formation in the digestive vacuole (DV) of *P. falciparum (Pf)* within the red blood cell (RBC) of a host. Haemoglobin (Hb) present in the RBC cytoplasm is ingested by *Pf* and transported to the DV by transport vesicles (a). Upon entering the DV (b), Hb is digested to peptides (c), which are further degraded to amino acids and used as a nutrient source for parasite growth and development (d). Free haem (Fe(II)PPIX) released as a by-product of Hb degradation (e), undergoes rapid oxidation to yield toxic haematin (Fe(III)PPIX) (f). As a detoxification mechanism, the Fe(III)PPIX is converted into haemozoin (malaria pigment) (g). Adapted from reference 26.

Taking into consideration that quinoline-containing antimalarial drugs demonstrate their antiplasmodial activity in the blood stage of the malaria parasite's life cycle,[27] it is important to realise that the parasite can be in danger to drug action at any given point while it is located within the host's RBCs. Two main ideas of drug action have been considered, namely the disruption of Hb degradation or the Fe(III)PPIX detoxification process, respectively.[27] Over the last few years, the latter process has been studied and investigated as the target of drug action, and understanding the structure and formation of haemozoin has been of great interest and importance in aiding the development of new therapeutic antimalarial drugs. The discovery of haemozoin crystals in other blood-feeding organisms, unrelated to the *Plasmodium* malaria parasite, including *Rhodnius prolixus* (insect),[27] *Schistosoma mansoni, Echinostoma trivolvis* and *Haemoproteus columbae* (helmith worms),[28,29,30] has contributed greatly to the overall interest in haemozoin over recent years.

1.4 Haemozoin

The first discovery of haemozoin dates back close to 150 years before the discovery of the malaria parasite. In the 18th century, Giovanni Maria Lancisi observed a black discolouration in the brains of cadavers of malaria victims.[5] Later, Johann Heinrich Meckel, a German physician, rediscovered the malaria pigment in 1847,[31] while Rudolf Virchow was the first to relate the presence of the pigment to malaria in 1849.[32] Initially the malaria pigment was believed to be melanin, however, W. H. Brown demonstrated that the chromophore responsible for the pigment's brown-black colour, is in fact haem.[33] For almost 80 years, no significant discoveries were made regarding haemozoin, until 1987, when Fitch and Kanjananggulpan demonstrated that haemozoin is comprised entirely of ferriprotoporphyrin IX (Fe(III)PPIX).[34] In 1991, it was Slater and co-workers who published a ground-breaking paper in which they confirmed Fitch and Kanjananggulpan's findings, and explained the chemical composition of haemozoin by elemental analysis.[35] This paper forms the basis of our understanding of haemozoin, however, numerous controversies have existed regarding its proposed structure.

1.4.1   Haemozoin Structure and Crystal Morphology

At first haemozoin was considered to be a linear polymer,[35] and later an antiparallel polymer.[36] However, more recently the structure of haemozoin has been described as a periodic array of cyclic dimers of Fe(III)PPIX.[37] The molecular structures of these various forms are shown below (Figure 1.5).
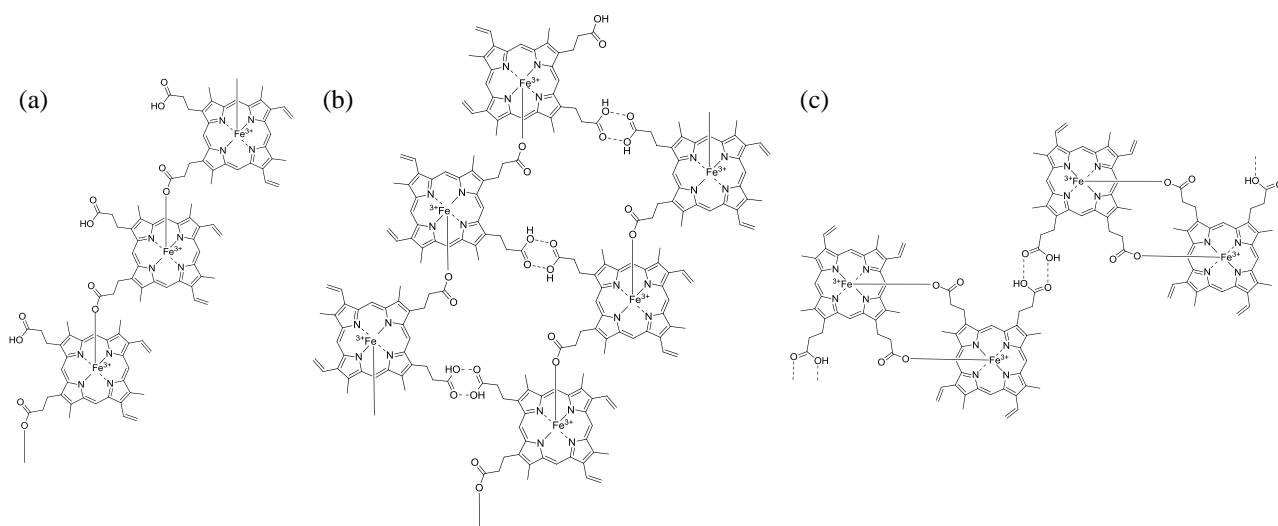
Figure 1.5 The proposed structures of haemozoin. (a) Slater *et al*. initially suggested that haemozoin was a linear polymer containing Fe(III)PPIX units linked *via* the coordination of propionate groups,[35] followed by the idea of (b) an antiparallel polymer by Bohle *et al*.[36] It was, however, shown than haemozoin was not a polymer, but rather contained (c) a periodic array of hydrogen-bonded cyclic dimers of Fe(III)PPIX.[37]

A synthetic product of Fe(III)PPIX, called β-haematin, precipitated from an aqueous solution with acetic acid, was first discovered and described in the 1930s by Hamsik, enabling the earliest study of the formation of haemozoin *in vitro*.[38] The haemozoin isolated by Fitch and Kanjananggulpan was suggested to be identical to this insoluble aggregate,[34] and solubilisation, infrared spectroscopy and powder X-ray diffraction (PXRD) studies by Slater *et al*. indeed confirmed this observation.[35] The authors initially proposed that haemozoin (and β-haematin) was a linear polymer, containing Fe(III)PPIX units linked *via* the coordination of a propionate group of one molecule to the iron centre of an adjacent monomer (Figure 1.5 (a)), which they concluded using extended X-ray adsorption fine structure (EXAFS) spectroscopy.[35] EXAFS was used to investigate the local environment of iron in haemozoin by identifying both the type and the distance of each shell of atoms around the absorbing metal. The strong absorbance bands present at 1211 cm⁻¹ and 1664 cm⁻¹ in the Fourier-transform infrared (FT-IR) spectrum of haemozoin and β-haematin confirmed this conclusion, and were assigned to the C−O and C=O stretching frequencies of the coordinated propionate group to the iron centre, respectively (Figure 1.6).[35]
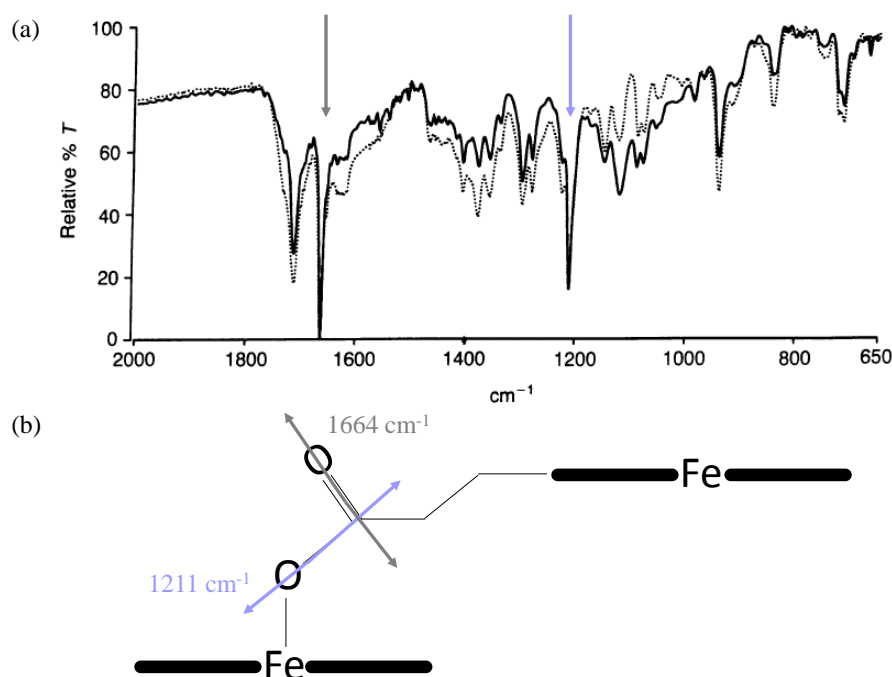
Figure 1.6 (a) The FT-IR spectrum of haemozoin (solid line) and β-haematin (broken line). The characteristic peaks are seen at 1211 and 1664 cm⁻¹ for the C-O and C=O stretching frequencies, respectively. Reproduced with permission from reference 35. (b) A schematic representation of the proposed linear haemozoin structure viewed side on. C−O and C=O stretching frequencies are indicated. The thick black lines represent the porphyrin plane.

It was only years later in 1997 when Bohle *et al*., using synchrotron PXRD, confirmed that haemozoin, is indeed identical to β-haematin. The sample of the latter material had been prepared by dehydrohalogenation of haematin with 2,6-lutidine in dry methanol.[36] In this study they were able to show that the β-haematin crystal

belongs to the centrosymmetric space group P1, and hence proposed that the structure of haemozoin (and β-haematin) was comprised of two antiparallel polymer chains linked to each other *via* hydrogen bonds (Figure 1.5 (b)).[36] Knowledge of the haemozoin crystal structure has progressed over time, and in 2000, Pagola *et al*. finally solved the structure of β-haematin from high resolution synchrotron PXRD patterns using Rietveld refinement.[37] The outcome, however, indicated that β-haematin was a crystal formed of discrete cyclic dimers of Fe(III)PPIX, rather than a polymer. It was shown that the propionate group of each Fe(III)PPIX molecule is coordinated to the iron centre of another molecule, while neighbouring dimers are connected by hydrogen bonds between the uncoordinated propionic acids groups (Figure 1.5 (c)).[37]

In 2002, Buller *et al*. published a paper in which they described the theoretical growth form and crystal morphology of β-haematin.[39] They determined a needle-like crystal morphology (extended along the c-axis) and explained that the relationship between the macroscopic morphology of the crystals and the unit cell structure is of importance to understand possible molecular mechanisms of haemozoin formation, and also its inhibition by antimalarial drugs (Figure 1.7 (a, c and d)).[39] More recently, Gildenhuys *et al.* obtained single crystals of solvated β-haematin from a CQ-containing DMSO solution (Figure 1.7 (b)).[40] The authors determined that the repeating unit in the crystal structure is a μ-propionato dimer of Fe(III)PPIX using single crystal X-ray diffraction (SCD), which is almost in agreement to what have been reported for β-haematin and haemozoin from PXRD data.[37] Based on the reported PXRD crystal structure of β-haematin,[37] Buller *et al*. further showed that the crystal form of β-haematin is similar in overall shape and form to that of haemozoin crystals using emission in-lens scanning electron microscopy (SEM) (Figure 1.7 (e, f and g)).[39]
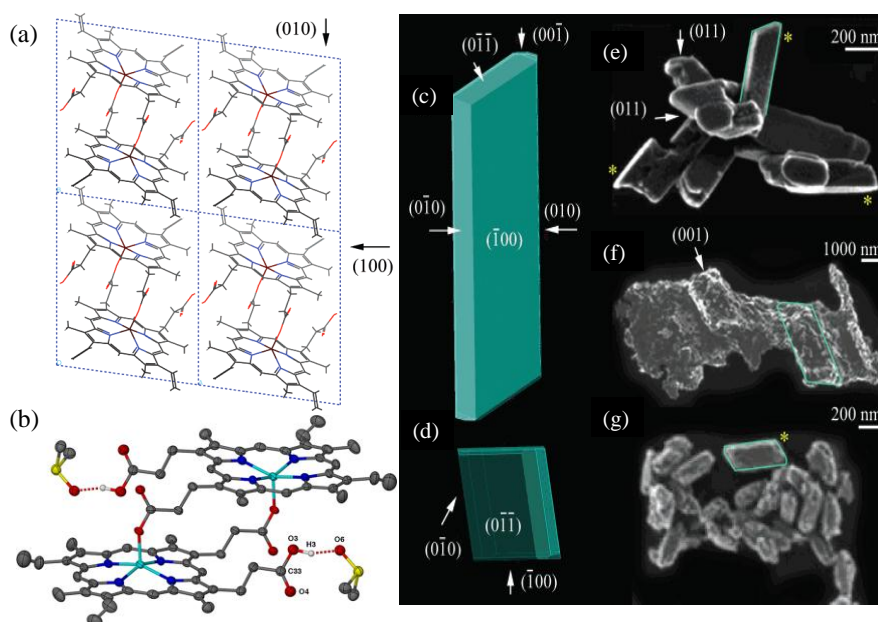
Figure 1.7 (a) The packing arrangement of β-haematin viewed along the c-axis. (b) The μ-propionato dimer of Fe(III)PPIX from solvated β-haematin obtained by single crystal X-ray diffraction. The theoretical growth form of β-haematin (c and d). Dominant faces include (100) and (010), while (011) is a lesser-developed face and (001) is a minor face. Field emission in-lens scanning electron microscopy images of haemozoin crystals purified from (e) *P. falciparum*, (f) *S. mansoni* and (g) *H. columbae*. (f). Reproduced with permission from reference 39 and 40.

1.4.2   Haemozoin Formation *In Vivo*

Haemozoin formation is a very effective method of Fe(III)PPIX detoxification, however, there is still much uncertainty regarding the mechanism of its formation. While it is believed that haemozoin formation occurs *via* a biocrystallisation process,[41] there is controversy surrounding whether proteins or lipids facilitate its formation.

1.4.2.1 Protein-Facilitated Haemozoin Formation

The proposal that proteins contribute to the formation of haemozoin dates back to when it was still considered to be a polymer. Sullivan *et al*. showed that histidine-rich protein (HRP) II, which is plentiful in *P. falciparum*, promoted haemozoin formation, and they proposed that HRP II may be responsible for initiating or catalysing haemozoin formation in the malaria parasite.[42] HRP II has further been shown to bind to Fe(III)PPIX[43,44] and later in 1999, Ziegler *et al*. indicated that a dendrimer, comprised of the long peptide repeat unit of HRP II (His-His-Ala-His-His-Ala-Ala-Asp) also promoted β-haematin and suggested that this specific peptide sequence may represent a biomineralising template.[45] In 2001, Papalexis *et al*. continued to study the role of HRPs and discovered using confocal immunofluorescence labelling of HRP II, that this protein is indeed present in the DV of the parasite, however, it is mainly localised in the RBC cytoplasm.[46] This observation was confirmed when only 3% of HRPII was located in the DV,[47] suggesting that the concentration of HRPII is too low to support haemozoin formation alone. The role of HRP in the formation of haemozoin was ultimately ruled out when it was later demonstrated that haemozoin formation occurred normally in a *P. falciparum* clone that lacked both genes for HRP II and HRP III.[48] Furthermore, no HRP homologues have been recognized in *P. vivax* or *P. berghei*, both malaria parasites being able to produce haemozoin.[49] More recently, Chugh *et al*. reported the presence of a protein complex containing several parasite proteins such as plasmepsin II and IV, histo-aspartic protease, falcipain 2 and most importantly, haem-detoxification protein (HDP), within the DV.[50] The authors developed an *in vitro* assay in which they showed that falcipain 2 and HDP coexist with one another to convert haem to haemozoin. Earlier in 1995, however, Dorn *et al*. reported that the parasite factor responsible for promoting β-haematin formation was not deactivated by boiling or protease activity and that both haemozoin and preformed β-haematin support β-haematin formation in the absence of proteins.[51]

1.4.2.2 Lipid-Facilitated Haemozoin Formation

Compared to the fading evidence for the contribution of HRP in haemozoin formation, the role that lipids play in the detoxification process has been expanding substantially since early studies on their possible involvement.[52,53] Fitch *et al*. performed a study where they investigated purified lipids, and showed that 70% of the initial β-haematin activity present in parasite-infected erythrocytes could be recovered from chloroform extraction, with no activity remaining in the residue.[54] They found that several unsaturated fatty acids, mono-

9

and dioleoylglycerol and a few detergents promoted β-haematin formation, while lipids incapable of β-haematin formation included trioleoylglycerol, cholesterol, dioleoylphosphatidylethanolamin, and both palmitic and stearic saturated fatty acids. The authors further proposed that the lipids play a role in haemozoin formation by co-precipitation with monomeric Fe(III)PPIX in the acidic DV, converting dissolved Fe(III)PPIX in the lipid into haemozoin.[54]

More recent studies in the last decade have suggested the role of neutral lipid bodies (NLBs) within the DV, after Jackson *et al.* investigated NLBs in *P. falciparum* by means of fluorescence microscopy (using Nile Red labelling) and transmission electron microscopy (TEM).[55] These NLBs were shown to contain mainly mono- and diacylglycerols, while a series of these, including triacylglycerols, were found to promote β-haematin formation. Shortly after this discovery, Coppens and Vielemeyer studied NLBs in apicomplexa and published for the first time a TEM image of a malaria parasite stained with malachite green (a substance which is used to fix neutral lipids), which indicated that haemozoin located in the DV is entirely encapsulated within a NLB (Figure 1.8 (a)).[56] This review followed a detailed investigation on NLBs and their ability to promote β-haematin by Pisciotta *et al.* in 2007 and included TEM images indicating haemozoin within vesicles referred to as lipid nanospheres (Figure 1.8 (b)).[57] Isolation and characterization of the lipids were made possible by sucrose cushion centrifugation, followed by thin layer chromatography, which indicated that the foremost components of these nanospheres are monoacylglycerols. Lipid hydrolysis followed by gas-liquid chromatography-mass spectrometry (GLC-MS) showed that the fatty acid components of the lipids are predominantly comprised of stearic- and palmitic acid, proposing that the nanospheres contains mostly monostearoylglycerol (MSG ($C_{21}H_{42}O_4$), Figure 1.8 (c)) and monopalmitoylglycerol (MPG ($C_{19}H_{38}O_4$)).[57]
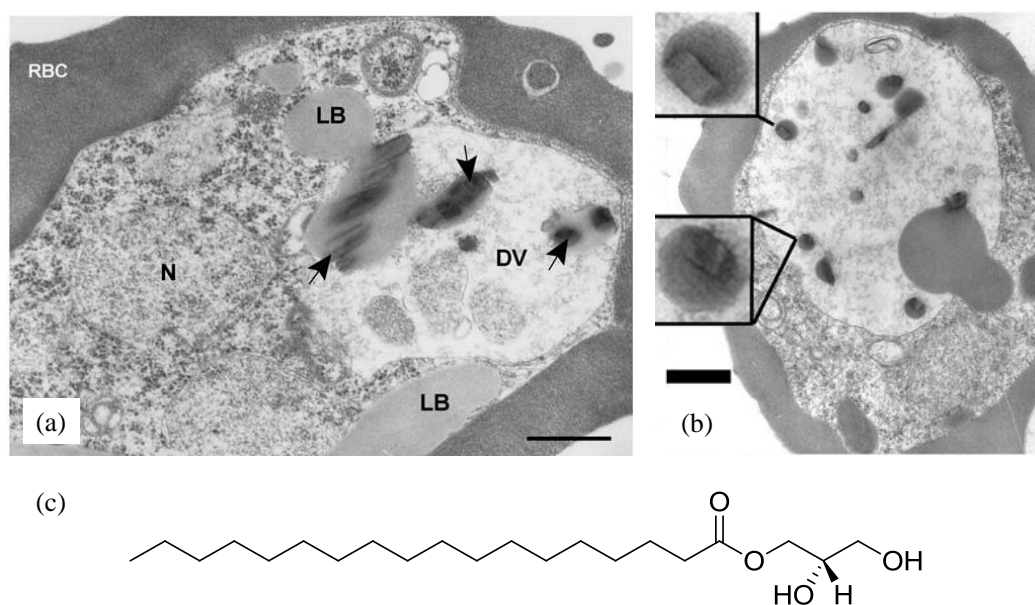
Figure 1.8 (a) Intravacuolar trophozoite of *P. falciparum* inside a human RBC. The arrows show the close association of neutral lipid deposits and haemozoin crystals. Reproduced with permission from reference 56. (b) Transmission electron microscopy image of trophozoites shows small haemozoin crystals surrounded by neutral lipid spheres inside the DV. Reproduced with permission from reference 57. (c) The molecular structure of monostearoylglycerol (MSG).

The association between haemozoin formation and lipids has further been established in other haemozoin forming organisms, which are unrelated to *P. falciparum*. Oliveira *et al*. indicated that the formation of haemozoin in *S. mansoni* also arises within lipid bodies, which are located in the gut of the worm (Figure 1.9 (a)), while the formation of haemozoin in *R. prolixus* appears to occur within bilayer membrane-bound vesicles (Figure 1.9 (b)).[58] In both cases the haemozoin is in direct contact with the lipid.
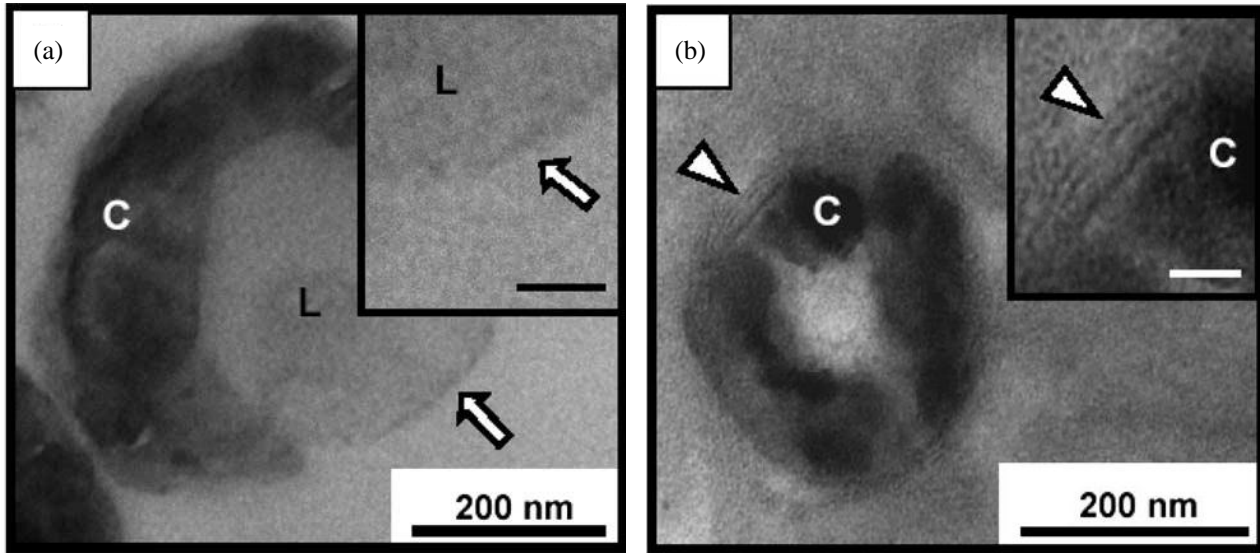
Figure 1.9 TEM images of haemozoin crystals (C) observed in (a) *S. mansoni* inside lipid droplets (L) and (b) *R. prolixus* inside membrane-bound vesicles. Arrows in (a) indicate the absence of a phospholipid double membrane in the lipid droplet-like particle, while the arrowheads in (b) indicate the presence of a phospholipid double membrane in perimicrovillar membranes. Reproduced with permission from reference 58.

The overall majority of information stemming from early to most recent studies strongly supports the contribution of lipids in the process of haemozoin formation.

1.4.3   β-Haematin Formation *In Vitro*

1.4.3.1 *β-Haematin Formation under Abiotic Conditions*

The formation of synthetic haemozoin, β-haematin, is readily performed in the laboratory, enabling one to investigate β-haematin crystal morphologies, structural properties and to develop an understanding of Fe(III)PPIX in different solvent environments. Understanding the mechanism of β-haematin formation *in vitro* is essential for understanding haemozoin formation *in vivo*. Previously, the majority of methods used for β-haematin synthesis made use of non-biological conditions; experiments were carried out either in an aqueous acetate solution from haematin (H_2O-Fe(III)PPIX),[35,53,59,51,60,61] or in dry methanol using haemin (Cl-Fe(III)PPIX) with 2,6-lutidine under anhydrous conditions.[36,62]

In 1991, Slater *et al.* synthesized β-haematin by dissolving haematin in 0.1 M sodium hydroxide (NaOH) and precipitating the porphyrin by the addition of acetic acid.[35] The reaction was run overnight at 70 °C, after which the precipitate was washed multiple times with distilled water. The β-haematin crystals were characterised by FT-IR and EXAFS spectroscopy, as well as PXRD. The first study in which the time course of β-haematin formation was reported was carried out by Adams *et al.* in 1996.[63] The authors monitored the progress of β-haematin formation at 60 °C in 4.5 M sodium acetate, pH 4.5, using Mössbauer spectroscopy. The results appeared to show that β-haematin formation is a zero-order process, continuing at a constant rate until completion.

In 2001, Egan *et al*. investigated the formation of β-haematin in a detailed study, using quantitative infrared spectroscopy, X-ray diffraction, SEM and TEM, to probe the parallel between haemozoin formation and biomineralisation processes.[64] The authors reported a method in which β-haematin was formed in less than an hour at 60 °C in 4.5 M acetate buffer, pH 4.5. The authors further investigated the kinetics of β-haematin formation and reported that the sigmoidal time dependence of formation could be accounted for by fitting the experimental data to the Avrami equation (Equation 1.1). The Avrami equation describes crystallization kinetics, and explains the transformation of solid materials from one phase into another at constant temperature during crystallisation.[65,66]

$$\frac{m_R}{m_0} = e^{-zt^n} \qquad \text{(Eq. 1.1)}$$

In the Avrami equation, m_R is the mass of the reactant (Fe(III)PPIX in this case) remaining after a specific time t, relative to the initial mass of the reactant, m_0. z is the experimental rate constant and n is the Avrami constant, which is generally an integer value between 1 and 4. The value of n describes the degrees of freedom and is a function of dimensionality of the growth process and the manner of crystal nucleation. When the Avrami constant is equal to 1, the model suggests that nuclei are preformed and crystal growth is in one dimension, resulting in linear crystal growth. However, when n is equal to 2 or 3, random or instantaneous nucleation is predicted and crystal growth is rod-like. Finally, when the Avrami constant is equal to 4, the reaction involves sporadic nucleation and crystal growth takes place in three dimensions. In the study by Egan *et al*., they showed that the best fit of the experimental time course data to the Avrami equation was when n was equal to 4 (Figure 1.10).[64]

In the experiment, β-haematin was formed from Fe(III)PPIX in a jacketed reaction vessel, and it was found that the reaction stirring rate influenced the geometry and the rate of crystal growth from the nucleation sites. Furthermore, it was shown that β-haematin formation was dependent on acetate concentration, reaction temperature and pH. The authors proposed that β-haematin formation occurred *via* rapid precipitation of amorphous Fe(III)PPIX, which was later converted into the desired product in the presence of acetate, which may have acted as a phase transfer catalyst in the dissolution and re-precipitation of haematin.[64]
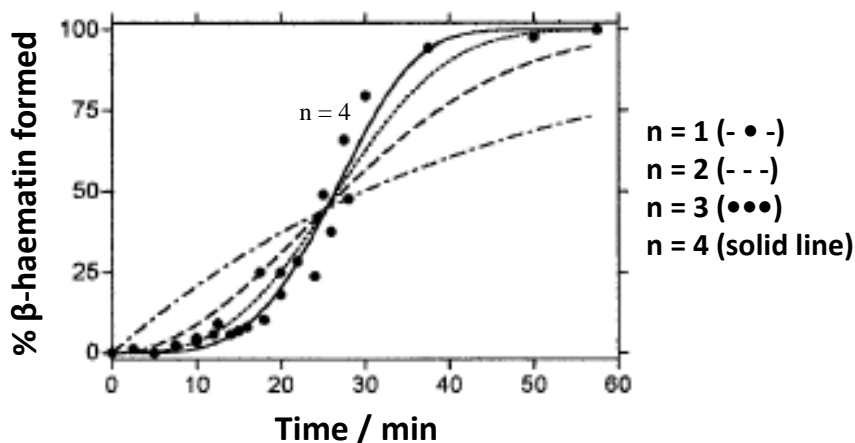
Figure 1.10 Time course of β-haematin formation in 4.5 M acetate, pH 4.5, 60 °C. The best fit through the experimental data (●) was achieved with n = 4 (solid line) in the Avrami equation. Reproduced with permission from reference 64.

Egan and Tshivhase reported a study in 2006 in which they investigated the formation of β-haematin in the presence of aqueous benzoic acid and derivatives of benzoic acid.[67] The experiments were otherwise carried out under the same the conditions as those used in the acetate medium. The authors showed that the acids are far more active in promoting β-haematin formation than acetic acid, in that β-haematin formed within 2 hours in the presence of 0.05 M benzoic acid (pH 4.5, 60 °C), compared to a higher concentration of acetate solution required (3.5 M) for β-haematin formation in a similar reaction time under the same conditions. The kinetics data were also fitted to the Avrami equation, with a value of n= 4 yielding the best fit. This indicated that β-haematin formation in the presence of benzoic acid, similar as in the acetate medium, involves sporadic nucleation and crystal growth in three dimensions. Egan and Tshivhase explained that the greater activity of benzoic acid compared to acetic acid may be accounted for by the ability of the benzene ring in the benzoic acid to π-stack over the Fe(III)PPIX molecule, assisting in the disruption of porphyrin-porphyrin interactions, and subsequently promoting the necessary rearrangements to form β-haematin. It was proposed that the role of the carboxylic acid was also to disrupt the hydrogen bond network in the Fe(III)PPIX molecule, and to assist in the formation of new hydrogen bonds, enabling β-haematin formation.[67]

A criticism of the above-mentioned work is the non-biologically relevant conditions. Consequently, studies began to focus on more biomimetic conditions to probe haemozoin formation. One way in which to mimic the lipid environment is the use of detergent-mediated methods for β-haematin formation. Various detergents have been studied as possible substitutes for the lipid environment in which β-haematin formation is performed, since detergents are less expensive materials and thus overall more affordable. In 1999, Fitch *et al.* carried out a study in which they showed that various detergents, including sodium dodecyl sulfate (SDS), n-octyl-glucopyranoside and Tween-80, actively promoted β-haematin formation by possibly increasing the solubility of monomeric Fe(III)PPIX.[54] In 2010, Carter *et al.* investigated a series of lipophilic agents as possible β-

13

haematin crystallisation promotors, from which they optimized and validated a Nonidet P-40 (NP40) detergent-mediated assay, which now serves as a screening mechanism for β-haematin inhibitors.[68] More recently, Sandlin *et al*. carried out studies in which they utilized the NP40 detergent-mediated assay in order to promote β-haematin formation as part of a high-throughput screen to identify β-haematin inhibitors, and to probe their β-haematin inhibitory activities.[69,70] In addition to the selection of detergents used for β-haematin formation, different solvent systems have been investigated as well. Huy *et al*. studied β-haematin formation induced by a series of short-chain alcohols, namely methanol, ethanol, *n*-propanol, and *n*-butanol. The authors showed that the induction of β-haematin formation by these alcohols is related with their respective degree of hydrophobicity and ability to solubilize heam.[71] In 2009 Stiebler *et al.* investigated the effect of water content on spontaneous β-haematin formation in dimethyl sulfoxide (DMSO) and a series of polyethyleneglycols. The authors demonstrated that reduced medium polarity increases haem solubility under acidic conditions, which in turn assisted in the nucleation of β-haematin crystals *in vitro* in the absence of any biological sample.[72]

While detergents such as NP40 are successful mediators of β-haematin formation, it is still ideal to carry out investigations using synthetic lipid particles in a biologically-relevant temperature and pH environment in order to facilitate β-haematin formation *in vitro.*

1.4.3.2 *β-Haematin Formation under Biologically-Relevant Conditions*

Given the attention that lipids have received regarding their role in the formation of haemozoin formation *in vivo*, lipid-mediated β-haematin formation has also been studied in the laboratory more recently.[54,73] In 2006, Egan *et al.* performed an independent study on the formation of β-haematin under biomimetic conditions, in order to investigate the possible role of lipids in this regard.[73] Two organic solvents, pentanol and octanol, as well as the model lipid monomyristoylglycerol (MMG), were used to mimic the lipid environment. The organic solvent or lipid solution (dissolved in acetone/methanol) was layered on top of aqueous citrate buffer to yield an interface. By introducing Fe(III)PPIX dissolved in 0.1 NaOH directly to the interface, the authors showed that β-haematin forms rapidly at 37 °C, pH 4.8,[19] near the pentanol-water, octanol-water and lipid-water interfaces. Kinetics of β-haematin formation in this system indicated an apparent first-order reaction, with a half-life of 5.3 minutes (Figure 1.11). Furthermore, the study indicated that no β-haematin formation occurred within 30 minutes in either the aqueous medium or organic solvents alone, pointing to the important role of the interface region. Compared to the previous non-biological methods for β-haematin formation,[64,67] the kinetics results in this particular study differ notably from the familiar sigmoidal profile observed in acetate. However, the experimental data were not analysed and according to the Avrami model, and a systematic study was not conducted until later.
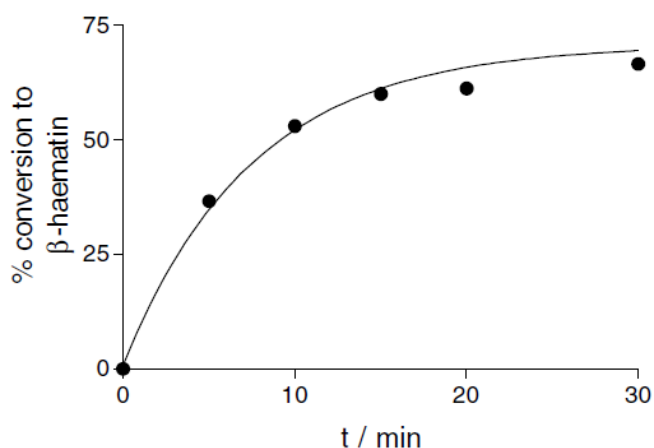
Figure 1.11 Kinetics of β-haematin formation brought about near the interface of MMG and water. The experimental data are fitted to a hyperbolic equation for a first-order reaction, corresponding to a half-life of 5.3 minutes. Reproduced with permission from reference 73.

Hoang *et al*. further investigated β-haematin formation at the lipid-water interface, using a model consisting of an emulsion of neutral lipid particles.[74] The effect of various neutral lipids, including mono-, di- and triglycerides, in promoting the formation of β-haematin under biologically-relevant conditions (37 °C, pH 4.8) indicated that monoglycerides, including MPG, MMG, MSG and rac-1-monooleoylglycerol (MOG), exhibit the highest efficiency in mediating β-haematin formation with yields of about 60-80% (Figure 1. 12). Kinetics studies indicated fast rates of β-haematin formation with half-lives of about 0.5 minutes for MPG, MMG and MSG, which are an order of magnitude faster than previously reported.[73] The data indicated that reactions were complete within five minutes, and additional experiments showed that the rate of the reaction stays constant, with a change in the percentage of β-haematin formation, when changing the surface area of the reaction vessel.
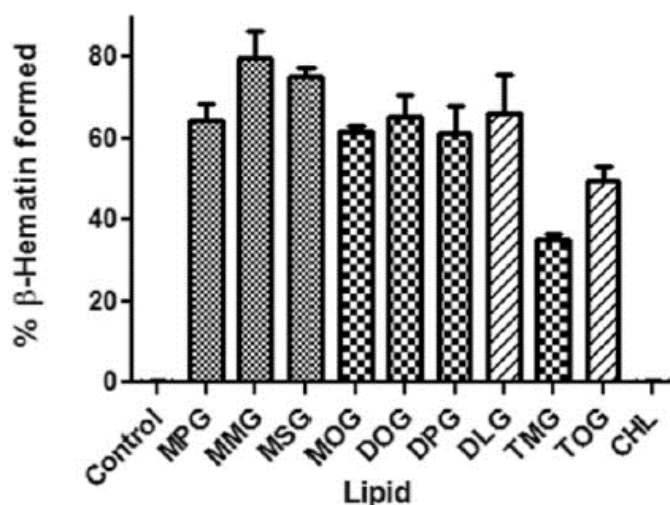
Figure 1.12 β-Haematin formation using various neutral lipids. The percentage yield of β-haematin formation using mono-, di- and tri-glycerides after 60 minutes incubation time. The monoglycerides show the highest yield of β-haematin formation, while the control reaction in which Fe(III)PPIX was incubated in pure aqueous medium, shows no yield. Reproduced with permission from reference 74.

15

Furthermore, Hoang *et al*. reported the presence of homogeneous lipid particles, which are spontaneously organised into a lipid emulsion, near the interface, using fluorescence, confocal and TEM imaging, as well as dynamic light scattering analysis.[74] β-Haematin crystals recovered from the lipid-water interface using MSG and MPG were confirmed by FT-IR spectroscopy, PXRD and TEM imaging. Further TEM images were obtained of Fe(III)PPIX-lipid samples after 10 minutes of incubation at the lipid-water interface (Figure 1.13), and indicated what appeared to be β-haematin crystals aligning along the interface for samples from both MSG and MPG.
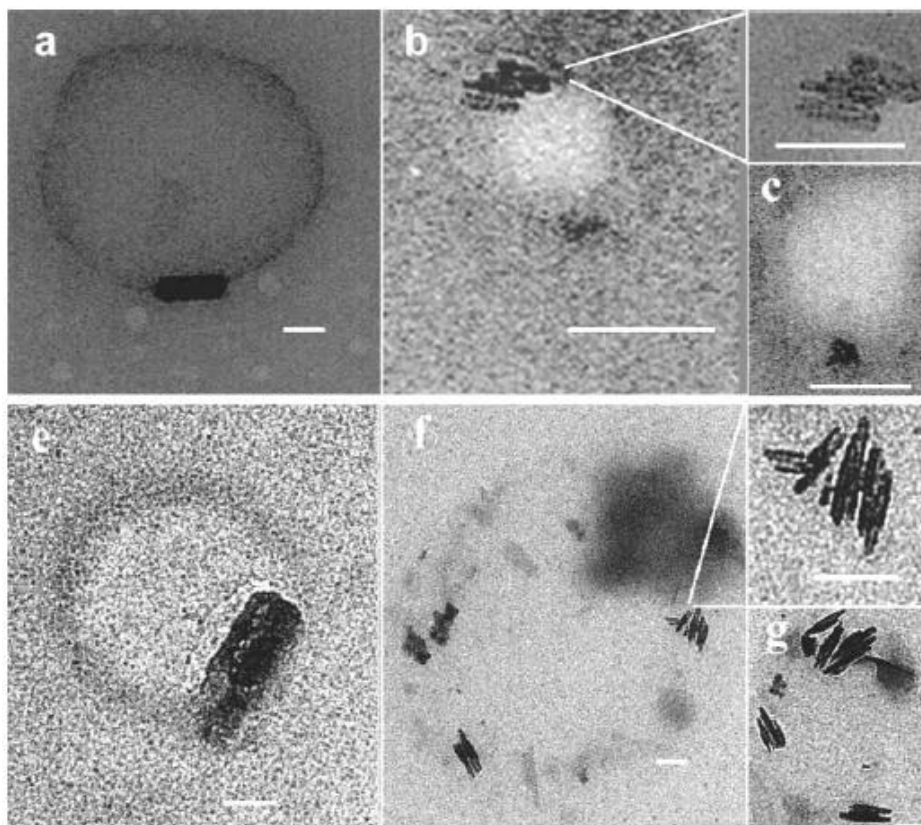
Figure 1.13 TEM images of β-haematin formed between the MSG-water (a-c) and MPG-water (e-g) interface after 10 minutes of incubation. β-Haematin crystals were observed aligned along the lipid-water interface (a and e), while clusters of β-haematin crystals are oriented parallel to each other and the lipid-water interface (b, c, e and f). Reproduced with permission from reference 74.

In 2013, Ketchum *et al*. compared the crystallisation of β-haematin from haematin in an aqueous buffer, pH 4.8, which is in agreement to the DV, to crystallisation in a water-saturated octanol solution, which is a mimic of a lipid nanosphere environment.[75] Investigating their crystal morphologies by atomic force microscopy, it was shown that β-haematin crystals grown in the octanol-water system are similar to biological haemozoin extracted from parasites. The authors also commented on the higher solubility of haematin at the water-saturated octanol interface compared to in the aqueous buffer, further suggesting that lipid bodies indeed play a role in facilitating haemozoin *in vivo*.[75,76] More recently, the formation of a monolayer of a phospholipid membrane surrounding β-haematin has also been shown.[77]

1.4.4   Proposed Mechanisms of Haemozoin Formation

To truly explain the molecular mechanism of haemozoin formation and the structure of Fe(III)PPIX complexes with antimalarial inhibitors, it is import to understand the behaviour and structure of Fe(III)PPIX in different solutions. Owing to its varied speciation in solution, it is important to comprehend under which conditions Fe(III)PPIX is most favourable for β-haematin formation.

Early studies on aqueous Fe(III)PPIX have recognised that the porphyrin self-associates in aqueous solution,[78,79] and it was widely accepted that Fe(III)PPIX spontaneously forms a μ-oxo dimer, whereby the iron centres of neighbouring porphyrins are connected by an oxo (Fe-O-Fe) bridge. This hypothesis, believed for almost 40 years, was based on infrared spectroscopic data obtained for the solid precipitated from an alkaline solution by the addition of solid NaOH or 1 M NaOH, or from an alkaline DMSO solution.[80] Brown *et al.* continued their research and further reported equilibrium constants for Fe(III)PPIX dimerization.[81] In an attempt to verify these dimerization constants, de Villiers *et al.* showed that spontaneous dimerization of H_2O-Fe(III)PPIX and HO-Fe(III)PPIX leads to π-π complexes in aqueous solution, rather than a μ-oxo dimer.[82] The π-π dimer is believed to form *via* a noncovalent interaction of the unligated face of the each porphyrin molecule, with the axial ligands pointing outwards (Figure 1. 14 (A, i)). The authors based their conclusion on both UV-visible and ¹H nuclear magnetic resonance (NMR) spectra of aqueous Fe(III)PPIX, which are markedly different from those of the μ-oxo dimer.[83,84] There is support in the literature for the formation of such π-π dimers given the reported X-ray crystal structures of Cl-Fe(III)PPIX[85] and aqua-iron(III)octaethylporphyrin,[86] which themselves pack in the solid state as π-π dimers. Furthermore, it has been shown that solvent concentration, temperature, pH and the presence of salts have an effect on Fe(III)PPIX speciation in different solvent systems,[87] however, from the study carried out by de Villiers *et al.*, it is clear that the formation of the π-π dimer species predominates in aqueous solution and understanding this structure is of importance in unravelling the mechanism of haemozoin formation.[82]

Molecular dynamics simulations have provided further insight into the possible molecular mechanism by which haemozoin may form at the lipid-water interface.[73] Egan *et al.* carried out simulations of the interactions of a π-stacked dimer of H_2O-Fe(III)PPIX in vacuum, and showed that the porphyrins rapidly reorganise to form a haemozoin precursor dimer (Figure 1.14 (B)), in which the positively charged iron centre of one Fe(III)PPIX molecule interacts with the negatively charged propionate group of the other.[73] Following displacement of the axial water molecules from the iron centres, and simultaneous bond formation between the iron centre and the propionate groups, the formation of haemozoin (β-haematin) takes place. It is further speculated that in the absence of competing hydrogen bonding from water solvent molecules, hydrogen bonding between the haemozoin dimers will be induced, facilitating in the formation of the haemozoin crystal. However, in the presence of water molecules, and hence competing hydrogen bonding, the simulation showed that the haemozoin precursor dimer is unstable, with the propionate groups preferentially interacting with the solvent water molecules, rather than the neighbouring iron centre. The molecular dynamics simulations therefore further suggest that a lipid environment (specifically a low dielectric medium) will better promote haemozoin crystal formation, owing to the lower water concentration.
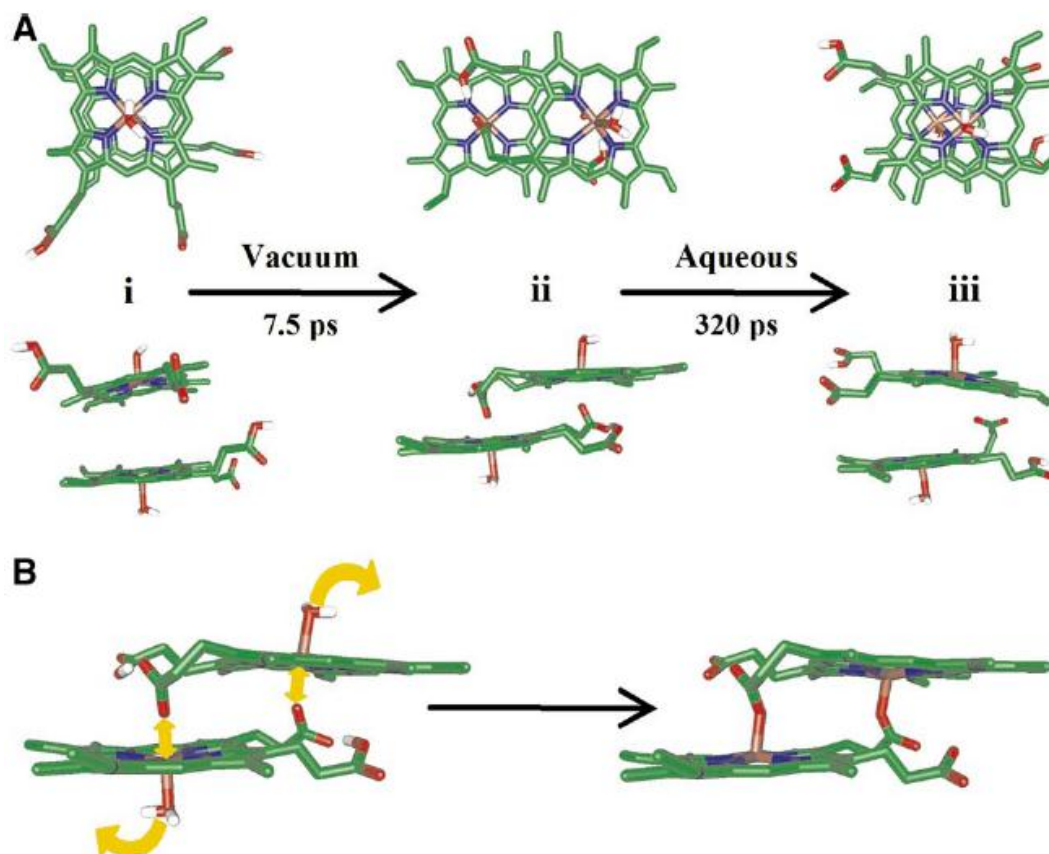
Figure 1.14 Molecular dynamics simulation of the interaction of H_2O-Fe(III)PPIX molecules. (A) The molecules were placed back-to-back as expected for a π-π dimer, with the propionate and propionic acid groups extended from the porphyrin core (i). In *vacuo*, the β-haematin precursor is rapidly formed (ii). In an aqueous environment, the precursor breaks down and the propionate groups interact with the solvent molecules (iii). Enlarged in (B), simulations suggest that the coordination of the propionate groups to the Fe(III) centre and the subsequent loss of an axial H_2O ligand will yield the precursor dimer (left) to the β-haematin dimer (right). Reproduced with permission from reference 73.

Based on the insight provided on Fe(III)PPIX π-π dimer species[82] and molecular dynamics simulations *in vacua*,[73] de Villiers *et al*. hypothesised how aqueous Fe(III)PPIX, in its π-π dimer form (Figure 1.15, 1), may be converted into haemozoin (β-haematin).[88] The molecular dynamics simulations suggest that when Fe(III)PPIX enters a lipid environment, which is a low dielectric medium, it forms an intermolecular haemozoin precursor dimer molecule (Figure 1.15, 2), which may convert to a haemozoin dimer by reciprocal coordination of the iron centre with the propionate groups and displacement of water ligands (Figure 1.15, 3). Upon hydrogen bonding between haemozoin dimers, the haemozoin crystal is formed (Figure 1.15, 4).

In 2009, de Villiers *et al.* investigated the orientation of β-haematin crystals nucleated by MMG on the water surface using grazing incidence synchrotron X-ray diffraction (GIXD).[89] The authors showed that β-haematin nanocrystals, prepared from premixed haematin with MMG, were orientated with the (100) face parallel to the water surface. They explained this observation in that the methanol-acetone-aqueous NaOH spreading solution allowed molecular aggregation of MMG into clusters, exposing the OH groups and oxygen lone-pair electrons that interact with the respective haematin molecules. These interactions induced oriented β-haematin formation, with crystal growth predominantly taking place in one dimension along the *c*-axis[89]

18
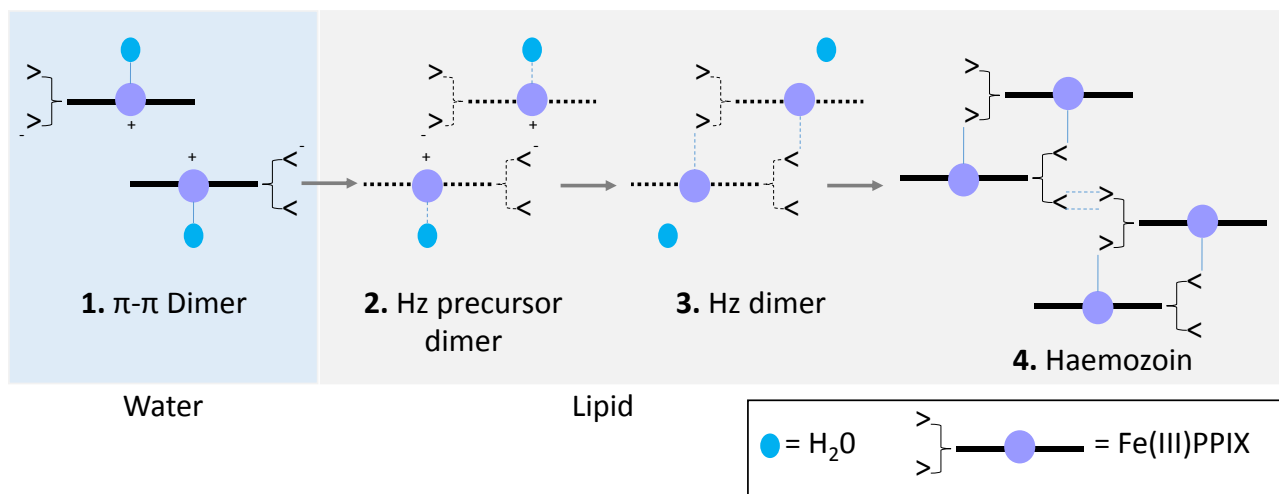
Figure 1.15 Schematic representation of the proposed route of haemozoin (Hz) formation.[88] The aqueous π-π dimer **(1)** enters the lipid environment and forms the haemozoin precursor **(2)**, which goes on to form the haemozoin dimer **(3)** by the reciprocal coordination of the propionate groups with the Fe(III) centre and the displacement of H_2O ligands. Upon hydrogen bonding between the dimers, the haemozoin crystal **(4)** is formed. Adapted from reference 88.

1.5 Quinoline Antimalarial Drugs

1.5.1   Site of Drug Action

As mentioned in section 1.3.1, clinically known symptoms that are related to malaria infection are associated with the blood stage (intraerythrocytic stage) of the malaria parasite's life cycle. While residing inside the host RBCs, *P.falciparum* may be exposed to antimalarial drug action at multiple stages, of which the potential targets for drug action have been broadly classified into three categories by Olliaro *et al*.[27] The categories include (1) processes arising in the DV of *P.falciparum*, including haem detoxification and haemoglobin digestion; (2) enzymes involved in metabolite and macromolecular synthesis; and (3) those responsible for membrane processes and signalling. Several studies have drawn focus to processes occurring in the DV. Saliba *et al*. confirmed the involvement of the DV of the parasite in the mechanism of CQ resistance, by showing that CQ-resistant (CQR) strains have a decreased CQ accumulation in comparison to CQ-sensitive (CQS) strains.[90] CQ and other quinoline antimalarial drugs have been shown to be active against the trophozoite stage of the parasite life cycle,[91] while Yayon *et al*. demonstrated the accumulation of CQ in malaria-infected erythrocytes by fluoromicroscopic examination.[92] Overall, the most likely drug targets in the DV of the parasite are the interruption of either haemoglobin degradation or haematin detoxification, resulting in the death of the parasite in either case.

The quinoline antimalarial drugs accumulate in the DV by a mechanism known as pH trapping.[49] In their neutral weak base form, quinoline antimalarial drugs are able to traverse the lipid membrane and enter the acidic environment of the DV, where the drugs are protonated and become membrane-impermeable. The result is that the concentration of the antimalarial drugs is considerably higher inside the DV than outside.[93]

1.5.2 History and Discovery of Quinoline Antimalarial Drugs

The most successful and effective antimalarial drugs that have been used to date include the quinoline-based and related drug compounds; CQ, amodiaquine (AQ), quinidine (QD), quinine (QN), mefloquine (MQ) and halofantrine (Hf) (Figure 1.16).
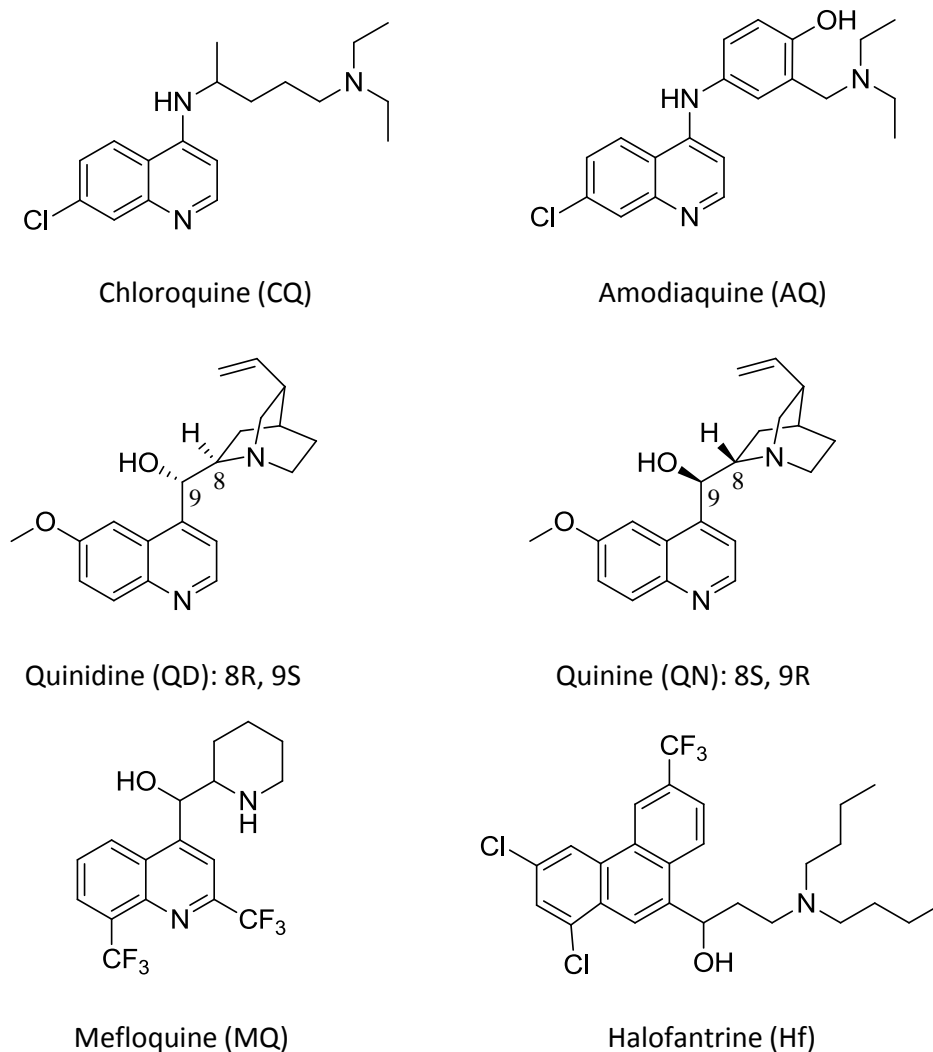
Figure 1.16 Molecular structures of several quinoline (CQ, AQ, QD, QN and MQ) and phenanthrene (Hf) antimalarial drugs.

For hundreds of years prior to understanding the mosquito or the malaria parasite life cycle, a herbal treatment, from *Cinchona* bark, was used to treat malaria.[94] In 1820, Pierre Pelletier and Joseph Caventou, two French chemists, were the first to isolate the pure alkaloids QN and cinchonine from the *Cinchona* bark.[95] From the 1940s, QN became the standard therapy for malaria-related fever worldwide, with the Dutch plantations of Java producing 97% of the world's supply of QN.[96,97] After the high demand of QN in World War I and especially in World War II, the Japanese takeover of Java saw the need for new antimalarial drugs to increase radically, which led to great research efforts by British and German scientists to develop alternative

treatments.[98] The first attempts in preparing synthetic antimalarials included the design of 8-aminoquinolines; plasmaquine (pamaquine) and primaquine, followed by the design of several 4-aminoquinolines, of which CQ was to be the most important.[98,99] CQ is recognized historically as the most effective antimalarial drug, owing to its efficacy, affordability and low toxicity.[94] AQ was, however, soon introduced as an alternative to CQ, owing to the widespread resistance against CQ since the 1960s, and is still used in some cases today for the treatment of uncomplicated malaria.[98,99] In the mid-1970s, another synthetic derivative of QN, MQ (Larium), a quinoline methanol compound, was introduced with potent antimalarial activity,[100,101] and has proven to be an effective antimalarial, especially against CQS strains of malaria.[102,103]

1.5.3   Quinoline Antimalarial Drug Resistance

A great deal of research has focussed on the development of new and effective antimalarial drugs, owing to the great increase in the appearance of drug resistance to clinically-relevant antimalarial drugs.

As mentioned above, a diprotic weak base such as CQ can be driven across the DV membranes of the parasite in its unprotonated form, by a pH gradient, to accumulate within the DV. It is believed that the resistance to CQ in *P. falciparum* is associated with an increased ability for the parasite to eject CQ out of the DV at a rate that does not allow CQ to reach the required levels needed for the inhibition of haemozoin formation.[104] Krongstad *et al*. investigated the reduced uptake of CQ and showed that this CQ efflux occurs at a rate of 40 to 50 times faster in CQR parasites than in CQS parasites.[105] The rapid efflux of CQ out of the DV of CQR parasites, compared to CQS parasites, may be accounted for by a possible enhanced permeation pathway for CQ across the DV membrane,[93] possibly through a channel, or *via* active transportation across the membrane, since the pH gradient across the DV membranes of both the CQR and CQS parasite shows no significant difference.[19]

Furthermore, at a molecular level, it has been shown that CQ resistance is related to mutations in two genes that encode transmembrane proteins. The 424 amino acid transmembrane protein, *P. falciparum* CQ-resistance transporter (*Pf*CRT), which is located on the surface of the DV, is coded for by the gene *pfcrt* on chromosome 7.[106] A mutation at position 76 in the amino acid sequence of the protein (K76T), is associated with the CQR strain.[107] In this mutation, the lysine α-amino acid (K) is replaced by the threonine α-amino acid (T). *P. falciparum* multidrug resistance gene 1 (*Pf*mdr1), located on chromosome 5, is another DV transporter protein which is associated with drug resistance, and encodes P-glycoprotein homologue 1 (Pgh1).[108] Cowman *et al*. demonstrated that resistance to QN, MQ and HF is caused by an over-expression of Pgh1.[109] Ferdig *et al*. showed that even though the mechanism for QN resistance is poorly understood, it is also associated to *P. falciparum* sodium proton exchanger (pfnhe-1).[110] At first the exact mechanism of CQ resistance by mutated *Pf*CRT proteins was not definitively understood, however, Sanchez *et al*. later proposed that *Pf*CRT acts either as a channel, allowing CQ to passively move out of the DV *via* an electrochemical gradient, or as a transporter, in which CQ is actively transported out of the DV.[93]

P. falciparum is one of the most well-known human pathogens that repeatedly encounters drug pressure and within-host competition among different malaria parasite strains.[111] Fidock and co-workers have been investigating the role of *Pf*CRT in antimalarial drug resistance over the last few years. Results show that *Pf*CRT variants can affect parasite fitness, alter *P. falciparum* vulnerability to current therapies and protect immature gametocytes against CQ drug action, and these authors have subsequently investigated the selection and dissemination of geographically diverse halotypes (a set of DNA variations) of *Pf*CRT genetically.[111,112]

1.5.4   Proposed Mechanisms of Antimalarial Drug Action

It is known that the quinoline antimalarial drugs CQ, AQ, QD, QN and MQ inhibit the formation of β-haematin under various conditions.[59,51,113,114,115] The exact mechanism of action of these antimalarial drugs is, however, not entirely understood and substantial research has been devoted to understand this phenomenon. To date, two main hypothesis exist regarding the mechanism by which inhibition occurs. It has been suggested that antimalarial drug compounds form complexes with free Fe(III)PPIX in the aqueous solution of the DV of the parasite, either *via* π-stacking or coordination, preventing the conversion of Fe(III)PPIX into β-haematin.[116,117,118] Early studies demonstrated that nitrogen-containing compounds and nitrogen-donor ligands are able to complex with Fe(III)PPIX species.[78,119,120] Alternatively, the other hypothesis proposes that drugs adsorb onto the fastest growing crystal face (001) of β-haematin, impeding further growth.[39,114] Owing to the diverse speciation of Fe(III)PPIX (as a monomer, μ-oxo dimer , π-π dimer or cyclic dimer precursor for the formation of haemozoin formation),[87] the possible drug interactions with Fe(III)PPIX which could be of importance in antimalarial drug action are endless. Investigating quinoline drug-Fe(III)PPIX complexes is one way of understanding their mode of action.

1.5.4.1 Drug-Fe(III)PPIX Complexation

Drug complexes with free Fe(III)PPIX are proposed to prevent the formation of haemozoin and possibly influence the overall toxicity within the parasite, leading to its overall death. The exact structures of the 4-aminoquinoline and quinoline methanol drug complexes have been widely debated and resolving these structures has been of great interest. Recently, the structures of the complexes of several quinoline methanol drugs and Fe(III)PPIX have been resolved. On the other hand, there is great controversy with respect to the proposed structure of 4-aminoquinoline complexes, such as CQ-Fe(III)PPIX.

1.5.4.1.1   Quinoline Methanol Complexes with Fe(III)PPIX

In 2008, de Villiers *et al*. reported the first crystal structure of a Fe(III)PPIX complex with an antimalarial drug.[88] The structure of the coordination complex formed between Fe(III)PPIX and Hf was determined using

SCD and shows coordination of Hf to the iron centre of the Fe(III)PPIX through the deprotonated aryl alcohol functionality of Hf, along with π-stacking of the phenanthrene ring over the porphyrin, resulting in a five-coordinate complex (Figure 1.17 (a)). Intermolecular hydrogen bonding between the propionate group of Fe(III)PPIX and the protonated nitrogen atom of Hf, as well as hydrogen bonding between the same propionate group and the propionic acid group of the neighbouring Fe(III)PPIX molecule also occurs. The structure further shows that Fe(III)PPIX is a monomer, rather than a μ-oxo dimer, in its interaction with Hf, and the length of the Fe–O bond is consistent with the length of an Fe-alkoxide bond.[121,122,123]

Furthermore, owing to structural resemblances between Hf and the quinoline methanol antimalarial drugs, QD and QN, de Villiers *et al.* carried out an *in vacuo* molecular mechanics modelling investigation of the complexes of QD and QN, and their respective inactive epimers, 9-epiquinidine (EQD) and 9-epiquinine (EQN) with Fe(III)PPIX.[88] The comparable spectral changes observed when titrating Fe(III)PPIX with Hf and QD free bases in acetonitrile, respectively, provided qualitative support for their above reasoning and suggested homologous coordination in Hf and QD. The molecular mechanics modelling proposed that the formation of the haemozoin precursor dimer may be prevented by the formation of an important intramolecular salt bridge between the protonated quinuclidine tertiary amino group and the unprotonated haem propionate group. The theoretical studies further indicated that the formation of the salt bridge is readily permitted by QD and QN, which can adopt the required lower energy conformations.

On the contrary, this was not the case for EQD and EQN. It has previously been shown that QD, QN, EQD and EQN associate with Fe(III)PPIX in an aqueous environment, allowing Fe(III)PPIX to exist as a π-π dimer (through its unligated faces).[118] The authors thus further proposed that as the association complexes of the inactive isomers enter the lipid environment, haemozoin precursor dimer formation dominates complex formation, due to their inability to form the salt bridge, allowing normal haemozoin formation to continue. On the other hand, when complexes of the active isomers enter the lipid environment, the salt bridge forms and therefore interrupts haemozoin precursor dimer formation, which in turn impedes haemozoin formation.[88] The inhibition of haemozoin formation *via* the interaction of the *Cinchona* alkaloids with monomeric Fe(III)PPIX is in agreement with previous studies.[124,125]

Structural evidence in support of the hypothesis discussed above was recently obtained. Importantly, the crystal structures of complexes formed between Fe(III)PPIX and the two *Cinchona* alkaloids, QD and QN, respectively, were determined by means of SCD (Figure 1.17 (b and c)).[126] The crystal structures confirm the formation of five-coordinate complexes between QD and QN with Fe(III)PPIX, respectively, through their benzylic alcohol functional group and the length of the Fe-O bond is also consistent with that of the length of an Fe-alkoxide bond, rather than an alcohol.[88] The crystal packing in both complexes indicates additional π-stacking between the unligated faces of Fe(III)PPIX of neighbouring alkaloid-Fe(III)PPIX moieties. The offset π-π dimerization is consistent with the Fe(III)PPIX speciation expected in aqueous[82] and aqueous methanol solutions.[87] Intermolecular hydrogen bonding between Fe(III)PPIX propionic acid side chains and propionate groups, allows the interaction of neighbouring π-π dimers. The authors further discussed that additional stability in the alkaloid complexes is provided by the intramolecular hydrogen bond which is observed between

the protonated quinuclidine nitrogen atom of each alkaloid and a propionate side chain of Fe(III)PPIX. It is proposed that these interactions, namely coordination, π-stacking and intramolecular hydrogen bonding, may be responsible for preventing the conversion of Fe(III)PPIX into haemozoin.
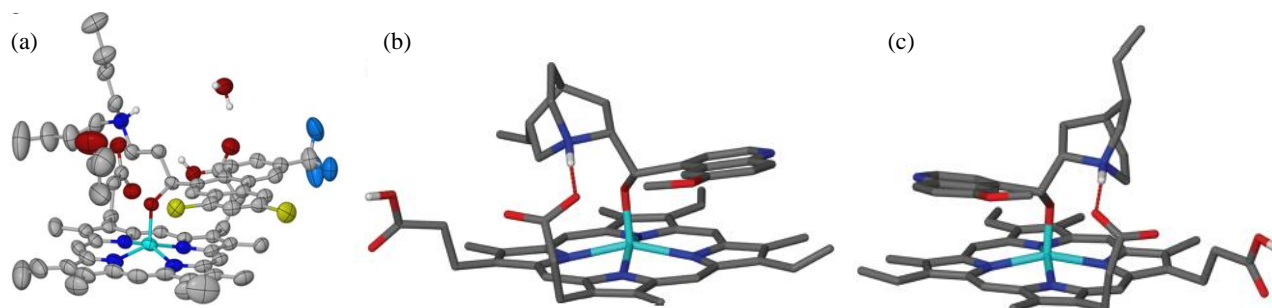
Figure 1.17 The single crystal X-ray diffraction structures of (a) Hf-Fe(III)PPIX, (b) QD-Fe(III)PPIX and (c) QN-Fe(III)PPIX. For (a) thermal ellipses are drawn at 50% probability and for (b and c) solvent molecules are omitted and hydrogen bonds are shown red dashed lines. Atom colour coding: C – grey, H – white, Cl – lime green, F – Prussian blue, Fe – cyan, N – blue and O – red. Reproduced with permission from reference 88 and 126.

Most recently, Gildenhuys *et al.* determined the crystal structure of the complexes formed between racemic *erythro* MQ and Fe(III)PPIX using SCD, and showed that alkoxide coordination is an important interaction in the solid state.[127]

1.5.4.1.2   4-Aminoquinoline Complexes with Fe(III)PPIX

The main focus of 4-aminoquinoline-Fe(III)PPIX complexes has been on CQ. Early spectrophotometric studies by Cohen *et al.* in 1964 were the first to qualitatively provide evidence of a CQ-Fe(III)PPIX complex in solution,[116] and interest in the CQ-ferrihaem complex remains high, even today. To date, various studies have suggested different structures of the CQ-Fe(III)PPIX complex. In 2003, De Dios *et al.* proposed that CQ coordinates to the iron centre of monomeric Fe(III)PPIX *via* its quinolinyl nitrogen atom to form a covalent complex (Figure 1.18 (a)).[128] The authors proposed the structure on the basis of solid state nuclear magnetic resonance (NMR) spectra of acid-precipitated CQ-Fe(III)PPIX aggregates formed in an aqueous solution. NMR inversion recovery experiments by Leed *et al.*, followed by the studies of Natarajan *et al.* a few years later, suggested that CQ rather forms a non-covalent complex in solution with the μ-oxo dimer of Fe(III)PPIX *via* π-stacking with the outer unligated face of Fe(III)PPIX (Figure 1.18 (b)).[129,130] It was suggested that CQ-Fe(III)PPIX complex was stabilised through these π-π interactions between the tetrapyrrole region of the porphyrin and the aromatic rings of CQ. Furthermore, Schwedhelm *et al.* proposed that two CQ drug molecules π-stack with the outer faces of a Fe(III)PPIX tetramer adduct, in which the two μ-oxo Fe(III)PPIX dimers are coordinated through neighbouring iron centres and propionate side chains (Figure 1.18 (c)).[131] Later, using excitonic Raman enhancement, Webster *et al.* suggested that CQ drug molecules acts as molecular spacers

which bind noncovalently to the unligated faces of µ-oxo dimeric Fe(III)PPIX aggregates via π-π interactions and dispersion forces (Figure 1.18 (d)).[132] This has also been suggested by Morau *et al*., using NMR spectroscopic studies.[133] Recently, Acharige and Durrant showed using quantum mechanical calculations that CQ may form hydrogen bonds *via* its 4-amino substituent group and tertiary amine to the axial ligand and propionate side chains of Fe(III)PPIX, respectively (Figure 1.18 (e)).[134] It is clear from these findings that there is no consensus regarding the CQ-Fe(III)PPIX complex structure in solution, resulting in much controversy.
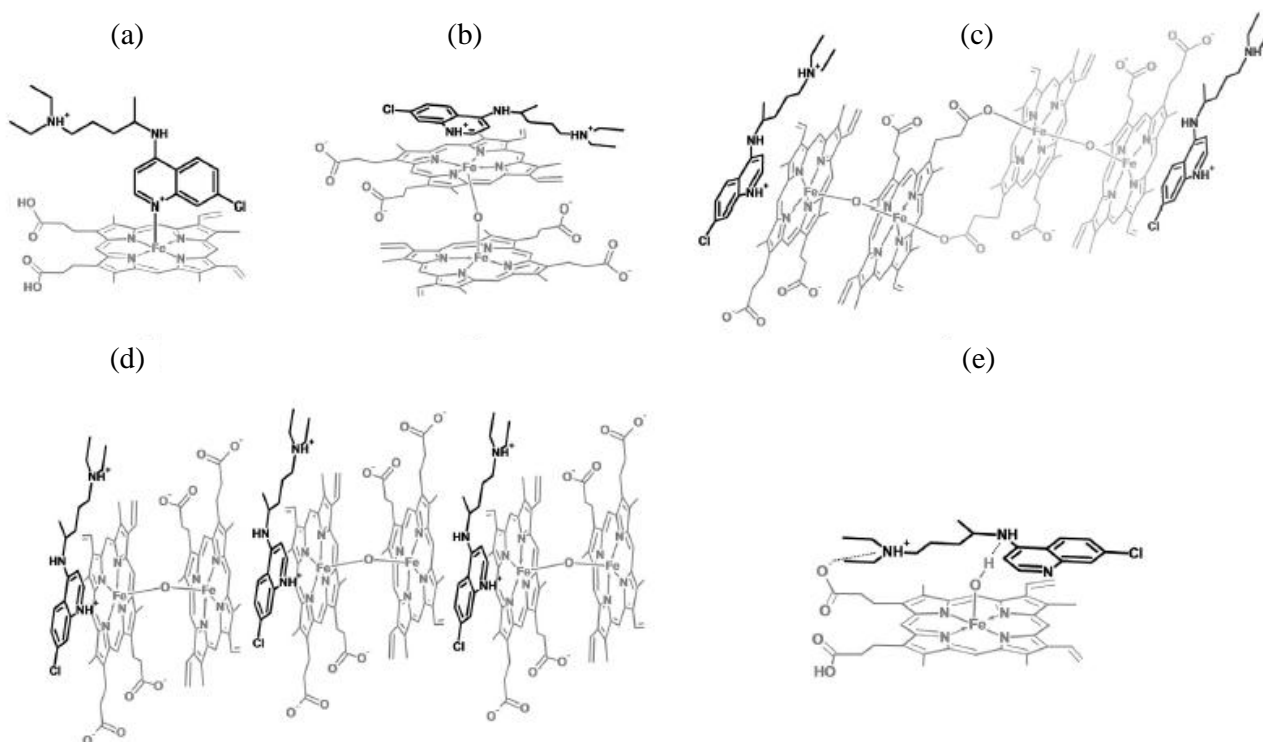
Figure 1.18 Proposed structures of CQ-Fe(III)PPX complexes. (a) CQ coordinated to monomeric Fe(III)PPIX,[128] (b) CQ π-stacked to µ-oxo Fe(III)PPIX dimer,[129,130] (c) two CQ molecules π-stacked to µ-oxo Fe(III)PPIX tetramer adduct,[131] (d) CQ molecules π-stacked between µ-oxo Fe(III)PPIX dimers[132,133] and (e) CQ hydrogen-bonded to Fe(III)PPIX.[134] Reproduced with permission from reference 135.

Most recently, Kuter *et al.* undertook a computational investigation of the CQ-Fe(III)PPIX complex structure, in which they probed two possible conformations of the complex using molecular dynamics (MD) simulations.[135] In light of previous studies suggesting that CQ induces µ-oxo dimer formation,[129,136] two CQ-[µ-oxo-Fe(III)PPIX] complexes were considered. The first structure was similar to previously discussed,[129,130,133] in which CQ π-stacked over the unligated face of the µ-oxo dimer (Figure 1.18 (b)). This structure is referred to as the π-stacked model. The second structure was novel, in that the CQ molecule is positioned between the two porphyrin rings with the protonated quinolinium nitrogen atom facing towards the bridging oxide ligand (Figure 1.19 (a)).[135] This structure is referred to as the docked model. Subsequent experimental EXAFS spectra, as well as magnetic and infrared spectroscopic data, most importantly the assymmetric Fe−O−Fe stretch that shifts lower in frequency (744 cm^{-1}) with H_2O^{18}, were consistent in

suggesting that the CQ drug molecule docks between the porphyrin rings of μ-oxo Fe(III)PPIX in aqueous solution. The authors further indicated that important interactions between CQ and the μ-oxo Fe (III)PPIX dimer in the docked model of the CQ-[μ-oxo-Fe(III)PPIX] complex can be observed (Figure 1.19(b)). Intermolecular hydrogen bonds are formed between the protonated quinolinium nitrogen atom of CQ and the oxide bridge of μ-oxo Fe(III)PPIX (i), while π- π interactions are formed between the porphyrin ring system and the quinoline ring of CQ (ii). Hydrogen-chlorine contacts are also observed between the methyl hydrogen atoms of the porphyrin ring system (yellow) and the 7-chloro substituent of CQ (green) (iii).[135]
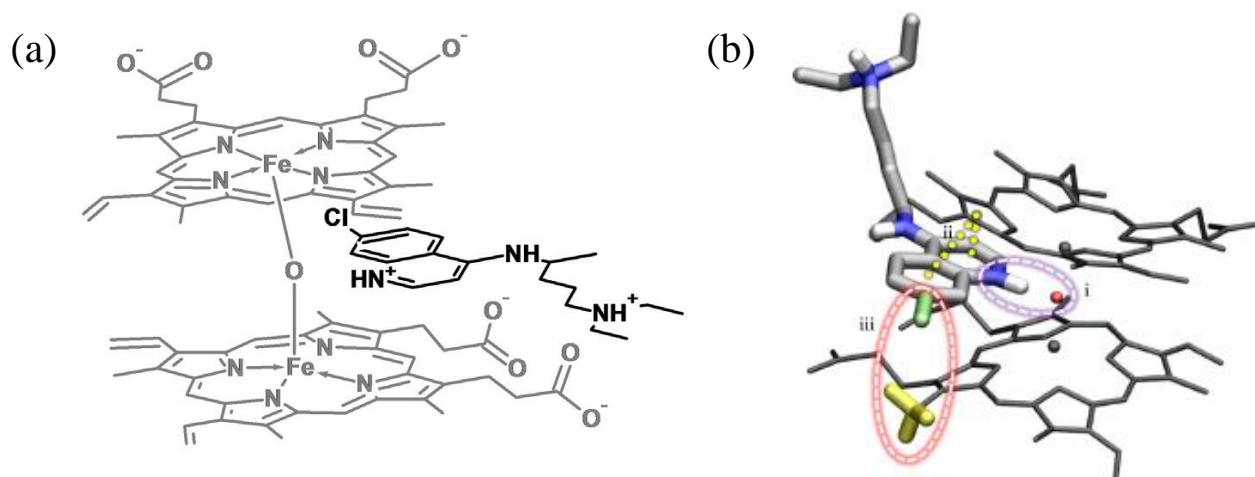
Figure 1.19 Model of the (a) docked CQ-Fe(III)PPIX complex simulated in the MD study. (b) Important interactions between CQ and the μ-oxo Fe(III)PPIX dimer in the docked model of the CQ-[μ-oxo-Fe(III)PPIX] complex. Reproduced with permission from reference 135.

1.5.4.2 Quinoline Interactions with Haemozoin

An alternative hypothesis regarding the inhibition of β-haematin formation is the direct interaction between the antimalarial drug and the fastest growing surface of β-haematin crystals. [37,39,114] In 1996, Sullivan *et al*. detected CQ in close association with haemozoin crystals in a study in which they investigated the distribution of [³H]-labelled CQ inside parasitized RBCs, using electron microscope autoradiography (Figure 1.20 (a)).[114] The authors further showed that *in vitro*, binding of the [³H]-labelled quinoline inhibitor to the haemozoin crystal strongly depends on the addition of haem substrate, which they suggested pointed to a haem-quinoline complex being incorporated into the growing haemozoin to impede further haemozoin formation (Figure 1.20 (b)). This process was referred to as haemozoin crystal capping.[114]
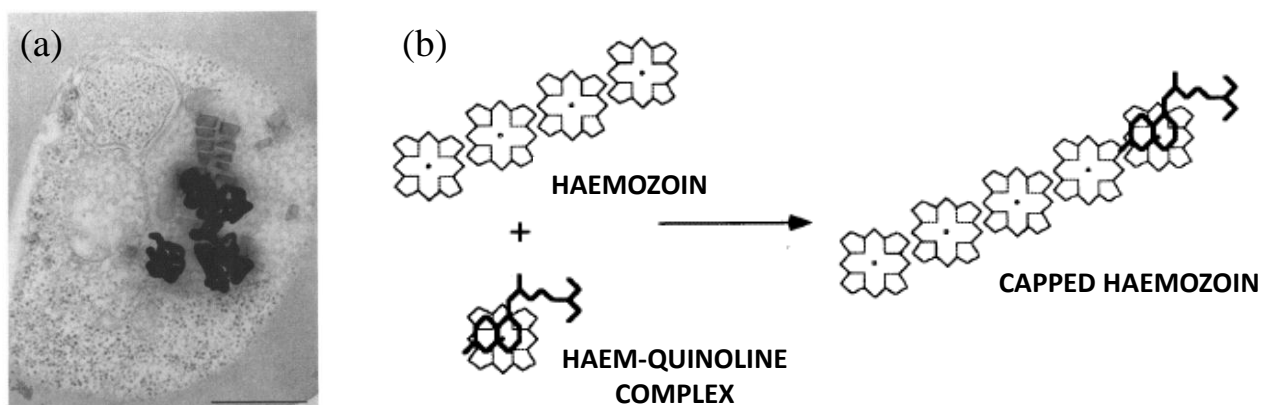
Figure 1.20 (a) An electron microscope autodiograph of [³H] CQ distribution in the digestive vacuole. There is direct overlap with the haemozoin crystals. (b) Proposed model for the inhibition of haemozoin formation. The incorporation of the haem-quinoline complex into growing haemozoin, thought to be a polymer at the time. The capping was thought to prevent further elongation. Reproduced with permission from reference 114.

A few years later, Buller *et al.* identified the fastest growing β-haematin crystal face (001), and subsequently showed theoretically that quinoline antimalarial drugs are able to bind into crevices created at this face and are stabilised by exposed functional groups of Fe(III)PPIX (Figure 1.21 (a)).[39] These functional groups include methyl and vinyl groups, propionic acid and aromatic surfaces (running parallel to the *a*-axis). When CQ (monoprotonated) is bound to the (001) β-haematin crystal face, energetically-favourable hydrogen bonding interactions include $Cl_{drug}\cdots H_3C_{porphyrin}$ (3.0 Å), $N_{drug}\cdots HC=C_{porphyrin}$ (2.4 Å), $NH_{drug}\cdots O_2C_{porphyrin}$ (2.7 Å) and $NH_{drug}\cdots C=C_{porphyrin}$ (2.7 Å) (Figure 1.21 (b)). Once adsorbed, the authors proposed that CQ is more tightly bound within the crevices than QN, owing to the exocyclic amine chain of CQ being longer and more flexible than that of QN. The authors were able to compare the antimalarial activity of the various quinolines to their theoretical surface binding sites to the (001) face.

More recently, similar structural aspects were observed when Dodd *et al*. demonstrated that CQ is able to form a complex with the Gallium(III) protoporphyrin IX μ-propionato dimer ([Ga(III)PPIX]₂) in both methanol solution and solid state.[137] The structure of the CQ-Ga(III)PPIX reciprocal dimer complex provides a structural model for the haem-drug interaction of CQ and a μ-propionato dimer of Fe(III)PPIX as observed in haemozoin (outlined in grey dashed line (b)). The crystal structure of [Ga(III)PPIX]₂ (Figure 1.21 (c)), determined by crystallography, reveals a six-coordinate metal centre, with CQ forming hydrogen bonds to both the axial methoxide ligand and the propionate side chain through the quinolinyl nitrogen atom and the tertiary amino group, respectively. When the Fe(III) centre of Fe(III)PPIX in aqueous solution is in a low spin state with a water molecule as the sixth ligand, the authors further proposed a similar complex structure may form between CQ and Fe(III)PPIX, as that of [Ga(III)PPIX]₂.[137] However, the existence of a CQ-(μ-propionato-Fe(III)PPIX) complex as the dominant species in specifically an aqueous solution is much less certain.[138,139] The structure does, however, provide experimental evidence of the interaction that are likely within the binding pocket on the crystal surface. There, the unligated face of the Fe(III)PPIX μ-propionato dimer is exposed to the inhibitor, and CQ may interact similarly with the latter as observed for the Ga μ-propionato dimer.
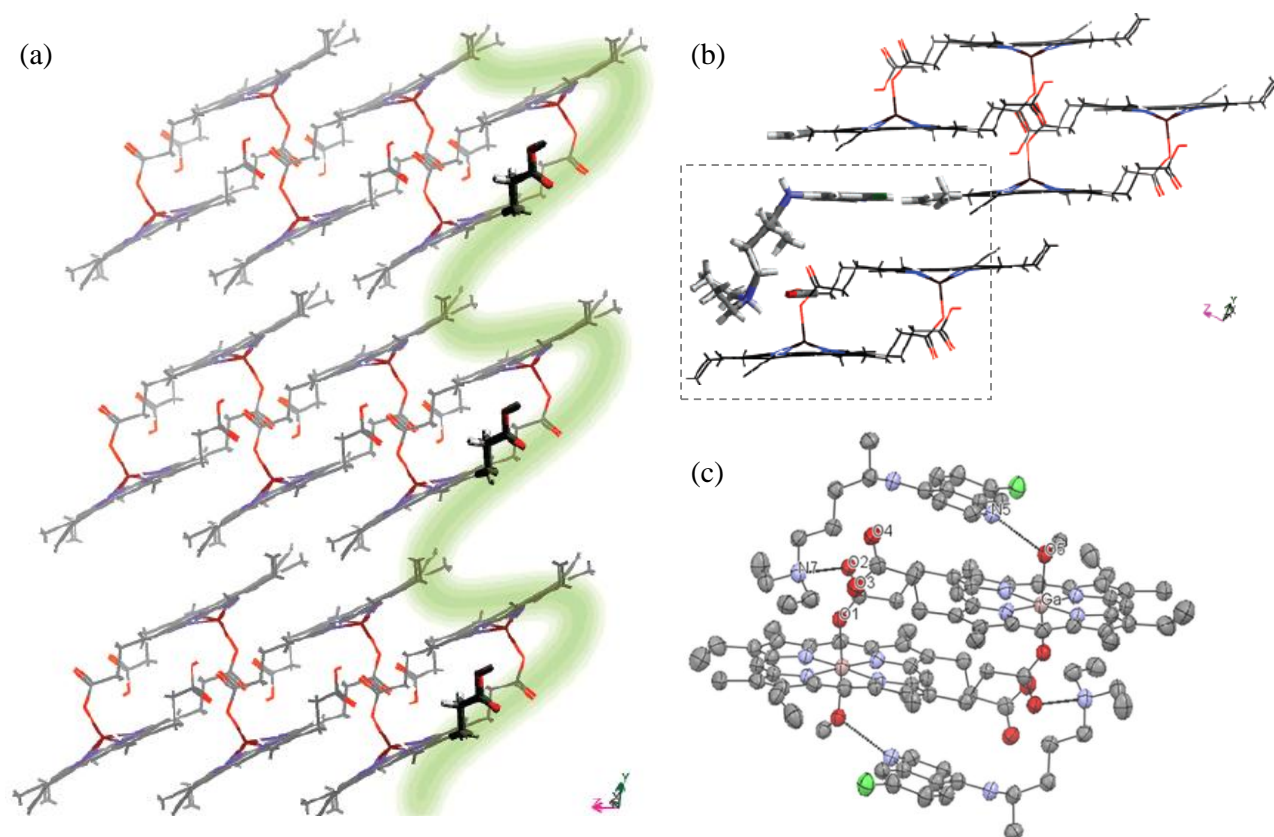
Figure 1.21 β-haematin crystal capping. (**a**) A model of β-haematin viewed along the *a*-axis, showing exposed propionic acid, aromatic surfaces, vinyl and methyl groups at the (001) face. The crevices outlined in green, are binding sites proposed for quinoline antimalarial drugs. Quinolines are able to dock into the grooves. (b) CQ bound to the (001) β-haematin crystal face along the *a*-axis. Reproduced from reference 39. (c) The crystal structure of [Ga(PPIX)(OMe)(CQ)]$_2$. A propionate bridged dimer is generated by inversion symmetry of the two CQ enantiomers which are hydrogen bonded to the propionate carboxylate. Reproduced with permission from reference 137.

1.5.4.3 *The Inhibition of β-Haematin Formation*

1.5.4.3.1 Pyridine Hemichrome Inhibition of β-Haematin (Phiβ) Assay

A large amount of literature has shown the ability of quinoline antimalarial drugs and related compounds to inhibit β-haematin formation.[59,51,115,114] In light of these observations and evidence suggesting that the inhibition of haemozoin formation is the most probable target of antimalarial drugs, the discovery of new antimalarial compounds has been of great interest. One of the main approaches in discovering such compounds is the development of assays to screen compounds for β-haematin inhibitory activity.

Since the earliest measurement of the inhibition of β-haematin formation in 1992 by Slater and Cerami,[115] numerous approaches to detecting and measuring β-haematin inhibition have been developed,[140,141,142,143,144] most of which had several disadvantages for high-throughput screening. Owing to this, Ncokazi and Egan developed a reliable, fast and cheap colorimetric pyridine (ferri)hemichrome inhibition of β-haematin (Phiβ) assay, which is based on the solubilisation of free Fe(III)PPIX by 5% (v/v) aqueous pyridine pH 7.5.[145] The interaction of pyridine with free haem results in the formation of a characteristic orange-pink monomeric low-

spin *bis*-pyridyl complex in solution (Figure 1.22 (a)), which can be monitored at an absorbance maximum at 405 nm, which allows quantitation of the percentage free Fe(III)PPIX in a Fe(III)PPIX-β-haematin mixture.

With increasing pyridine concentration, the authors showed that the broad and relatively weak Soret band of the aqueous Fe(III)PPIX π-π dimer species at 389 nm displays a red shift to a longer wavelength of 404 nm (Figure 1.22 (b)). The sharper and more intense peak is an indication of monomerisation of the iron porphyrin, which together with the other spectroscopic changes at longer wavelengths, are consistent with the coordination of two pyridine ligands to the iron centre of the porphyrin (pyr-Fe-pyr). The pyridine molecules displace the axial water molecule of 5-coordinate haematin and form a low-spin complex.[119] It was importantly noted that conditions under which pyridine only reacts with Fe(III)PPIX, rather than β-haematin, should be investigated. The authors found that pure pyridine and strongly basic aqueous pyridine solutions decompose β-haematin to form a Fe(III)PPIX-pyridine complex, while neutral or mildly basic aqueous solutions containing 5-10% (v/v) pyridine (pH 7.5) do not react with β-haematin.
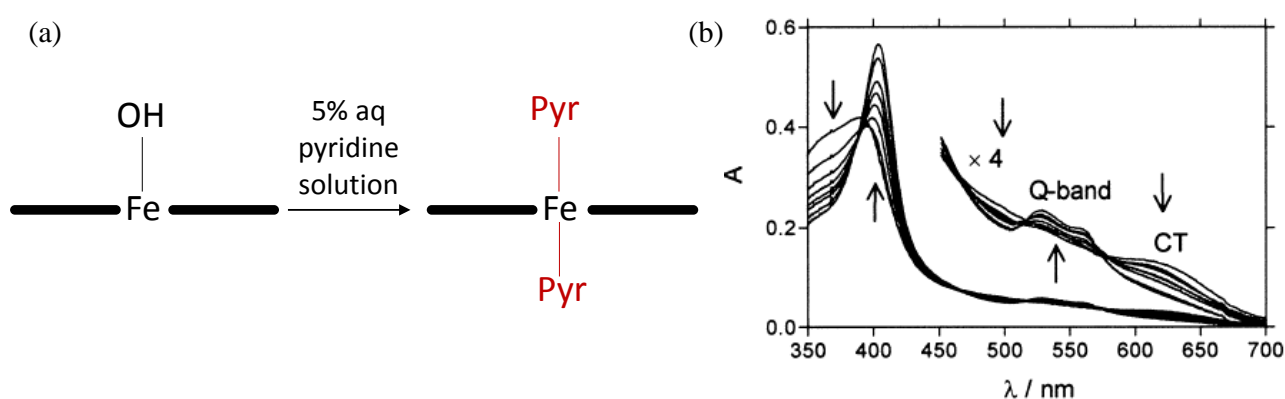
Figure 1.22 Interaction of pyridine with Fe(III)PPIX. (a) A schematic of the low-spin *bis*-pyridyl complex of Fe(III)PPIX in 5% (v/v) aqueous pyridine solution. (b) The effect of increasing pyridine on the spectrum of Fe(III)PPIX in aqueous solution indicates a red shift in the Soret band. The arrows indicate the direction of change as the pyridine concentration is increased. The spectral changes are consistent with coordination of two pyridine ligands to the iron centre of Fe(III)PPIX. Reproduced with permission from reference 145.

The Phiβ assay was subsequently used in the study to quantify the inhibition of β-haematin formation by quinoline antimalarials and related compounds. The Phiβ assay is now routinely used to identify β-haematin inhibitors (Figure 1.23), where a more intense orange-pink colour is a result of greater quantities of unreacted Fe(III)PPIX, indicating greater β-haematin inhibitory activity by test compounds.[145] The absorbance data obtained from the Phiβ assay can further be manipulated in order to reflect the percentage β-haematin formed for a given inhibitor concentration.
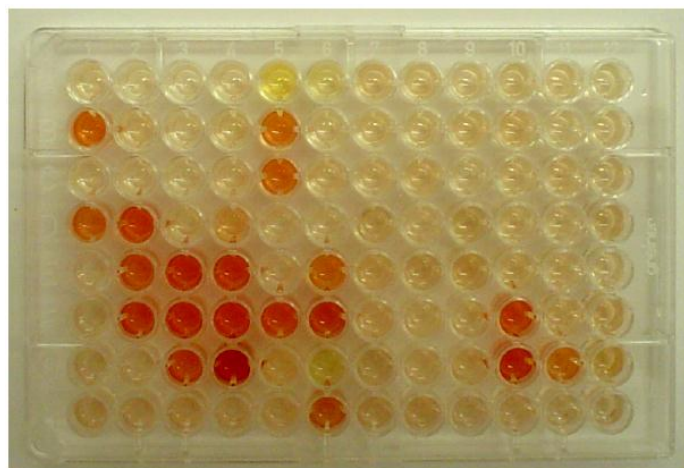
Figure 1.23 An example of a 96-well plate in which 47 compounds were screened for their ability to inhibit β-haematin formation using the Phiβ assay. 5% (v/v) aqueous pyridine (pH 7.5) was used to quench the reaction in order for the β-haematin inhibitors to be identified by direct visual inspection (orange-pink colour). Reproduced with permission from reference 145.

1.5.4.3.2   The Effect of Quinoline Antimalarial Drugs on the Kinetics of β-Haematin Formation

Despite the knowledge that antimalarial drugs are able to inhibit β-haematin formation, little is known about the effect of quinoline antimalarial drugs and related compounds on the kinetics of the growth process. Previous studies reported only the effects of quinoline antimalarials on Fe(III)PPIX crystal growth at fixed time points.[141,146,147,148] In an attempt to study the kinetics of Fe(III)PPIX crystal growth, Chong and Sullivan developed a spectrophotometric high-throughput β-haematin crystal growth determination assay which is based on the differential solubility of free Fe(III)PPIX versus crystalline Fe(III)PPIX.[149] They found that the inhibition of Fe(III)PPIX crystal growth is reversible in the presence of both CQ and QD, and that the activity of the inhibiting compounds decreases at longer time periods, suggesting that the IC_{50} value of a compound, which is the concentration at which β-haematin is inhibited by 50%, is dependent on incubation time.

In 2005, Egan and Ncokazi[150] confirmed the observations made by Chong and Sullivan[149] by investigating the inhibition of β-haematin formation in the presence of quinoline antimalarial drugs CQ, AQ, QD and QN. β-Haematin formation was brought about using 4.5 M acetate, pH 4.5 at 60 °C and the unreacted haematin was monitored using the Phiβ assay. A decrease in absorbance of the Fe(III)PPIX-pyridine complex at 405 nm was observed in the presence of both CQ and QN as a function of time (Figure 1.24 (a)). Infrared spectroscopy and XRD were used to confirm that the decrease in absorbance indeed corresponds to β-haematin formation. The authors thus found that β-haematin was able to form in the presence of the antimalarial drugs, albeit at longer incubation times. This suggests that the compounds act by decreasing the rate of β-haematin formation, rather than inhibiting the process overall.[150] A sigmoidal dependence of β-haematin formation on drug concentration was observed (Figure 1.24 (b)) and is based on β-haematin formation taking place in three stages; namely induction/nucleation, growth/propagation and termination. The authors further indicated the importance of incubation time on the inhibitory activity of the quinoline antimalarial drugs.
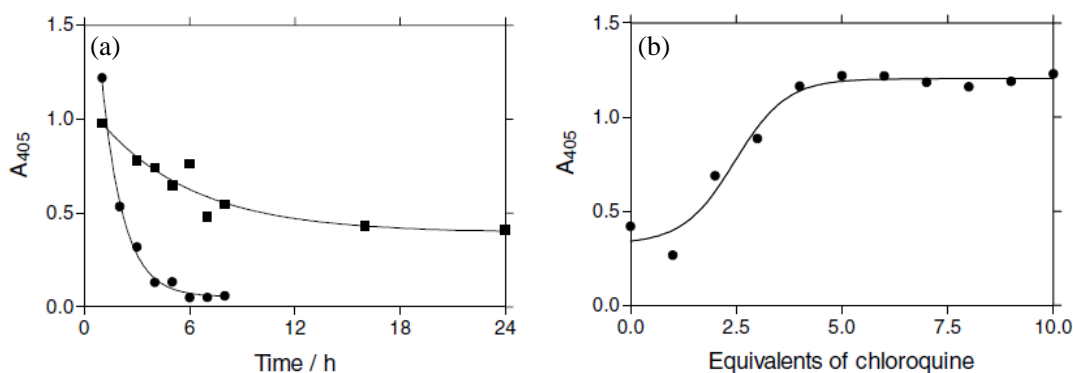
Figure 1.24 Inhibition of β-haematin formation by CQ and QN. (a) The absorbance values observed at 405 nm in the presence of CQ (●) and QN (■) at various incubation times. The experimental data predicts first-order rate constants. The decrease in absorbance is ascribed to β-haematin formation. (b) The dose-response curve for the inhibition of β-haematin formation by CQ. Reproduced with permission from reference 150.

In both independent kinetics studies discussed above, β-haematin formation was brought about in the presence of acidic acetate buffers, either at high incubation temperatures or long incubation periods. Previous kinetics studies performed in model-lipid mixtures, however, have returned biologically relevant half-life values for the formation of β-haematin.[73,74,151] Recently, Gildenhuys *et al.* carried out a detailed kinetics investigation on the formation of β-haematin in the presence of CQ, and QD[40], and subsequently, AQ and QN.[152] In contrast to previous kinetics studies, they made use of biomimetic lipid emulsion conditions (pH 4.8, 37 °C) to mediate β-haematin formation. The experimental procedure was performed in 15 mL Falcon centrifuge tubes, which was overall time-consuming. However, in studying the effects of quinoline antimalarial drugs on the kinetics of β-haematin formation at a lipid-water interface, the authors found that there is a decrease in the rate at which β-haematin is formed at low drug concentrations, while a decrease in the final yield of β-haematin is observed at high drug concentrations (Figure 1.25).
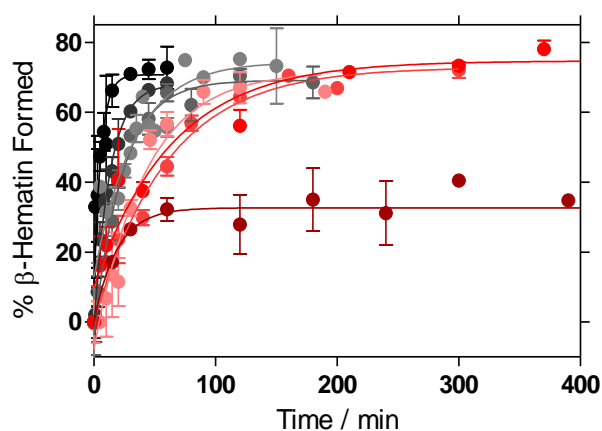
Figure 1.25 The effect of chloroquine on the kinetics of β-haematin formation. Differences in the rate of β-haematin formation are observed for increasing drug concentrations at low concentrations (black to red) with the same yield of β-haematin forming. At high drug concentrations (maroon), a decrease in the final yield of β-haematin is observed. Reproduced with permission by reference 40.

In order to verify that the observed decrease in absorbance measured as a function of time is indeed caused by the formation of β-haematin, and not the formation of an unknown aggregate of Fe(III)PPIX or a Fe(III)PPIX-drug complex, they used infrared spectroscopy and PXRD to confirm β-haematin formation in the presence of CQ and QD.[152]

In order to further account for the observed effects of the quinoline antimalarial drugs on the rate and yield of β-haematin formation, Gildenhuys *et al.* derived their own theoretical model to explain these observations (Equation 1.2).[40]

$$\%\beta_{(s)} = \frac{100Yz}{(z+k_2[I]^2+k_2K_{ads}[I]^3)}\left\{1 - e^{-\left(\frac{z+k_2[I]^2+k_2K_{ads}[I]^3}{1+K_{ads}[I]}\right)t}\right\} \qquad \text{(Eq. 1.2)}$$

In the above equation, the percentage β-haematin formation depends on various parameters. Y represents the fractional yield of β-haematin formation expected in the MPG lipid-mediated system at any given concentration, since MPG is unable to convert H_{aq} into β-haematin with an 100% yield.[74] z is the rate of β-haematin formation in the absence of an inhibitor, while k_2 is the rate of a proposed irreversible precipitation of an inhibitor-haematin complex. [I] is the inhibitor concentration used in each individual experiment and K_{ads} is the adsorption equilibrium constant that represents the strength of adsorption of each inhibitor to the fastest growing face of β-haematin crystals. The theoretical kinetics model is dependent on time and the amount of free sites available for continued β-haematin crystal growth. For the full derivation of the kinetics model, the reader is kindly referred to reference 40 and 152.

The authors hypothesized that β-haematin crystal growth is the rate-determining process, and therefore the rate of β-haematin formation would be expected to depend on the rates of crystal nucleation and growth, respectively. In light of this, they developed this crystal growth kinetic model. Based on the hypothesis that antimalarial drugs are able to adsorb onto the fastest growing face of β-haematin crystals in order to impede further growth, an idea originally put forward by Leisorowitz and co-workers[39,153] as a proposed mechanism for the inhibition of β-haematin formation, a mechanistic explanation of the effect of antimalarial drugs on the rate of β-haematin formation was considered (Scheme 1). The processes shown in the scheme account for the parameters included in the theoretical kinetics model (Equation 1.2).

In Scheme 1, the growth of β-haematin crystals, $\beta H_{(s)}$, proceeds as free haematin, $H_{(aq)}$, is incorporated at free surface binding sites, S, with z, the rate constant of β-haematin formation (i). In the presence of an inhibitor, $I_{(aq)}$, this process is slowed down, since the inhibitor now competes with free haematin for the free sites. This is considered to be a reversible adsorption process since the drug adsorbs and desorbs to the crystals with K_{ads} as the equilibrium adsorption constant, which indicates the strength of adsorption of each inhibitor (ii). When present in high concentration, an inhibitor may show preference to bind to free haematin to form a precipitated inhibitor-haematin complex, $IH_{(s)}$, therefore preventing the inclusion of free haematin into β-haematin. This

latter process results in a decrease in the yield of β-haematin formation, with k_2 being the rate constant of the precipitation reaction. It is proposed that z_{obs} is expected to dominate k_2 at low drug concentrations, however, at relatively higher concentrations, k_2 is expected to have an influence and cause the observed decrease in the overall yield of β-haematin.
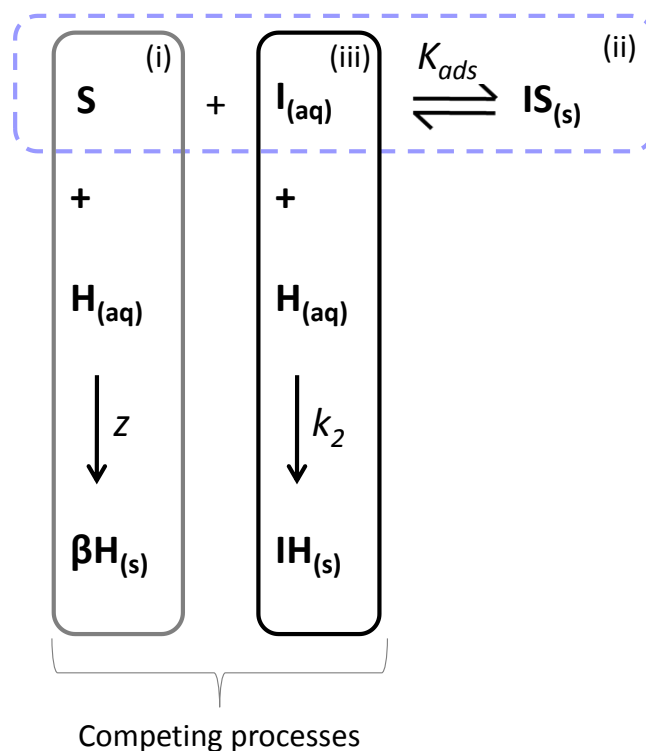
Scheme 1 The proposed kinetic model to explain the effect of quinoline antimalarial drugs on the rate and yield of β-haematin formation. Free Fe(III)PPIX, $H_{(aq)}$, competes for the free surface binding sites, S, in the presence of an inhibitor, I_{aq}. The formation of β-haematin, $βH_{(s)}$, (i) thus slows down by the adsorption of an inhibitor onto the β-haematin crystal surface, $IS_{(s)}$, in a reversible adsorption process with an adsorption equilibrium constant, K_{ads} (ii). In the presence of high inhibitor concentrations, the inhibitor may show preference to bind to free Fe(III)PPIX, forming a precipitated inhibitor-Fe(III)PPIX complex, $IH_{(s)}$ with a rate constant k_2. Adapted from reference 40 and 152.

Using the Avrami equation (Equation 1.1), which has been used to model crystallisation processes as previously described in section 1.4.3.1, the observed exponential kinetics were modelled. In previous studies in which β-haematin formation was brought about in an acetate buffer medium, the kinetics of formation appeared to exhibit a sigmoidal time dependence, with the Avrami constant (n) equal to 4, indicating sporadic nucleation and crystal growth in three dimensions.[64] The yield of β-haematin in the lipid-mediated system as a function of time, however, was shown to display an exponential dependence. This too can be accounted for by the Avrami equation (Equation 1.1), however, with the Avrami constant equal to 1. In this case, the equation becomes mathematically indistinguishable from that of first order kinetics. As mentioned before, when the Avrami constant is equal to 1, β-haematin formation involves a fixed number of preformed nuclei and crystal growth in one dimension (i.e. linear), the former being provided by the lipid[154] and the latter being consistent

with the long needle-like morphology of β-haematin crystals observed in previous studies.[155,156] In the crystal growth kinetic model, adsorption of an inhibitor onto the growing face of β-haematin crystals is reminiscent of adsorption predicted by the Langmuir isotherm, where the extent of monolayer coverage of a solid surface by an adsorbent gas molecule is related to the partial pressure of the absorbent. In this case, however, the degree of adsorption, θ, is dependent on the concentration of the drug in solution, [I], and K_{ads} is the adsorption equilibrium constant (Equation 1.3).

$$\theta = \frac{K_{ads}[I]}{1+K_{ads}[I]}$$
(Eq. 1.3)

Using the kinetic model represented by equation 1.2, the kinetics of β-haematin formation in the absence and presence of an inhibitor may be predicted, and are found to adhere to exponential behaviour (Figure 1.26). It is observed that the final yield of β-haematin remains almost constant at low drug concentration, however, with a decrease in the rate of β-haematin formation. On the other hand, the yield decreases at a higher drug dose.
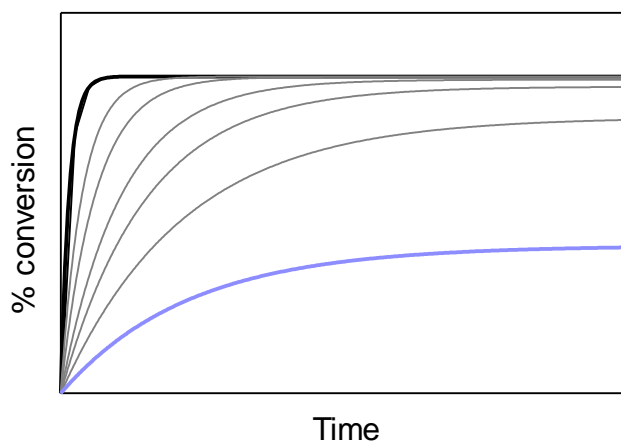
Figure 1.26 The kinetics profile of β-haematin formation predicted by the kinetic model (Eq. 1.2) in the absence (black line) and the presence of increasing inhibitor concentration (grey lines). The trace obtained in the presence of the highest inhibitor concentration is shown in purple. Adapted from reference 40 and 152.

Furthermore, according to the adsorption model, at drug concentrations where Langmuir adsorption is likely to dominate (Equation 1.4), it is predicted that a plot of the inverse of z_{obs}, the observed rate constants, as a function of increasing drug concentration will be linear at low concentrations (Figure 1.27). Linear regression in this region allows the rate constant of β-haematin formation in the absence of an inhibitor, z, as well as K_{ads}, to be determined from the y-intercept (y_0) and slope values, respectively (Equation 1.5 and 1.6)

34

$$\frac{1}{z_{obs}} = \frac{1 + K_{ads}[I]}{z} = \frac{K_{ads}}{z}[I] + \frac{1}{z} \qquad \text{(Eq. 1.4)}$$
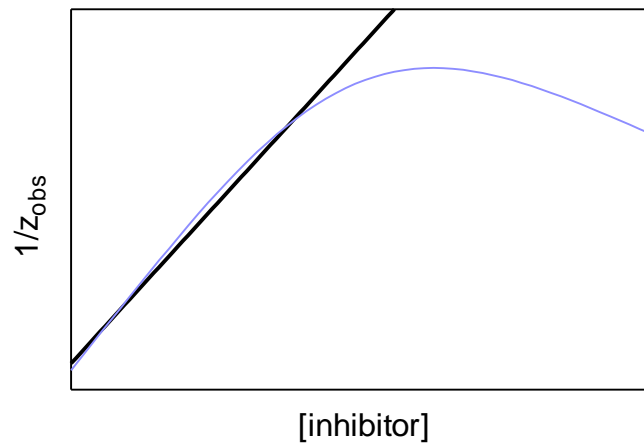
Figure1.27 The plot of the inverse of the observed rate constants, z_{obs}, as a function of increasing inhibitor concentration (purple line, fitted to Eq. 1.4), is predicted to be linear at low concentrations (black line). Linear regression in this region allows both z and K_{ads} to be determined (Eq. 1.5 and 1.6). Adapted from reference 40 and 152.

$$y_0 = \frac{1}{z} \qquad \text{(Eq. 1.5)}$$

$$slope = \frac{K_{ads}}{z} \qquad \text{(Eq. 1.6)}$$

The kinetic model further proposes that it is possible to predict the dose-response behaviour of a drug from the respective kinetics profile by investigating expected yields of β-haematin at individual time points as a function of increasing drug concentration (Figure 1.28 (a) and (b)). The model gives rise to sigmoidal dose-response curves at longer incubation times, while at shorter incubation times, the dose-response curves adhere to a simple hyperbolic function. Finally, the kinetic model is also able to predict that IC_{50} values, the concentration at which β-haematin formation is inhibited by at least 50%, extracted from the generated dose-response curves, are dependent on incubation time (Figure 1.28 (c)). The dependence of IC_{50} on time is most pronounced at short incubation times. Overall the data conform to a hyperbolic function; at longer incubation times, the individual dose-response curves are predicted to converge with relatively no change expected in the IC_{50} value. At longer incubation times it is observed that a slice through the kinetics profile at any given incubation time (dash lines together in Figure 1.28 (a)) will generate similar dose-response curves (grey line in Figure 1.28 (b)), which will in turn result in similar IC_{50} values. This observation accounts for the hyperbolic shape in Figure 1.28 (c). The hyperbolic increase in IC_{50} values as a function of time observed here is in agreement to what Egan *et al.* observed in 2005.[150] The authors also reported that the IC_{50} values become larger as the incubation time is increased, and that the IC_{50} increases steeply with shorter incubation times and more gradually at longer incubation times.
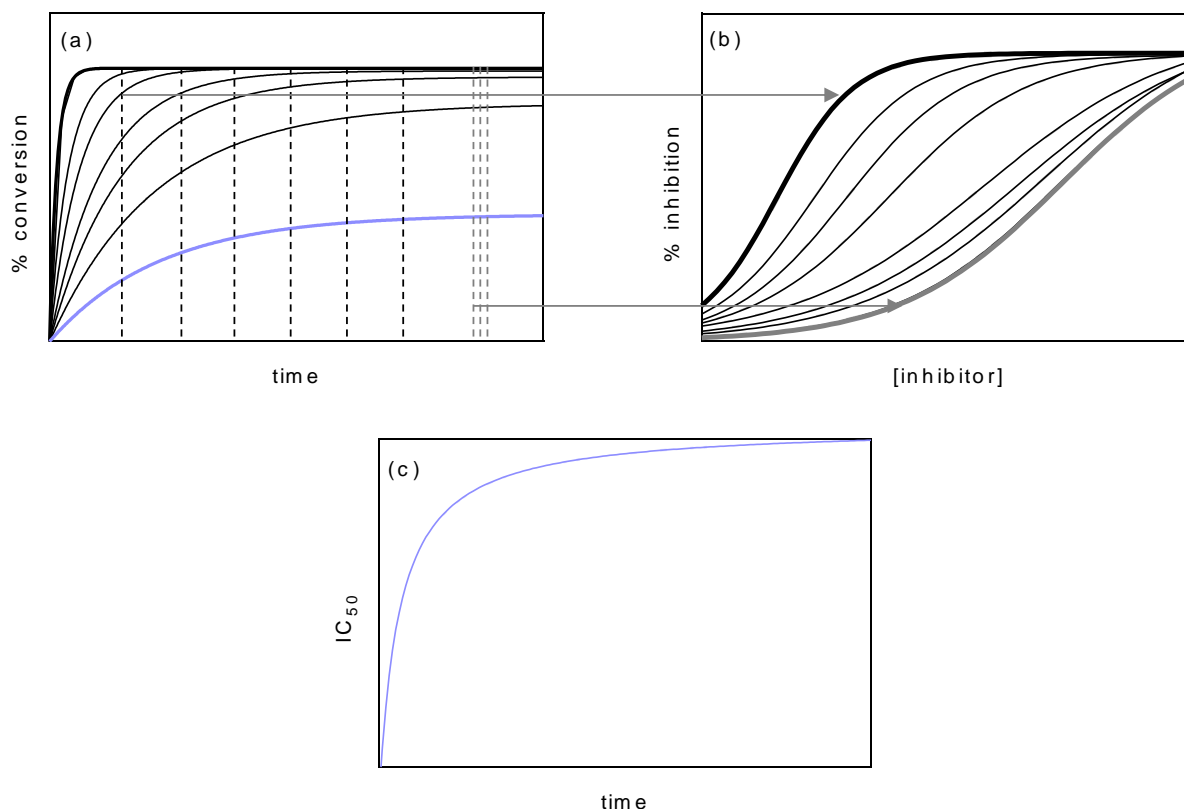
Figure 1.28 The kinetics of β-haematin formation predicted by the kinetic model (Eq. 1.2). (a) Taking slices through the kinetics profile at several time points (broken lines), the dose-response curve of an inhibitor can be predicted. (b) The dose-response curves as the best fits of the numerical output generated at different times from (a). At longer incubation time, dose-response curves are sigmoidal (grey line), compared to hyperbolic at short incubation times (black line). (c) The dependence of IC_{50} values on incubation times. Based on the theoretical outputs in (a), the corresponding IC_{50} values from each curve are predicted. The hyperbolic function shows that the effect on the IC_{50} values is more pronounced at shorter incubation times. Reproduced from reference 40 and 152.

Following data analysis using the derived kinetics model, a linear correlation was observed between the IC_{50} values obtained in the lipid system and the biological activities reported against the chloroquine-sensitive (3D7 and HB3) and –resistant (K1 and PH3) parasite strains (Figure 1.29 (a)). The observed linear correlation is a strong indicator that the lipid emulsions provide a valid system in which to investigate drug activity.[40]

The K_{ads} values determined for each antimalarial drug were subsequently compared against the biological activity determined against the chloroquine-sensitive 3D7 parasite strain, in order to assess whether the hypotheses underpinning the theoretical model (namely adsorption) could be related to the biological mechanism of quinoline antimalarials in any way (Figure 1.29 (b)).[152] The linear correlation between the experimental and biological data further suggest that the strength by which a compound is able to adsorb to the surface of β-haematin crystals may indeed be related to its β-haematin inhibitory activity.
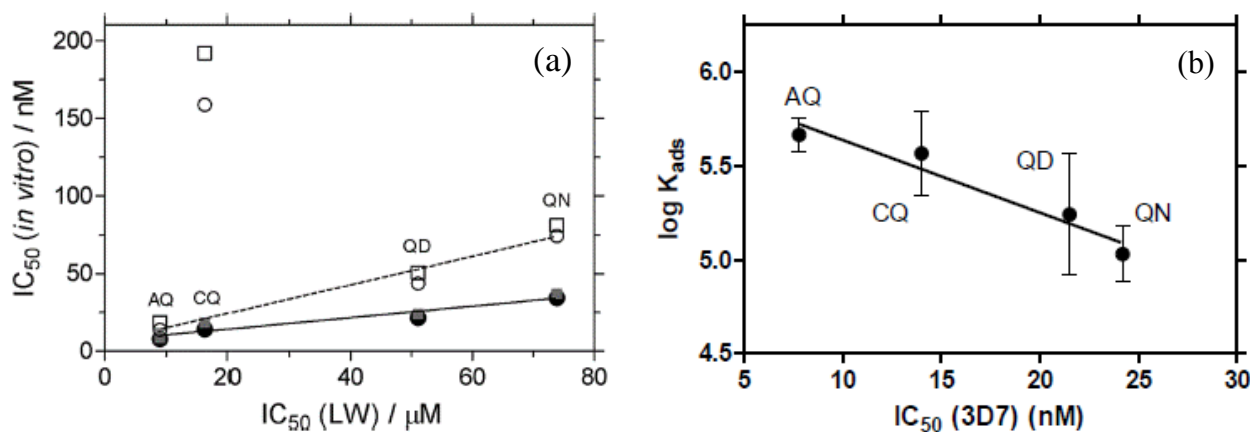
Figure 1.29 Inhibition of β-haematin formation in the presence of antimalarial drugs at the lipid-water interface. (a) Linear correlations of the IC_{50} values obtained independently after 30 minute with biological activity against CQS strains (3D7 (●) and HB3 (■), solid line, $r^2 = 0.92$) and CQR strains (PH3 (○) and K1 (□), dashed line, $r^2 = 0.97$). The data points for CQ against the CQR strains have been excluded from the linear regression analysis. Reproduced with permission from reference 40. (b) Linear correlation ($r^2 = 0.69$) between the observed K_{ads} values and the IC_{50} for the biological activity against CQS 3D7 strain for AQ, CQ, QD and QN. Reproduced with permission from reference 152.

The kinetics data provided by Gildenhuys *et al.*[40] strongly support a mechanism of quinoline antimalarial drug action by adsorption to the growing face of haemozoin in the lipid-mediated system. It is, however, essential that the theoretical model be tested by further investigating the effects of other β-haematin inhibitory compounds, including non-quinolines, on the kinetics of β-haematin formation. The current experimental system involving 15 mL Falcon tubes would not, however, be efficient to investigate larger numbers of compounds. In addition, a significant shortfall of the model is that independent measurements of drug adsorption to β-haematin crystals are also required to further support the kinetics data. To date no such data has been reported to support the hypothetical adsorption behaviour.

37

1.6 Aims and Objectives

1.6.1   Aims

Following a careful literature review of malaria, the *Plasmodium falciparum* parasite, haemozoin and the current understanding on the possible mechanisms of antimalarial drug action on haemozoin formation, the aim of the current study is to:

Investigate the effect of diverse β-haematin inhibitors on the kinetics of β-haematin formation, using the lipid-mediated system.

This aim is underpinned by the hypothesis that *the β-haematin inhibitory activity of a compound is related to its strength of adsorption to free surface binding sites on the fastest growing face of β-haematin crystals.*

1.6.2   Objectives

In order to achieve the above-mentioned aim, the specific objectives set out in this research project were to:

1. Develop a new, improved-throughput lipid-mediated assay in which to investigate the inhibition of β-haematin formation.
2. Validate the newly-optimized assay as a means of assaying drug activity by introducing clinically-relevant antimalarial drugs into the system.
3. Introduce a larger set of quinoline-based β-haematin inhibitors into the system and investigate their effects on the kinetics of β-haematin formation.
4. Introduce a set of non-quinoline inhibitors into the system and investigate their effects on the kinetics of β-haematin formation.
5. Investigate the strength of direct adsorption of β-haematin inhibitors independently.

1.6.3   Proposed Compounds to be Investigated

Owing to the increase in resistance to clinically-relevant antimalarial drugs,[1,157] there is a crucial need to develop novel antimalarial haemozoin inhibitors. Understanding haemozoin formation and the mechanism of antimalarial drug action is central to this. In particular, investigating the effect of inhibitors other than quinoline antimalarial drugs on the kinetics of β-haematin formation is important. The two groups of compounds investigated in this study include short-chain CQ analogues (Figure 1.30 (a)),[158] as well as a series of benzamide non-quinolines (Figure 1.30 (b)), with all compounds having β-haematin inhibitory activity.

(a)

Q-Cl **Q-I** **Q-CF₃**

Q-OMe **Q-SCF₃**

(b)

nQ-KW16 **nQ-KW17** **nQ-KW23**

nQ-KW31 **nQ-KW32** **nQ-KW33**
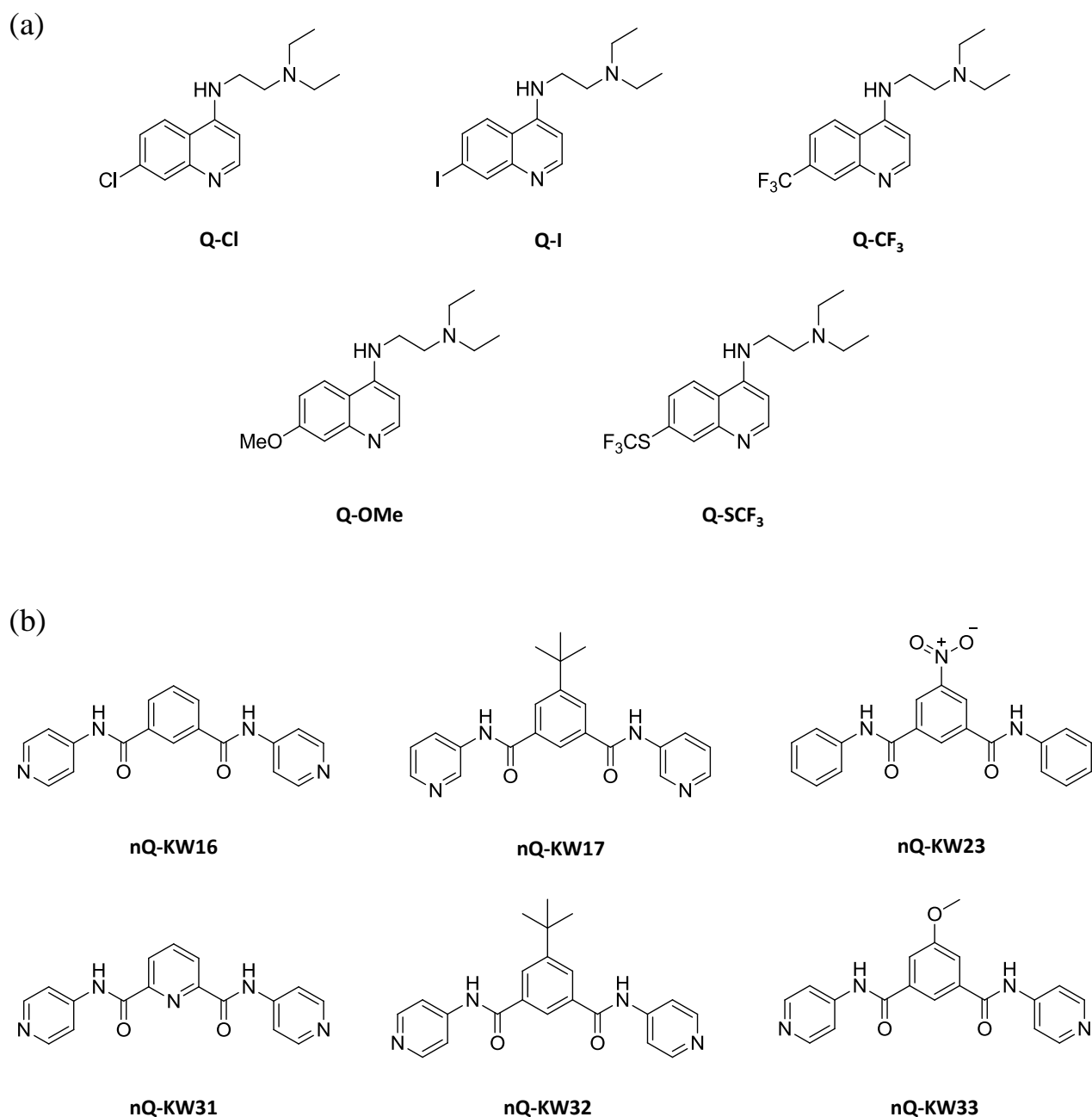
Figure 1.30 (a) A series of N1, N1-diethyl-N2-(4-quinolinyl)-1, 2-ethanediamine compounds with different substituents at the 7-position on the quinoline ring includes the 7-chloro (Q-Cl), -iodo (Q-I), -trifluoromethyl (Q-CF₃), -methoxy (Q-MeO) and –trifluoromethylthio (Q-SCF₃) 4-aminoquinolines.[158] (b) A series of benzamide non-quinoline inhibitors with different substituents on the central aromatic ring, nQ-KW16, -17, -23, -31, -32, and -33.

Chapter 2. Materials, Instrumentation and General Methods

2.1 Materials

All of the materials that were used in this research project were of the highest purity and analytical grade, and were purchased from known commercial suppliers. All of the materials were used as obtained, without further purification, and are listed in Table 2.1.

Table 2.1 Materials used throughout the study and their suppliers

MATERIALS	SUPPLIERS
Solids	
Citric acid monohydrate	Sigma-Aldrich
DL-α-Palmitin	Sigma-Aldrich
Haemin (bovine)	Sigma-Aldrich
Haematin (porcine)	Sigma-Aldrich
N-2-[hydroxyethyl]piperizine-N'-[2-ethanesulfonic acid] (HEPES)	Sigma-Aldrich
Sodium hydroxide pellets	Sigma-Aldrich
Sodium acetate trihydrate	Sigma-Aldrich
Sodium citrate tribasic dihydrate	Sigma-Aldrich
Phosphorus pentoxide	Sigma-Aldrich
Liquids and Solvents	
Acetone AR	Kimix Chemicals
Acetonitrile	Sigma-Aldrich
Ethylacetate	Sigma-Aldrich
Dimethylsulfoxide	Sigma-Aldrich
Methanol AR	Kimix Chemicals
Nitric acid AR	Kimix Chemicals
1-Pentanol	Sigma-Aldrich
Pyridine	Sigma-Aldrich
Antimalarial drugs	
Amodiaquine dihydrochloride dihydrate	Sigma-Aldrich
Chloroquine diphosphate	Sigma-Aldrich
Mefloquine hydrochloride	Sigma-Aldrich
Atovaquone	Sigma-Aldrich
Quinidine sulphate dihydrate	Sigma-Aldrich
Quinine hemisulphate hydrate	Sigma-Aldrich
Quinoline and non-quinoline inhibitors	
Quinolines: Short-chain CQ analogues[158]	Re-synthesized by Mr J. B. Hay (US)
Non-quinolines: Benzamide series	Synthesized by Dr K. J. Wicht (UCT)

2.2 Instrumentation

2.2.1   Analytical Balance

An A&D Company HR-200 standard balance scale was used to weigh off materials weighing more than 10 mg and a Sartorius GMBH Göttingen sensitive balance scale was used to weigh off smaller quantities.

2.2.2   Centrifuge

A Hermle Labortechnik centrifuge (Z 206) with a maximum speed of 6000 rpm was used to centrifuge large-volume samples in 15 mL Greiner Falcon centrifuge tubes. A Z 233 M-2 Hermle Labortechnik GbmH centrifuge, with a maximum speed of 15000 rmp, was used to centrifuge smaller volumes in 2 mL eppendorf tubes.

2.2.3   High Vacuum Pump

An Edwards Max high vacuum pump was used to dry materials overnight.

2.2.4   Infrared Spectroscopy

A Nexus[TM] FT-IR spectrometer from Thermo Nicolet Instruments fitted with a Golden Gate attenuated total reflection (ATR) accessory was used to record ATR-IR spectra.

2.2.5   Magnetic Stirrer Hot Plate

Heidolph MR-2002 and JKI JK-MSH-PRO standard magnetic stirrer hot plates were used to stir and heat solutions.

2.2.6   Micro Glass Syringes

Microliter glass syringes (10 µL, 25 µL and 50 µL), obtained from Hamilton, were used for the accurate delivery of small volumes of solutions. Glass is also preferred when handling solutions of haematin as it has been shown to adsorb to plastic.[82,87]

2.2.7   Oven

Kinetics experiments were performed in a fan-assisted oven set at the required temperature (37 ± 1 °C).

2.2.8   pH Meter

A Mettler Toledo FE20 pH meter was used to perform all of the pH measurements. The electrode was calibrated using pH buffer solutions (pH 4 and pH 7) obtained from Crison.

2.2.9   Powder X-Ray Diffraction

A PANalytical X-ray Powder Diffractometer was used to record PXRD data.

2.2.10   Scanning Electron Microscopy

A Leo 1430 VP scanning electron microscope was used to obtain structural images of samples. The images show the surface morphology of the material.

2.2.11   Single- and Multi-Channel Micro Pipettes

For volumes greater than 25.0 µL, micro-pipettes were routinely used. Axygen Scientific single-channel (AP-20, AP-200, AP-1000 and AP-5000) and Gilson multi-channel (P8X20 and P8X200) pipettes were used.

2.2.12   Ultrasonic Water Bath

An Elma TranssonicDigital ultrasonic water bath was used for direct adsorption studies. An operating temperature of 37 ± 1 °C was maintained for the duration of the measurements, for which the ultrasound power level 2 was used.

2.2.13   UV-Visible Spectroscopy

A Thermo Scientific Multisakan GO UV-Visible spectrophotometer was used to record single wavelength readings as well as UV-visible spectra.

2.2.14 Vortex

A VORTEX V1-plus device was used to mix solutions thoroughly.

2.2.15 Water Bath

In some cases, experiments were performed at the required temperature (37 ± 1 °C) using a MEMMERT water bath.

2.3 Computer Software

Different computer software and programmes were used in this study to obtain and analyse data (Table 2.2).

Table 2.2 Computer software and programmes used throughout the study

PROGRAMME	VERSION	USE
Chem Draw Ultra	12.0	Drawing molecular structures of compounds
GraphPad Prism	6.0	Analysis and graphing of data
Mendeley	1.14	Referencing and Bibliography
Microsoft Excel	2010	Handling and analysis of raw data
OMNIC	7.2	Recording ATR-IR spectra of samples
PANalytical Data Collector	4.1.0.25	Collect PXRD data
SkanIt Multiskan GO	3.2	Obtaining UV-vis absorbance readings
SmartSem	5.05	Scanning electron imaging of samples
X'Pert HighScore Plus	2.2.5	Processing of PXRD data

2.4 General Precautions in Sample Preparations and Handling Washing of Glassware and Plasticware

Glass-distilled water was used to prepare water solvent solutions throughout the experiments. All glass- and plasticware was washed with soap-water and rinsed with glass-distilled water and wash-acetone. Fe(III)PPIX-contaminated glass syringes, cuvettes, glass- and plasticware were allowed to soak in 0.1 M NaOH for at least one hour. After rinsing extensively with water, the cuvettes, glass- and plasticware were washed with 1 M HNO₃, followed by extensive rinsing with water. This procedure is important since Fe(III)PPIX adsorbs to glass- and plasticware.[82,87] All glassware were either air dried or dried in an oven at 37 °C after washing. All pyridine-contaminated 24- and 96-well plates and lids were discarded immediately after use. New sterile plates were used for every new experiment.

2.5 General Preparations

This section describes the solutions that were prepared often owing to their frequent use in the different experiments carried out. The materials that were used to prepare these solutions have previously been listed in Table 2.1.

2.5.1   50.0 mM Stock Solution of Citrate Buffer, pH 4.8

Citric acid monohydrate (5.255 g, 24.95 mmol) was dissolved in 450.0 mL distilled water. On adding a concentrated solution of sodium hydroxide dropwise, the pH was adjusted to 4.8. The solution was then made to volume in a 500 mL volumetric flask.

2.5.2   1:9 (v/v) Acetone: Methanol Solution

A solution was prepared in a 100.0 mL volumetric flask consisting of 10.0 mL of acetone, after which the solution was made to volume with methanol.

2.5.3   0.10 M NaOH Solution

Solid NaOH pellets (1.000 g, 250.0 mmol) were dissolved in distilled water to a volume of 250.0 mL in a volumetric flask.

2.5.4   2.0 M Stock Solution of HEPES Buffer, pH 7.5

HEPES acid (47.66 g, 200.0 mmol) was dissolved in 80.00 mL distilled water. On adding a concentrated solution of sodium hydroxide dropwise, the pH was adjusted to 7.5. The solution was then made to volume with distilled water in a 100 mL volumetric flask.

2.5.5   3.03 mM Lipid Solution

The neutral lipid, 1-monopalmitoyl-*rac*-glycerol (MPG), (10.0 mg, 30.26 μmol) was dissolved in 10.0 mL of the 1:9 acetone: methanol solution. A fresh solution was prepared for each set of experiments.

2.5.6   3.16 mM Haematin Solution

Haematin (10.0 mg, 15.79 μmol) was dissolved in 2.00 mL of 0.10 M NaOH in a 15 mL Greiner Falcon centrifuge tube. 3.00 mL of the 1:9 acetone: methanol solution was added after complete dissolution. A fresh solution was prepared for each set of experiments.

2.5.7   30:30:40 (v/v) Pyridine: Aqueous Buffer: Acetone Solution

10.0 mL of 2.0 M HEPES buffer and 30.0 mL of pyridine were added to 40.0 mL acetone and thoroughly mixed together. The solution was made up to 100.0 mL in a volumetric flask by adding distilled water.

2.5.8   0.20 M Stock Solution of HEPES Buffer, pH 7.5

HEPES acid (4.766 g, 20.0 mmol) was dissolved in 80.00 mL distilled water. On adding a concentrated solution of sodium hydroxide dropwise, the pH was adjusted to 7.5. The solution was made up with distilled water to 100.0 mL in a volumetric flask.

2.5.9   5: 45: 50 (v/v) Pyridine: Aqueous Buffer: Acetone Solution

10.0 mL of 0.20 M HEPES buffer and 5.00 mL of pyridine were added to 50.0 mL acetone and thoroughly mixed together. The solution was made up to 100.0 mL in a volumetric flask by adding distilled water.

Chapter 3. The Effect of Quinoline Inhibitors on the Formation of β-Haematin at the Lipid-Water Interface

3.1 Introduction

The inhibition of β-haematin (synthetic haemozoin) formation by clinically-relevant antimalarial drugs has been of interest for a long period of time and to date, different systems have been investigated to probe their mode of action in this regard.[59,149,150] In a recent study conducted in our laboratory, the inhibition of β-haematin formation has been investigated in a lipid-water interface system using the modified Phiβ assay,[40] in which the amount of free Fe(III)PPIX in a Fe(III)PPIX-β-haematin mixture is quantified (see section 1.5.4.3.1 for details of the Phiβ assay). The study made use of monopalmitoyl-*rac*-glycerol (MPG) as a model lipid, and was the first to systematically investigate the kinetic effect of four quinoline antimalarial drugs on the formation of β-haematin under biomimetic conditions. A kinetic model underpinned by the Langmuir adsorption isotherm was used to analyse the data, and the authors suggested that the β-haematin inhibitory activity of a compound is related to its strength of adsorption to free surface binding sites on the growing β-haematin crystals.[40] These initial findings warranted further investigation, the most important being to study the effect of additional inhibitors, in order to validate the hypothesis. Furthermore, the assay used in the original study was time-consuming, and by improving the turnaround time per compound, it was proposed that a larger set of compounds could be investigated. In the current study, clinically-relevant antimalarial drugs were initially used to optimize an improved-throughput assay compared to the previous work. Having successfully developed this more efficient assay, it has been possible to extend the data set to include a series of short-chain chloroquine analogues,[158] all of which contain the quinoline nucleus. Investigating a larger set of compounds is of great importance to validate the hypothesis and substantiate the proposed theoretical kinetic model. For each compound, activity and kinetics experiments have been carried out.

This chapter provides a detailed discussion of the experimental methods followed and results found, regarding both the activity- and kinetics studies for quinoline-based β-haematin inhibitors.

3.2 Optimization of the Phiβ Assay using known Antimalarial Drugs

The antimalarial drugs used in the first part of the study were the clinically-relevant quinoline compounds, namely amodiaquine (AQ), chloroquine (CQ), quinidine (QD), quinine (QN) and mefloquine (MQ). Their molecular structures have been presented previously in Figure 1.16.

3.2.1   Experimental Methods

3.2.1.1 Introducing Antimalarial Drugs into the Aqueous Citrate Buffer

Four quinoline antimalarial drugs, namely AQ, CQ, QD and QN, were all used in their salt forms, enabling them to be readily solubilised in the aqueous citrate buffer. A drug-containing stock solution of citric acid monohydrate (50.0 mM, pH 4.8) was prepared in a similar manner as described in section 2.5.1, however, the appropriate quantity of each antimalarial drug (Table 3.1) was also included. Further optimization was required to introduce MQ into the system, as it is monoprotic and not readily soluble in aqueous solution. MQ was therefore dissolved in the 1:9 acetone: methanol solution (section 2.5.2), which was used to dissolve and introduce the lipid into the system. This will be discussed in further detail in section 3.2.1.3

Table 3.1 Quantities of antimalarial drugs in salt form required to prepare a 100.0 mL[†] stock solution in 50.0 mM citrate buffer, pH 4.8.

Antimalarial Drug	Molecular Mass (g.mol⁻¹)	Stock Concentration (mM)	Mass (mg)
AQ	464.80	0.02	0.9
CQ	515.86	0.10	5.2
QD	391.45	0.20	7.9
QN	391.45	0.30	11.4
MQ[‡]	414.08	0.20	8.3

[†] The volume can be adjusted according to the amount needed for a specific experiment. [‡] MQ is insoluble in the aqueous citrate buffer. The mass represented here is the mass needed to prepare 100.0 mL of a 0.2 mM solution, however, it was dissolved and introduced in a 1:9 acetone: methanol solution. This is discussed in section 3.2.1.3.

3.2.1.2 Antimalarial Drug Activity Studies

Studies were carried out to determine the IC_{50} value, which is the concentration required to inhibit β-haematin formation by 50%, for each antimalarial drug in the lipid-water interface system. In these experiments, the incubation time was fixed while the concentrations of all antimalarial drugs were varied.

All of the experiments were performed in sterile 24-well polystyrene cell culture plates. Each well has an internal diameter of 1.6 cm and has a maximum volume capacity of 3.5 mL. The plates were incubated in an oven to ensure a consistent temperature of 37 °C throughout the experiment. The concentration range of each antimalarial drug was chosen in close proximity to what had previously been determined by Gildenhuys *et*

al.[40] and the relative β-haematin inhibitory activity of each drug in the Phiβ and NP40 assays was also considered. A series of at least ten to twelve different drug concentrations were prepared by diluting the drug-containing stock solution (section 3.2.1.1.) with drug-free citrate buffer (section 2.5.1) using calibrated micro-pipettes.

Two plates were used to accommodate twelve different concentrations simultaneously, each column representing a different concentration (columns 0-11, Figure 3.1). Each test well contained 1.0 mL of drug-containing citrate buffer in total. Moving from left to right over the plate the concentrations increased from zero drug to the highest drug stock concentration. Each concentration was measured in triplicate (rows A-C) and a single control was also included for each concentration (row D). The plates, which had been loaded with the buffer, were pre-incubated in the oven at 37 °C for 45 minutes, during which time the lipid and Fe(III)PPIX solutions were freshly prepared.
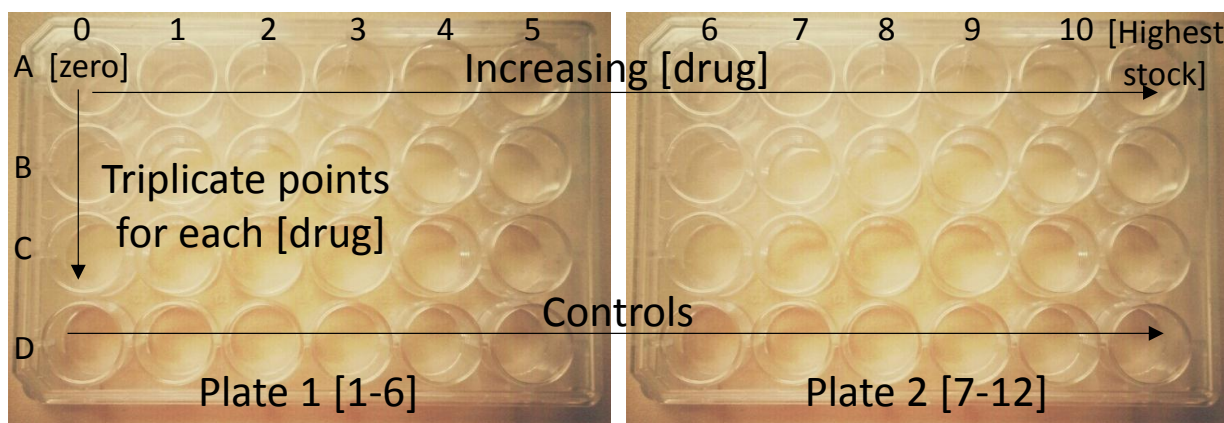
Figure 3.1 Representation of two 24-well plates used during drug activity experiments. Increasing drug concentrations are loaded from left to right over the plate and each drug concentration is measure in triplicate. A control is also included for each drug concentration.

Solutions containing 200.0 µL of lipid and 5.00 µL of Fe(III)PPIX stock solutions (sections 2.5.5 and 2.5.6) were premixed in the wells of a 96-well plate, using multi-channel micro pipettes. Excluding the twelve control wells this adds up to 36 pre-mix solutions that needed to be prepared per drug activity study (three triplicate of each concentration × twelve different concentrations). The control wells (row D) were used to monitor the state of the buffer and the lipid solution only, and thus did not contain the Fe(III)PPIX solution. The aliquots of lipid-Fe(III)PPIX solution were added dropwise to the pre-incubated buffer using a syringe with a needle diameter of 0.5 mm, yielding an interface between the hydrophobic lipid emulsion droplets and hydrophilic buffer regions after solvent mixing. The plates were allowed to incubate in the oven for a further four hours, which was chosen arbitrarily in initial experiments.

Following the incubation period, the reaction was quenched by adding 241.0 µL of the 30:30:40 (v/v) pyridine: aqueous buffer: acetone solution (section 2.5.7) into each well to yield an end solution that contained 5% (v/v)

pyridine overall. After manually agitating the plate for one minute to ensure that the pyridine had interacted fully with any unreacted Fe(III)PPIX, the plate was left to stand for 15 minutes to allow visible lipid precipitate to settle. A 200.0 µL aliquot of the supernatant in each well was then transferred to an empty well in a clean 96-well plate and the absorbance value for each well was measured at 405 nm. This absorbance value was compared to that of the zero-drug control, and was used as a measure of the amount of unreacted Fe(III)PPIX remaining at each drug concentration, from which the IC_{50} value could be determined.

Measurements were conducted in triplicate for each antimalarial drug to improve the reliability of the results. The observed absorbance values were plotted as a function of increasing drug concentration and fitted to a sigmoidal or hyperbolic function, using nonlinear least squares fitting in GraphPad Prism. The IC_{50} value for each antimalarial drug was then determined from the dose-response curves by as described in Figure 3.2.
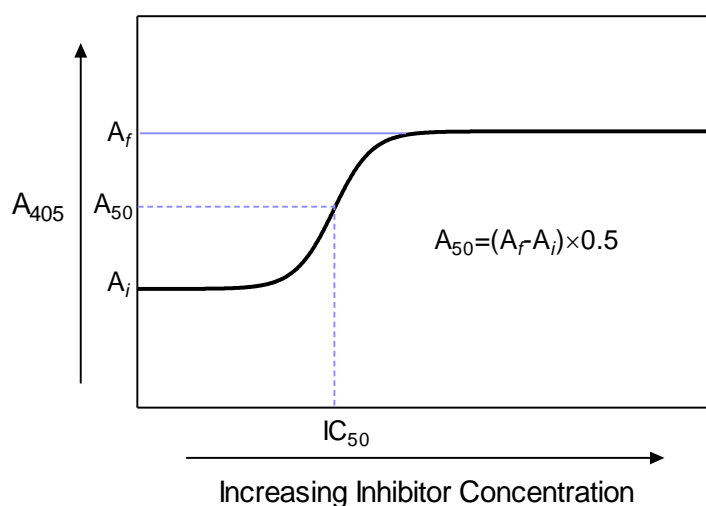
Figure 3.2 A schematic indication of how the absorbance values at A_{405} were used to calculate the IC_{50} values for each drug. Inhibition of β-haematin formation by 50% was determined by subtracting the absorbance of Fe(III)PPIX measured in the absence of drug (A_i) from that obtained at high drug concentration (A_f) and multiplying the product by 0.5. The drug concentration corresponding to this absorbance value (A_{50}) is the concentration of drug required to inhibit 50% of β-haematin formation and is termed the IC_{50} value.

3.2.1.3 Non-Aqueous Soluble Antimalarial Drugs

As mentioned above, MQ is insoluble in the aqueous citrate buffer solution, and hence has been treated differently compared to the other antimalarial drugs. MQ was therefore dissolved in a 1:9 acetone: methanol solution and incorporated into the aqueous citrate buffer in each well within a 100.0 µL aliquot before the pre-incubation period. The quantity of MQ dissolved in the acetone: methanol stock solution was equal to the amount that would be expected in an aqueous citrate buffer stock solution if the drug was soluble. The concentrations were thus calculated relative to the total volume of the system in each well. The lipid-Fe(III)PPIX premix solution was prepared in the remaining 100.0 µL of 1:9 acetone: methanol solution, which was therefore double the concentration used previously to ensure the same lipid- and Fe(III)PPIX final

concentrations in each well compared to the aqueous-soluble compounds. The premix solution was added dropwise into each well as described above (section 3.2.1.2).

3.2.1.4 The Effect of Incubation Time on Drug IC_{50} Values

A study investigating the effect of time on drug activity (IC_{50}) was conducted for CQ and QD. The procedure described in section 3.2.1.2 was followed, except that for each experiment, varying time periods ranging between one and one hundred hours (1, 2, 4, 5, 8, 16, 24, 32 and 100 hours) were used for incubation. The reactions were monitored, and data were analysed, as described previously.

3.2.1.5 Antimalarial Drug Kinetics Studies

Kinetics studies were carried out in order to determine the equilibrium adsorption constant, K_{ads}, for each antimalarial drug in the lipid-water interface system. In these experiments, the incubation time, as well as the concentration of each antimalarial drug, were varied in order to obtain a full profile for each β-haematin inhibiting compound.

The same procedure as outlined for the drug activity studies in section 3.2.1.2 was followed to monitor the kinetics of β-haematin formation in the presence of different drug concentrations. The solutions were prepared and introduced into the 24-well plates in a similar manner as before. The number of concentrations that were investigated ranged from six to eight, with six being most common. The range of concentrations investigated was different for each drug, depending on the β-haematin inhibitory activity, which was determined in the drug activity studies, as mentioned above. Lower concentrations were introduced into the aqueous buffer for more active drugs, compared to less active drugs that required higher doses. For convenience, and to prevent disturbance of the interface, one plate was prepared per incubation time. Nine different incubation time periods were chosen, ranging from 0 up to 32 hours (0, 0.5, 1, 2, 4, 8, 16, 24 and 32 hours).

The premix solution delivered to each well contained 200.0 μL of lipid- and only 2.00 μL of Fe(III)PPIX solution.[74] After the incubation period, the reaction was quenched by adding 240.4 μL of the 30:30:40 (v/v) pyridine: aqueous buffer: acetone solution into each well. As before, the absorbance of a 200.0 μL sample was measured in a dry 96-well plate at 405 nm.

Kinetics studies were also conducted in triplicate for each antimalarial drug to improve the accuracy of the results. All of the data were plotted and analysed by non-linear least squares fitting, using GraphPad Prism. The K_{ads} value for each antimalarial drug was then determined from the respective analyses as described in section 3.2.1.6, as well as in Chapter 1, and further discussed in the following section. The experimental procedures described for drug activity- and kinetics studies in sections 3.2.1.2 and 3.2.1.5 are shown in the flow diagram in Figure 3.3.
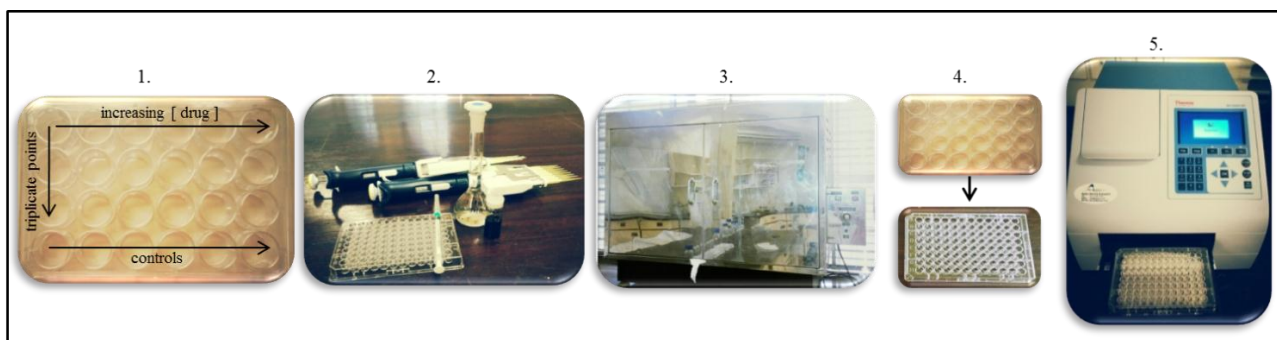
Figure 3.3 Flow diagram of the experimental procedures for inhibitor activity- and kinetic studies. (1) 24-well plates were prepared with drug-containing buffer and pre-incubated for 45 minutes in a 37 °C oven. (2) Premix solutions containing 200 µL lipid- and 5.00 µL (activity studies) or 2.00 µL (kinetic studies) Fe(III)PPIX were prepared in 96-well plates and introduced into each well with a 0.5 mm needle syringe. (3) Plates were left to incubate in an oven set at 37 °C for four hours (activity studies) and up to 32 hours (kinetic studies). After quenching the reaction in each well with the 30:30:40 pyridine: aqueous buffer: acetone solution to ensure 5 % (v/v) pyridine in the end, a 200 µL aliquot of the supernatant was transferred to a 96-well plate (4) and the absorbance at 405 nm was read as a measure of the amount of unreacted Fe(III)PPPIX (5).

3.2.1.6 Analysis of Kinetics Data

The experimental absorbance data obtained at 405 nm represents the amount of free Fe(III)PPIX that remains in the system at the end of a specific incubation period. The data were compared to a zero-drug control value, following which they were converted into a percentage value, quantifying the amount of β-haematin formed in a given time. By plotting these values as a function of time, and fitting them to a simple exponential kinetic equation, the observed rate constant, z_{obs}, for the formation of β-haematin in the presence of a particular drug concentration was determined. According to the adsorption model based on the Langmuir isotherm (Equation 1.4), it is predicted that a plot of the inverse of z_{obs} as a function of increasing drug concentration will generate a linear correlation at low drug concentration (Figure 3.4 (a)). Linear regression in this region allows for both the slope and y-intercept values to be determined, which in turn assists in calculating the rate constant for β-haematin formation in the absence of an inhibitor, z, as well as K_{ads} (using the equations inserted in Figure 3.4 (a)). By fitting the kinetics data to Equation 1.2 (repeated below as Eq. 3.1 for ease of reference), known parameters, namely, K_{ads}, z, the inhibitor concentration and the fractional yield of β-haematin formation expected in the MPG lipid-mediated system, are used as constraints in the equation. The values of K_{ads} and z were determined from the linear regression analysis, while the rate constant for the precipitation of a proposed drug-haem complex, k_2, was allowed to refine freely in order to generate the best fit of the experimental data to the model (Figure3.4 (b)). Since this competing precipitation process is still poorly understood, accurate values for k_2 were not investigated in the current study and it is found that the k_2 value can generally accommodate a wide range of values.

$$\%\beta_{(s)} = \frac{100Yz}{(z+k_2[I]^2+k_2 K_{ads}[I]^3)}\left\{1 - e^{-\left(\frac{z+k_2[I]^2+k_2 K_{ads}[I]^3}{1+K_{ads}[I]}\right)t}\right\} \tag{Eq. 3.1}$$

51
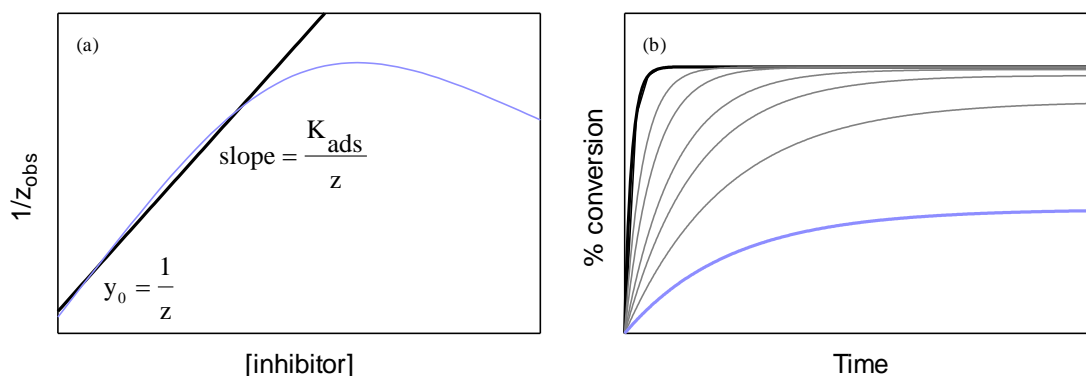
Figure 3.4 Predicted kinetics of β-haematin formation in the presence of an inhibitor.[40] (a) A plot of the inverse of the observed rate constants, z_{obs}, as a function of increasing inhibitor concentration (purple line) yields a linear correlation at low concentrations (black line). Linear regression in this region allows the K_{ads} and z values to be calculated from the slope and intercept values, respectively. (b) Kinetic traces observed in the absence (black line) and presence of increasing inhibitor concentrations (grey lines). The trace obtained in the presence of the highest inhibitor concentration is shown in purple.

3.2.2   Results

The previously-modified Phiβ assay used to investigate the inhibition of β-haematin at a lipid-water interface,[40] has several disadvantages and limitations from the point of view of medium- to high-throughput screening of β-haematin inhibitors. The assay is overall time-consuming, used unnecessarily large quantities of materials, had multiple centrifugation steps, and used less efficient absorbance measurement reading methods, all of which resulted in a slow turnaround time per compound. This prompted the revisions and further optimizations carried out in the current study, which has allowed a greater number of compounds to be investigated. The results obtained have facilitated a broader understanding of the inhibition phenomenon in a biomimetic system.

3.2.2.1 Optimization of Assay

The assay was optimized by introducing 24-well plates as the reaction vessel, as opposed to the 15 mL Greiner Falcon centrifuge tubes that were used previously. 24-well plates were chosen since the internal diameter of a single well is identical to that of a tube (1.6 cm). In keeping the internal diameter constant, the surface area in each vessel remains unchanged, which in turn meant that the maximum percentage yield of β-haematin formed would also be consistent.[74]

Experiments were initially incubated by floating the 24-well plates in a water bath. However, longer incubation times were required using this approach since there is considerably less area that is in contact with the water in the case of the wells as compared to the fully immersed tubes. Furthermore, non-reproducible and inconsistent results were obtained, possibly as a consequence of irregular heat distribution across the well, but also as a result of condensation that formed on well lids. In the case of the latter, this produced changes in solvent composition within the well, as well as changes to concentrations of the reagents. Exchanging the water

bath for a fan-assisted oven produced more consistent results as better temperature control was achieved and condensation was eliminated. An added benefit of using the oven over a water bath was the greater number of plates that could be incubated in the former, facilitating more efficient means with which to conduct the study. The oven is advantageous over the water bath in that it provides greater consistency and better results overall.

An equal volume of the lipid-Fe(III)PPIX premix solutions was introduced into the system as before, while the volume of aqueous citrate buffer was decreased due to the smaller well capacity. Since the surface area of each well was the same as previous experiments carried out in tubes, as mentioned above, the difference in the buffer bulk was not expected to interfere in the formation of β-haematin.

UV-visible measurements by means of a single cuvette (2.0 mL) were also improved upon by introducing 96-well plates for simultaneous measurement of multiple samples.

Under these revised conditions, the yield of β-haematin in the absence of an inhibitor was found to be the same as in the original approach. Interestingly, however, a ten-fold decrease in the rate of β-haematin formation was observed, with the rate decreasing from 0.171 ± 0.04 min^{-1} to 0.019 ± 0.002 min^{-1} (Figure 3.5).
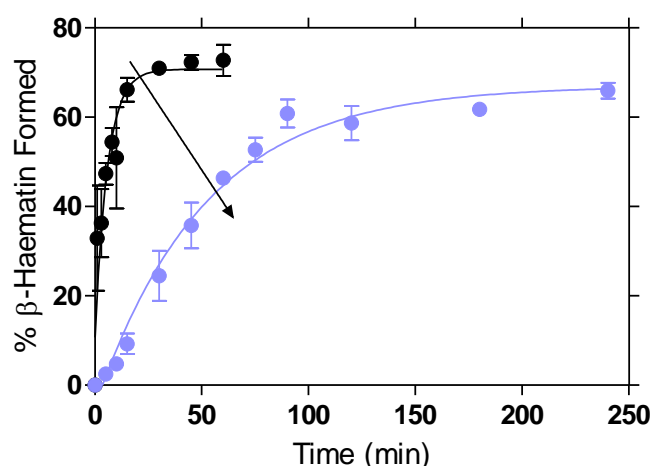
Figure 3.5 Rate of β-haematin formation in the absence of an inhibitor. The previous rate observed using 15 mL Greiner Falcon tubes (●) is ten-fold faster compared to the rate determined in 24-well plates (●). A decrease in the rate of β-haematin formation is observed (arrow). The observed rate constants determined from these curves are 0.171 ± 0.04 min^{-1} and 0.019 ± 0.002 min^{-1}, respectively.

In an attempt to understand the observed ten-fold decrease in the rate constant of β-haematin formation in the absence of an inhibitor, an independent study was performed to investigate the influence of the solvent concentrations in the 24-well system. Since all other quantities were the same, the difference in rate was presumed to arise from the larger proportion of acetone: methanol used relative to the buffer volume in the 24-well method as opposed to in the tubes. To probe this, β-haematin formation was performed in 15 mL Falcon tubes, as demonstrated in the previous study,[40] however, with an increased proportion of the acetone: methanol

53

solution relative to the buffer, such that the ration was the same as in the wells. It was first considered to decrease the acetone: methanol volume relative to the buffer in the wells in order that it is the same as that previously used in the tubes, however, this resulted in very small quantities to work with. Keeping the lipid- and Fe(III)PPIX premix solution the same as before, an additional volume of acetone: methanol solution was therefore introduced into the aqueous citrate buffer to ensure that the final acetone: methanol concentration in each tube was the same compared to the concentration in each well. The experiment was carried out over a period of time, ranging from 0 to 32 hours incubation time, followed by quenching with 1.0 mL of pyridine: aqueous buffer: acetone and single UV-vis measurement readings, using a cuvette.

Under these conditions, the yield of β-haematin in the absence of an inhibitor was found to be the same as in the original tube approach, as well as in the 24-well plate. Interestingly however, the same ten-fold reduction in the rate of β-haematin formation was obtained in this adapted system, thus confirming that the volume of acetone: methanol relative to the buffer affects the rate of β-haematin formation. The rate of β-haematin formation in the tubes decreased from 0.171 ± 0.04 min^{-1} to 0.023 ± 0.003 min^{-1}, which is consistent with the rate of β-haematin in the 24-well plates (Figure3.6).

Due to the significant decrease in the rate of β-haematin formation in the new assay (in the 24-well plates), overall incubation periods for both activity- and kinetics experiments were increased to 32 hours to ensure reaction completion. Even though shorter incubation times are preferable, increased incubation times are serendipitous, because previous incubation times were so short that they were difficult to measure. In increasing the incubation times, the kinetics can be more easily measured, and with greater accuracy. All of the important differences and similarities between the previous method and the new assay are summarized in Table 3.2.
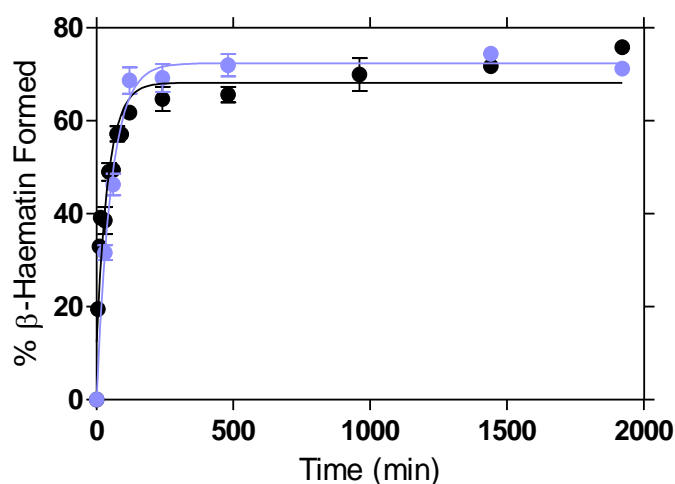
Figure 3.6 Kinetics of β-haematin formation in the absence of an inhibitor. The increased concentration of acetone: methanol in the tube method (●) produces a ten-fold reduction in the rate constant of β-haematin formation and is in good agreement with that determined using 24-well plates (●).The observed rate constants determined from the curves are 0.023 ± 0.003 min^{-1} and 0.019 ± 0.001 min^{-1}, respectively.

54

Table 3.2 A comparison between the previous and new assay to investigate the inhibition of β-haematin formation

Previous Assay	New, Optimized Assay
Equipment	
15 mL Falcon tubes	24-well sterile plates
Water bath, 37 °C	Oven, 37 °C
Reaction (Quantities)	
5 mL 50 mM Citrate buffer, pH 4.8	1 mL 50 mM Citrate buffer, pH 4.8
Pre-incubation time, 30 minutes	Pre-incubation time, 45 minutes
200 μL lipid	200 μL lipid
5 μL (activity), 2 μL (kinetic) Fe(III)PPIX	5 μL (activity), 2 μL (kinetic) Fe(III)PPIX
Incubation periods, 0-240 minutes	Incubation periods, 0-1920 minutes
Measurement	
1 mL 30: 30: 40 Pyridine: HEPES: Acetone	0.24 mL 30: 30: 40 Pyridine: HEPES: Acetone
10 minutes centrifuge and leave to settle	Manually agitated and leave to settle for 15 minutes
2.0 mL aliquot reading in cuvette	0.2 mL aliquot reading in 96-well plates

There is overall a vast improvement compared to the previous method used to investigate the inhibition of β-haematin at the lipid-water interface. The main advantage of the new assay is the faster turnaround time per compound to investigate both the drug activity- and kinetic studies, irrespective of the longer incubation periods required per compound. In order to validate the newly-optimized assay as a means of assaying drug activity against β-haematin formation in the lipid-water system, the observed drug activity- and kinetic adsorption results then needed to be compared to previously-determined results. In order to thus fully compare the two different protocols with each other, the new assay was first validated by investigating five known antimalarial drugs, namely CQ, AQ, QD, QN and MQ. Both drug activity and kinetic studies were carried out to investigate the effect these compounds would have on the formation of β-haematin.

3.2.2.2 Antimalarial Drug Activity Studies

Drug activity studies were performed independently to determine the IC_{50} value for each antimalarial compound (as described in section 3.2.1.2). The IC_{50} value determined for a specific inhibitor, as defined previously, is the drug concentration required to inhibit β-haematin formation by 50%. The dose-response curves for the inhibition of lipid-mediated β-haematin formation by AQ, CQ, QD, QN and MQ are shown in Figure 3.7. The data were collected after a four-hour incubation period, since longer incubation times are required in the 24-well plates in order to account for the ten-fold decrease in the observed rate. This incubation period is eight times longer than the 30 minutes incubation period used for the tube method, however, since the incubation time was chosen arbitrarily in the previous study, it was presumed to be sufficiently long enough. The data show how the proportion of free Fe(III)PPIX, measured spectroscopically as a *bis*-pyridyl Fe(III)PPIX complex at 405 nm,[74,145] changes as a function of increasing drug concentration. In all five cases, an increase in the absorbance at 405 nm is observed as a function of increasing drug concentration. This is

expected, since an increase in drug concentration would inhibit the conversion of free Fe(III)PPIX into β-haematin to a greater extent, and hence an increase in the absorbance of free Fe(III)PPIX will be observed.

The observed IC_{50} values for each drug (Table 3.3) were determined by fitting the experimental data to either a sigmoidal or a simple hyperbolic function as explained earlier in Figure 3.2. Interestingly, the dose-response curves for AQ, CQ and MQ conform to a sigmoidal fit, while those for QD and QN, conform to a hyperbolic function. According to the theoretical model, this suggests that an incubation time longer than four hours may be required for compounds such as QD and QN in order for the IC_{50} values to be meaningfully compared to the others.
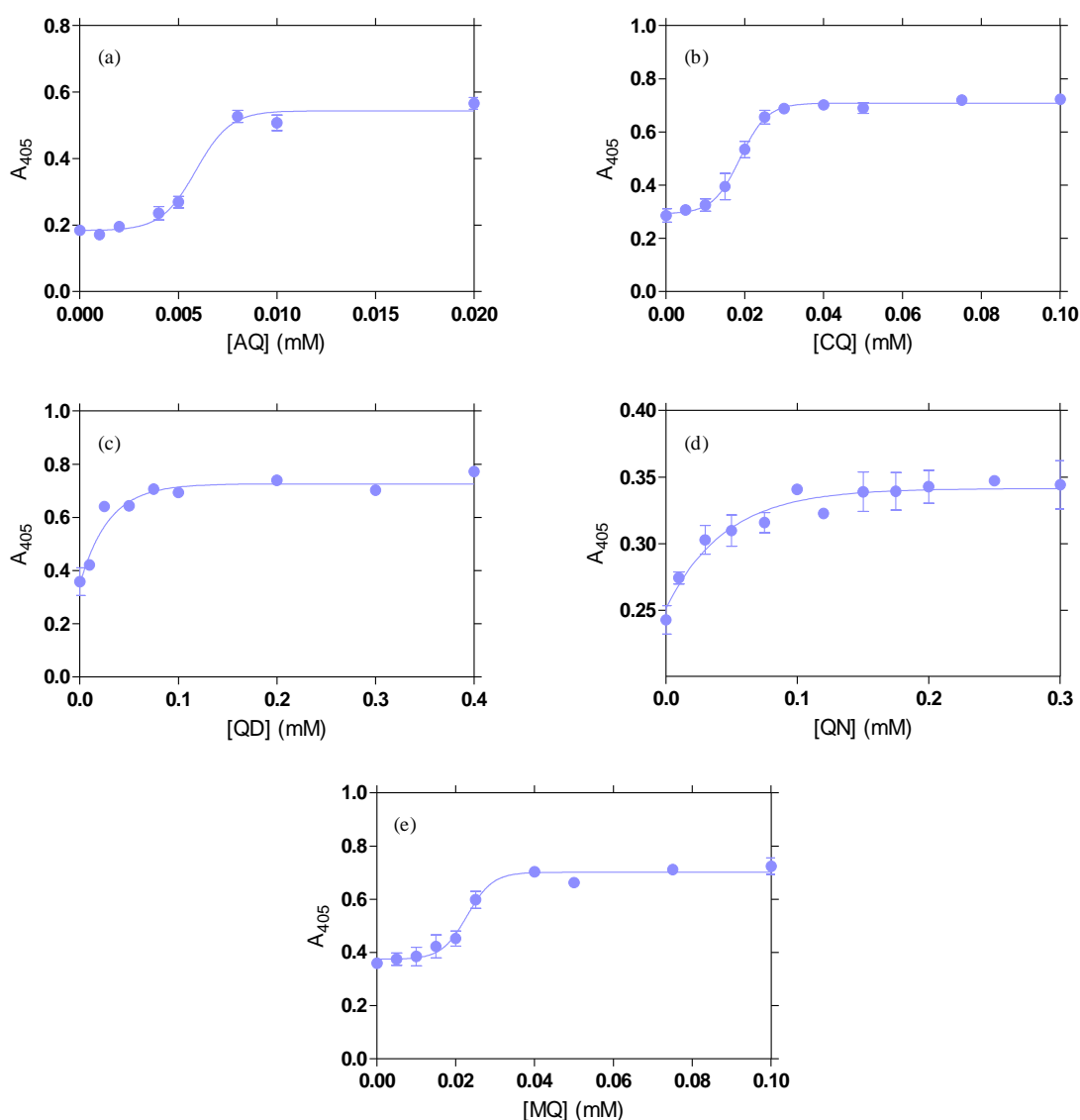
Figure 3.7 The inhibition of β-haematin formation by antimalarial drugs at the lipid-water interface using the newly-developed 24-well plate assay. Dose-response curves determined in drug activity studies after a four-hour incubation period as a function of increasing drug concentration for (a) AQ, (b) CQ, (c) QD, (d) QN and (e) MQ. The IC_{50} value for each drug is determined by fitting the data either to a sigmoidal (a, b and e) or a hyperbolic (c and d) function. The r^2 values are 0.94, 0.98, 0.93, 0.77 and 0.95, respectively.

56

Table 3.3 IC_{50} values obtained for the inhibition of β-haematin formation by antimalarial drugs at the lipid-water interface in 24-well plates compared to previously used tubes.[40,152]

Antimalarial Drug	24-Well Plates (μM)[†]	Falcon Tubes (μM)
AQ	5.9 ± 0.3	9.0 ± 0.4
CQ	18.8 ± 0.6	16.4 ± 0.5
QD	20.1 ± 4.1	51.1 ± 5.8
QN	31.0 ± 8.3	73.9 ± 12.8
MQ	22.9 ± 0.6	12.2 ± 0.1

[†]Error calculated as standard error of the mean (SEM), following three experimental repeats, each including triplicate data points.

While the absolute values do not agree, the IC_{50} values determined in the current study are in good agreement when compared to previously-determined IC_{50} values.[40,152] Both sets of values follow the same trend, with drug activity increasing from QN to AQ as follows; QN<QD<CQ<AQ. The linear correlation observed between these IC_{50} values is shown in Figure 3.8 (a), with an r^2 value of 0.78. The P value is larger than 0.05, however, indicating that the correlation is non-significant. This is most likely due to there being only four points in the correlation. MQ is not included in the evaluation between the previous and the new assay, since the drug was introduced differently into the lipid-water interface system in both cases. Despite the insignificant correlation, the good agreement between the IC_{50} values obtained *via* the two protocols did provide sufficient validation to progress with the study of additional compounds.

Different systems in which β-haematin formation is investigated are frequently compared to one another to establish or validate if their outcomes regarding the activity of a drug are related. Drug activities obtained in the current lipid-water system were thus compared to the drug activities determined *in vitro* in the Phiβ acetate assay[145] and the NP40 detergent-mediated assay.[159] A non-significant linear correlation, with an r^2 value of 0.68, is observed when comparing the IC_{50} values of each drug against the respective equivalents determined in the Phiβ acetate assay (Figure 3.8 (b)). When comparing the IC_{50} values to those determined in the NP40 assay, which is a lipid environment mimic, a significant linear correlation, with an r^2 value of 0.93 and P value < 0.05, is observed (Figure 3.8 (c)). These two relationships are important when considering the efficacy of the optimized 24-well plate method, as a means to determine inhibitory activities biomimetically.

Having demonstrated that the observed activity in the biomimetic system does correlate with β-haematin inhibitory activity determined in related systems, the observed IC_{50} values were also compared to the biological activities previously determined against a CQ-sensitive (CQS) strain of the malaria parasite, 3D7.[147] A linear correlation is observed (Figure 3.9), which is statistically significant, with an r^2 value of 0.91, and a P value < 0.05. Overall, taking the correlations in Figures 3.8 and 3.9 into account, the data indicate that the newly-optimized lipid-mediated assay is indeed a valid system in which to investigate drug activity.
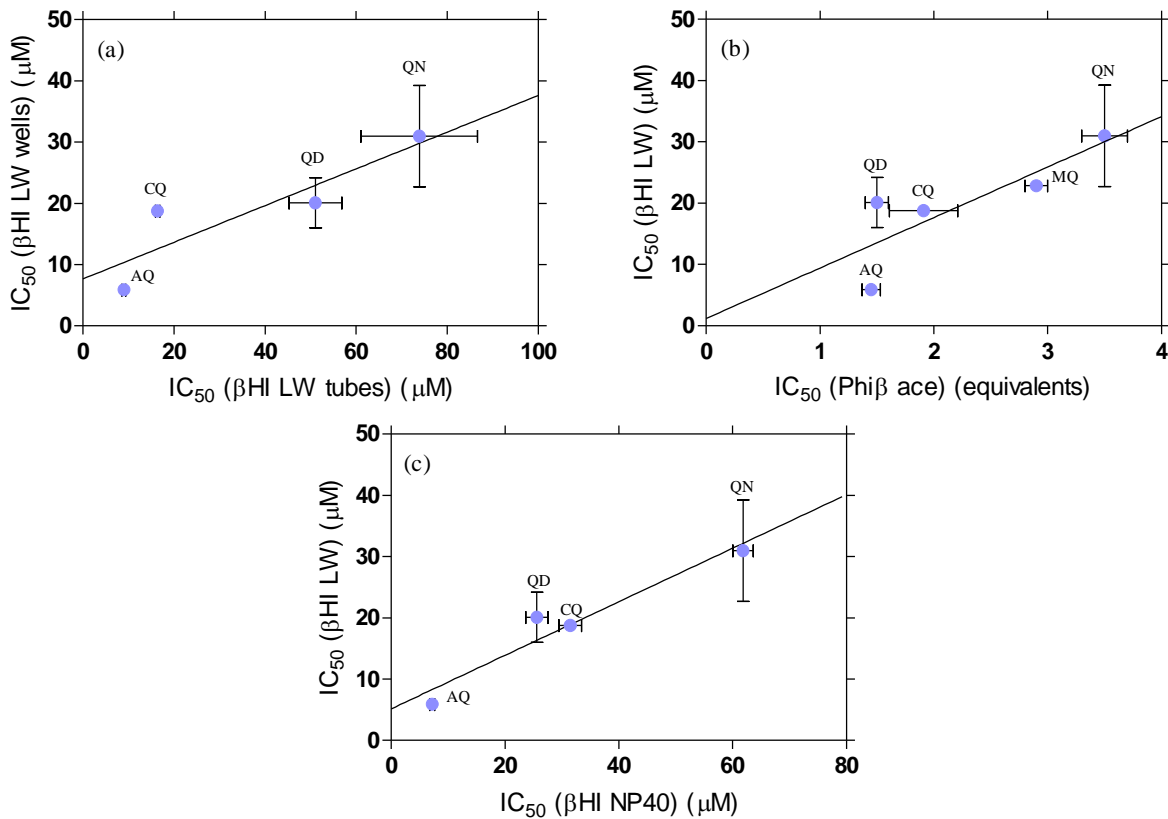
Figure 3.8 The inhibition of β-haematin formation by antimalarial drugs at the lipid-water interface. The correlation between the observed IC_{50} values, obtained after 4 hours in the 24-well plate assay, compared to previously determined (a) IC_{50} values in the Falcon tubes,[40] (b) IC_{50} equivalents in the Phiβ acetate assay[145] and (c) IC_{50} values in the NP40 detergent-mediated assay.[159] The r^2 values for the linear correlations are 0.78, 0.68 and 0.93, respectively, of which only the latter is a significant fit with a P value < 0.05.
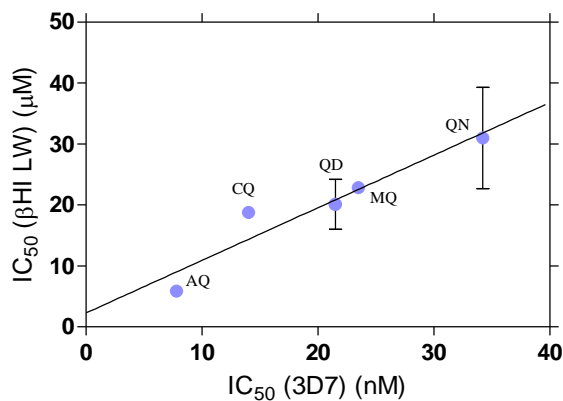
Figure 3.9 The inhibition of β-haematin formation by antimalarial drugs in the lipid-water interface system. The linear correlation between the observed IC_{50} values, obtained after 4 hours in 24-well plate assay, compared to previously determined biological activity against a CQ-sensitive strain, 3D7 (r^2 value of 0.91, P value < 0.05).[147]

3.2.2.3 The Effect of Incubation Time on Drug IC$_{50}$ Values

An additional independent study investigating the effect of incubation time on drug activity was carried out for CQ and QD. An increase in IC$_{50}$ values is observed as a function of increasing incubation time for both drugs (Figure 3.10). In both cases, the data showed a hyperbolic dependence in agreement with that predicted by the theoretical kinetic model (see section 1.5.4.3.2) These results are also consistent with what has previously been observed from time studies conducted in the tubes.[152] Together with the activity study, it is clear that the same trend is observed in the 24-well plates compared to the previously-used tubes, suggesting that the two systems yield the same information and are comparable.
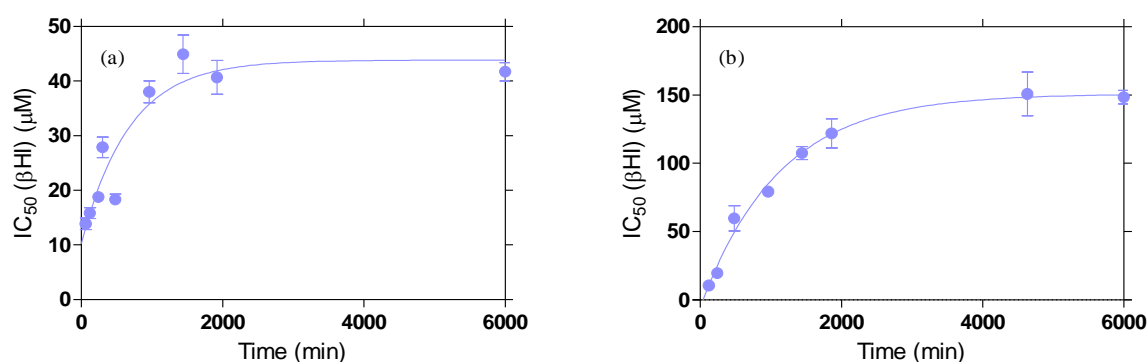
Figure 3.10 The influence of incubation time on the observed IC$_{50}$ values. The IC$_{50}$ values obtained in the lipid-water interface system using the new 24-well plate assay as a function of increasing incubation time for (a) CQ and (b) QD. Both datasets conform to a hyperbolic function with r^2 values of 0.88 and 0.99, respectively.

3.2.2.4 Antimalarial Drug Kinetics Studies

Due to the rapid rate at which β-haematin formation occurs in the lipid-water interface system (pH 4.8, 37 °C), compared to the acetate system (pH 4.5, 60 °C),[64] it has been feasible to investigate the kinetics of this process in the presence of various inhibitors. Kinetics studies using CQ were initially conducted to assist in the optimization of the modified Phiβ assay in 24-well plates. With the new method optimized, full kinetics profiles were collected for the formation of β-haematin in the presence of additional antimalarial drugs, namely AQ, QD, QN and MQ. Taking into account the proposed theoretical kinetic model,[40] which is based on the premise that adsorption of an inhibitor onto the growing crystal face of β-haematin is important, it has been possible to draw conclusions regarding the effect of each inhibitor on the formation of β-haematin. Furthermore, it has been possible to determine equilibrium adsorption constants, K_{ads}, which is essentially the main aim in this section. The model is based mathematically on the Langmuir isotherm, as well as the Avrami equation, as discussed previously in section 1.5.4.3.2.[40] This section focusses on the effect of each antimalarial drug on the formation of β-haematin, compared to what has previously been accounted for in the Falcon tubes. The effect of CQ is discussed in detail below, followed by a brief summary of the results obtained for the other

clinically-relevant quinoline antimalarial drugs. A detailed kinetic investigation of the formation of β-haematin in the absence and presence of CQ was carried out by introducing different concentrations of CQ into the aqueous phase of the biomimetic system. Given that CQ showed good β-haematin inhibitory activity in the lipid-water system (IC_{50} = 18.8 µM, which is equivalent to 0.0188 mM), a concentration range of 0.01 to 0.10 mM was considered. The concentration ranges used for the other antimalarial drugs were chosen according to their activity relative to that of CQ. The procedure outlined in section 3.2.1.6 was followed for kinetics data analysis. Both z and K_{ads} were calculated from the slope and intercept values determined from the linear region of the plot in Figure 3.11 (a). By fitting the kinetic data to Equation 3.1 and using these parameters as constraints, the best fit of the experimental kinetic data was generated and is found to be in good agreement with the proposed theoretical kinetic model (Figure 3.11 (b)). During the fitting process, the values for k_2 were allowed to refine freely. It is shown that the same percentage β-haematin yield is formed, however, a decrease in the rate of β-haematin formation is observed as the CQ concentration is increased. Following the incorporation of higher CQ concentrations, a notable decrease in the final yield of β-haematin is observed.
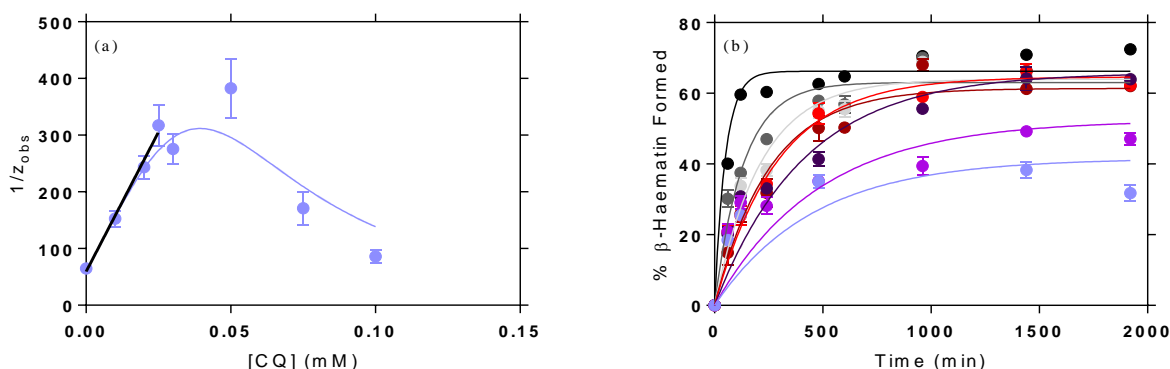
Figure 3.11 Kinetics of β-haematin formation in the presence of chloroquine. (a) A plot of the inverse of the rate constants, z_{obs}, as a function of increasing CQ concentration yields a linear correlation (black line) with an r^2 value of 0.99 at low concentrations. K_{ads} (165.9 ± 34.8 mM) and z (0.017 ± 0.003 min^{-1}) values were computed from the slope (9844 ± 697 min. mM^{-1}) and intercept values (59.3 ± 11.7 min). The best fit of the experimental data to Equation 1.4 is shown in purple and corresponds to an r^2 value of 0.84 (b) Kinetic traces observed in the absence (●) and presence of increasing concentrations of CQ: 0.01 (●), 0.02 (○), 0.025 (●), 0.03 (●) 0.05 (●), 0.075 (●) and 0.10 (●) mM. The r^2 values are 0.95, 0.93, 0.95, 0.91, 0.94, 0.86, 0.59 and 0.38, respectively.

A kinetics profile for each of the other antimalarial drugs is presented below, which includes the plot of the inverse of z_{obs} as a function of increasing drug concentration, fitted to Equation 1.4 (Figure 3.12, left panel), as well as the plot of the percentage β-haematin formed over time, fitted to the theoretical kinetic model (Equation 3.1) (Figure 3.12, right panel). A table summarizing the calculated K_{ads} and z values for each antimalarial drug is also provided (Tables 3.4). The kinetics effects of AQ, QD and QN have been investigated previously, however, this study is the first to investigate the effect of MQ on the lipid-mediated formation of β-haematin.

60
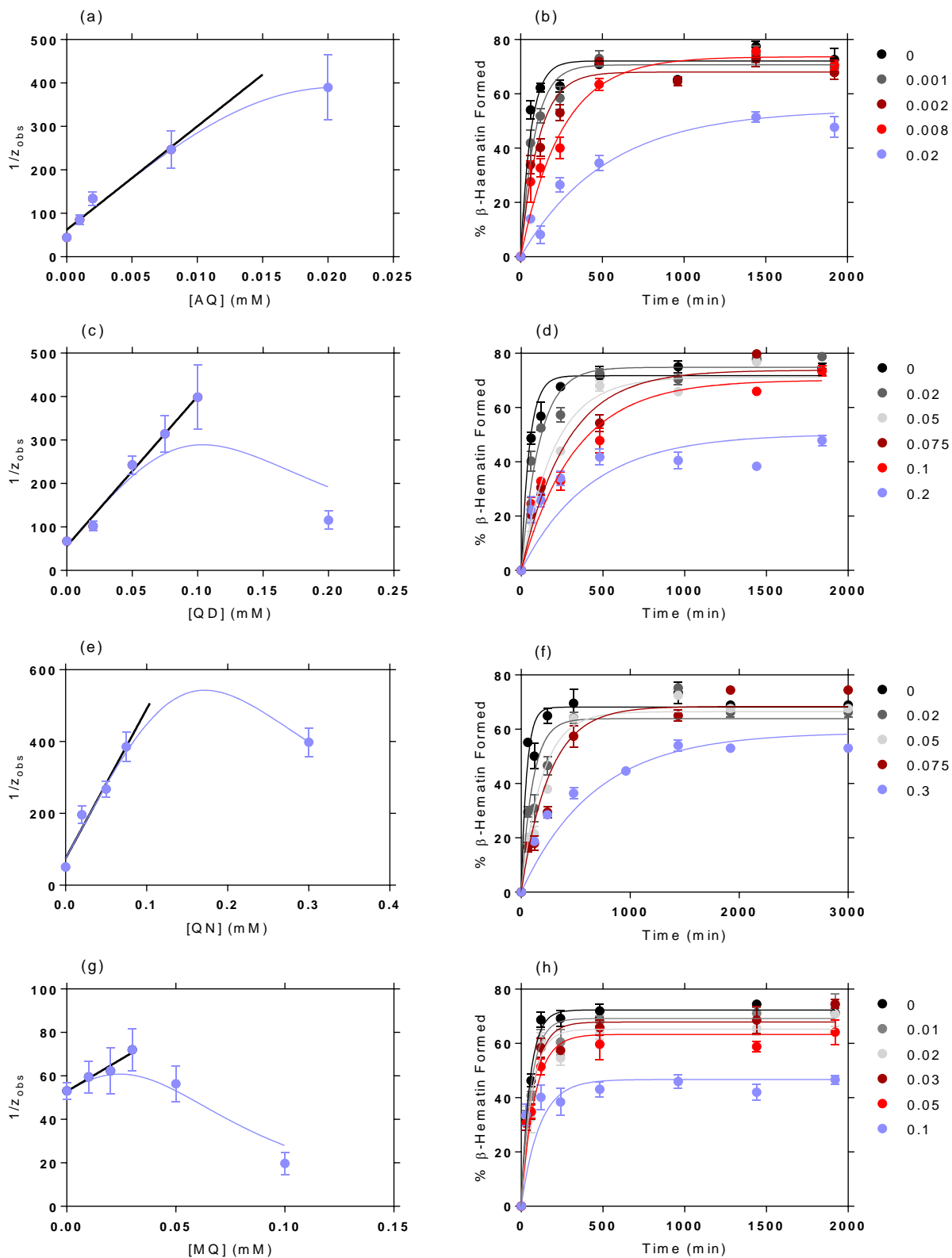
Figure 3.12 Kinetics of β-haemin formation in the presence of antimalarial drugs. Left panel (a, c, e, g): a plot of the inverse of the rate constant, z_{obs}, as a function of increasing drug concentration, yields a linear correlation (black line) at low concentrations from which the K_{ads} and z values were computed from the slope and y-intercept values. The best fit of the experimental data to Equation 1.4 is shown in purple. Right panel

(b, d, f, h): kinetic traces fitted to Equation 3.1 observed in the absence and presence of increasing inhibitor concentrations. The antimalarial drugs investigated were amodiaquine, quinidine, quinine and mefloquine.

The linear correlation (black line) and the best fit of the experimental data to Equation 1.4 (purple curve) shown in the left panel of Figure 4.5 (a, c, e and g), correspond to good r^2 values (0.99, 0.99, 0.96 and 0.96) and (0.99, 0.76, 0.97 and 0.86) for AQ, QD, QN and MQ, respectively. The kinetic traces fitted to Equation 3.1 in the right panel of Figure 3.12 (b, d, f and h) also correspond to good r^2 values for each drug at each respective concentration. In the case of CQ, the r^2 values for the fit of the data at each concentration range between 0.38 and 0.95. Fits with lower r^2 values are observed at higher concentrations ($r^2 = 0.38$ for 0.1 mM) and may possibly be attributed to the formation of the proposed drug-haem complex, for which the solubility in aqueous pyridine is still unknown. The r^2 values for the kinetics traces are between 0.89-0.93, 0.48-0.96, 0.88-0.95 and 0.72-0.97 for AQ, QD, QN and MQ, respectively.

Table 3.4 The best fit values to the theoretical kinetic model for β-haematin formation in the presence of AQ, QD, QN and MQ in 24-well plates.[†]

Antimalarial Drug	Slope (min.mM⁻¹)	Intercept (min)	z (min⁻¹)	k_2	K_{ads} (mM⁻¹)	Log K_{ads} (M⁻¹)
CQ	9844 ± 697	59.3 ± 11.7	0.017 ± 0.003	0.105	165.9 ± 34.8	5.22 ± 0.33
AQ	23830 ± 3461	62.1 ± 14.4	0.016 ± 0.004	0.155	384 ± 105	5.58 ± 0.44
QD	3447 ± 211	56.0 ± 12.9	0.018 ± 0.004	0.022	61.6 ± 14.7	4.79 ± 0.38
QN	4160 ± 591	74.3 ± 27.3	0.013 ± 0.005	0.004	55.9 ± 22.0	4.75 ± 0.63
MQ	594.7 ± 89.9	52.9 ± 1.7	0.019 ± 0.001	0.003	11.2 ± 0.3	4.05 ± 0.04

[†]Error calculated as standard error of the mean (SEM), following three experimental repeats, each including triplicate data points.

It is observed that the rate constant of β-haematin formation in the absence of an inhibitor, z, is statistically the same for the various antimalarial drugs. The value of z in all five cases is approximately 0.02 min⁻¹, which is ten-fold lower than that determined in the Falcon tubes. It was observed that the value of the rate constant for the proposed competing precipitation process, k_2, could take on a wide range of values, however, the reported values above were chosen in order to generate good fits to the theoretical model for each drug, respectively. For the antimalarial drugs, k_2 varied between values of 0.003 and 0.155. Interestingly, values of k_2 appear to decrease with a decrease in K_{ads} values, however, this was not investigated further. Important relationships are observed between the K_{ads} values determined for the antimalarial drugs and their respective IC_{50} values determined in the previous section. These relationships are discussed in the following section.

3.2.3   Relationships between Drug Activity and Strength of Adsorption

After performing both activity- and kinetic studies with the known antimalarial drugs at the lipid-water interface, the relationship between the observed IC_{50} and K_{ads} values was investigated. A linear correlation with an r^2 value of 0.83 (Figure 3.13 (a)) suggests that the inhibitory activity of a compound may very well be related to its strength of adsorption to the growing β-haematin crystal in the lipid-mediated system. This observation lends possible insight into understanding the mechanism of the inhibition of β-haematin formation in biomimetic systems. Subsequently, the K_{ads} values were compared against the biological activity reported against the CQS parasite strains, NF54,[160] 3D7[147] and D10.[160] Linear correlations, with r^2 values of 0.68, 0.93 and 0.60, respectively, are observed between these values (Figure 3.13 (b-d)) and indicate a good agreement between the biological and experimental data. These correlations are, however, not significant (except in the case of the 3D7 parasite strain), indicated by P values > 0.05. This is in part due to an insufficient number of data points included in the analysis, since MQ was omitted from these correlations. It was thus recognized that in order to draw any meaningful conclusions, it would be important to extend the data set further, by introducing other inhibitors into the system. This was achieved by investigating additional quinoline derivatives that had previously been shown to be β-haematin inhibitors.[158]
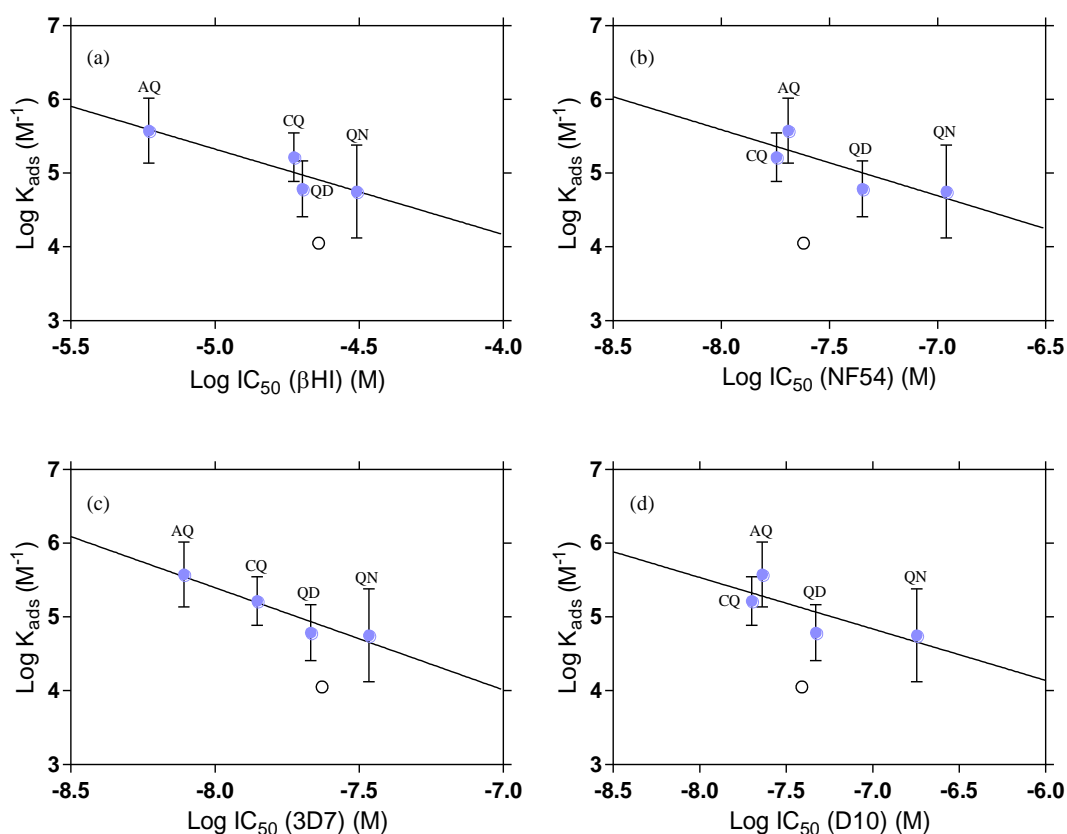
Figure 3.13 Important correlations observed for antimalarial drugs. The linear correlations between the observed K_{ads} values and (a) the IC_{50} values determined in the lipid-water interface system (24-well plates) and the biological IC_{50} values determined previously against the (b) NF54,[160] (c) 3D7[147] and (d) D10[160] CQ sensitive parasite strains. The r^2 values are 0.83, 0.68, 0.93 and 0.60, respectively. In all four correlations MQ has been omitted as an outlier (indicated by the open circle).

3.3 Extending the System to Other Quinoline-based β-Haematin Inhibitors

After optimizing and validating the 24-well plate method of the Phiβ assay to investigate the inhibition of β-haematin at the lipid-water interface, it was considered to extend the study in this system even further to include other β-haematin inhibitors. The 4-aminoquinoline inhibitors used in this section are short chain chloroquine derivatives with different substituents at the 7-position. These compounds were previously synthesized in a study by Kaschula *et al.*[158] to investigate structure-activity relationships and were chosen for use in the current study owing to their simple structures and based on their β-haematin inhibitory activities (referred to as BHIA$_{50}$ in the original reference). The compounds were kindly resynthesized by Mr J. Hay for the current study, and their molecular structures have been presented previously in Figure 1.30 (a).

3.3.1 Experimental Methods

3.3.1.1 Introducing the Chloroquine Derivatives into the Aqueous Citrate Buffer

A series of N^1, N^1-diethyl-N^2-(4-quinolinyl)-1, 2-ethanediamines with different substituents at the 7-position on the quinoline ring have been investigated previously.[158] The 7-chloro (Q-Cl), -iodo (Q-I), -trifluoromethyl (Q-CF$_3$), -methoxy (Q-OMe) and -trifluoromethylthio (Q-SCF$_3$) 4-aminoquinolines were, however, resynthesized for the purpose of this study, and were made available in their free base forms. As such, they are completely insoluble in the aqueous citrate buffer, however, can easily be converted into their salt forms by protonation at the terminal amine and quinoline nitrogen atoms (highlighted in blue in Figure 3.14). By dissolving each compound in a small amount of ethylacetate and protonating it by the addition of an excess of moderately strong acid, HNO$_3$, the salt form of the compound precipitated out of solution. After extensive washing with ethylacetate and allowing the product to dry overnight on a high vacuum pump, the desired salt could be recovered ([fb+2H]$^{2+}$(NO$_3^-$)$_2$, where fb = free base). Once in their salt form, these compounds were readily soluble in the aqueous citrate buffer. Stock solutions of the citric acid monohydrate buffer (50.0 mM, pH 4.8), including the appropriate mass of each 4-aminoquinoline inhibitor (Table 3.5), were prepared in a similar manner as described for the antimalarial drugs in section 3.2.1.1.
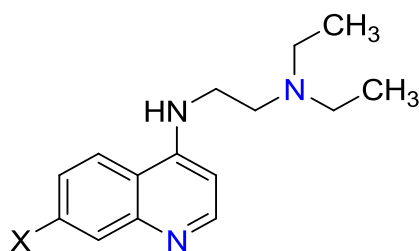
Figure 3.14 Structure of the short-chain CQ analogues investigated in this study. The terminal amine and quinoline nitrogen atoms, which are protonated to yield the salt form of these compounds, are indicated in blue, where X = Cl, I, CF$_3$, OMe or SCF$_3$, respectively.[158]

Table 3.5 Quantities of short-chain CQ analogue salts required to prepare a 100.0 mL[†] stock solution in 50.0 mM citrate buffer, pH 4.8.

Short-chain CQ Analogues	Molecular Mass (g.mol^{-1})	Stock Concentration (mM)	Mass (mg)
Q-Cl	403.81	0.10	4.0
Q-I	498.26	0.10	4.9
Q-CF$_3$	437.37	0.20	8.8
Q-OMe	399.39	0.40	16.0
Q-SCF$_3$	469.44	0.20	9.4

[†]The volume can be adjusted according to the amount needed for a specific experiment.

3.3.1.2 Short-chain CQ Analogue Activity Studies

Studies were carried out to determine the IC$_{50}$ value for the 4-aminoquinoline compounds in the lipid-water interface system. In these experiments, the incubation time was fixed, while the concentrations of each 4-aminoquinoline β-haematin inhibitor were varied. Due to a limited amount of compound provided, a complete activity study could unfortunately not be conducted for the 7-methoxy aminoquinoline derivative.

The procedure described in section 3.2.1.2 was followed to investigate the activity of the remaining four 4-aminoquinoline compounds, however, due to limited quantities of each compound provided, triplicate studies could not be repeated three times for all the compounds as before.

3.3.1.3 Short-chain CQ Analogue Kinetics Studies

Kinetics studies were carried out in order to determine the K_{ads} value of each 4-aminoquinoline compound in the lipid-water interface system. In these experiments, the incubation time, as well as the concentration of each β-haematin inhibitor, were varied in order to obtain a full profile for each compound.

The procedure described in section 3.2.1.5 was followed to investigate the kinetics of β-haematin formation in the presence of the 4-aminoquinoline compounds, however, due to limited quantities of each compound provided, triplicate studies could not be repeated three times for all of the compounds.

3.3.2   Results

3.3.2.1 Short-chain CQ Analogue Activity Studies

Similarly to the antimalarial drugs, inhibitor activity studies were performed independently of the kinetics studies to determine the IC$_{50}$ value for each short-chain CQ analogue (as described in section 3.2.1.2). The dose-response curves for the inhibition of β-haematin formation by Q-Cl, -I, -CF$_3$ and –SCF$_3$ are shown in Figure 3.15. The observed IC$_{50}$ values for each inhibitor (Table 3.6) were determined by fitting the data to either a sigmoidal or a simple hyperbolic function. Three of the inhibitors, namely Q-Cl, -I and –SCF$_3$, yielded

a good sigmoidal fit with r^2 values of 0.94, 0.99 and 0.64, respectively. The data for Q-CF$_3$ conformed to a hyperbolic function with an r^2 value of 0.90. Again, this may suggest that an incubation period longer than four hours is required for complete inhibition by Q-CF$_3$. In all four cases, an increase in the absorbance at 405 nm is observed as a function of increasing inhibitor concentration. This is expected, since an increase in inhibitor concentration would inhibit the conversion of free Fe(III)PPIX into β-haematin to a greater extent, and hence an increase in the absorbance of free Fe(III)PPIX will be observed.
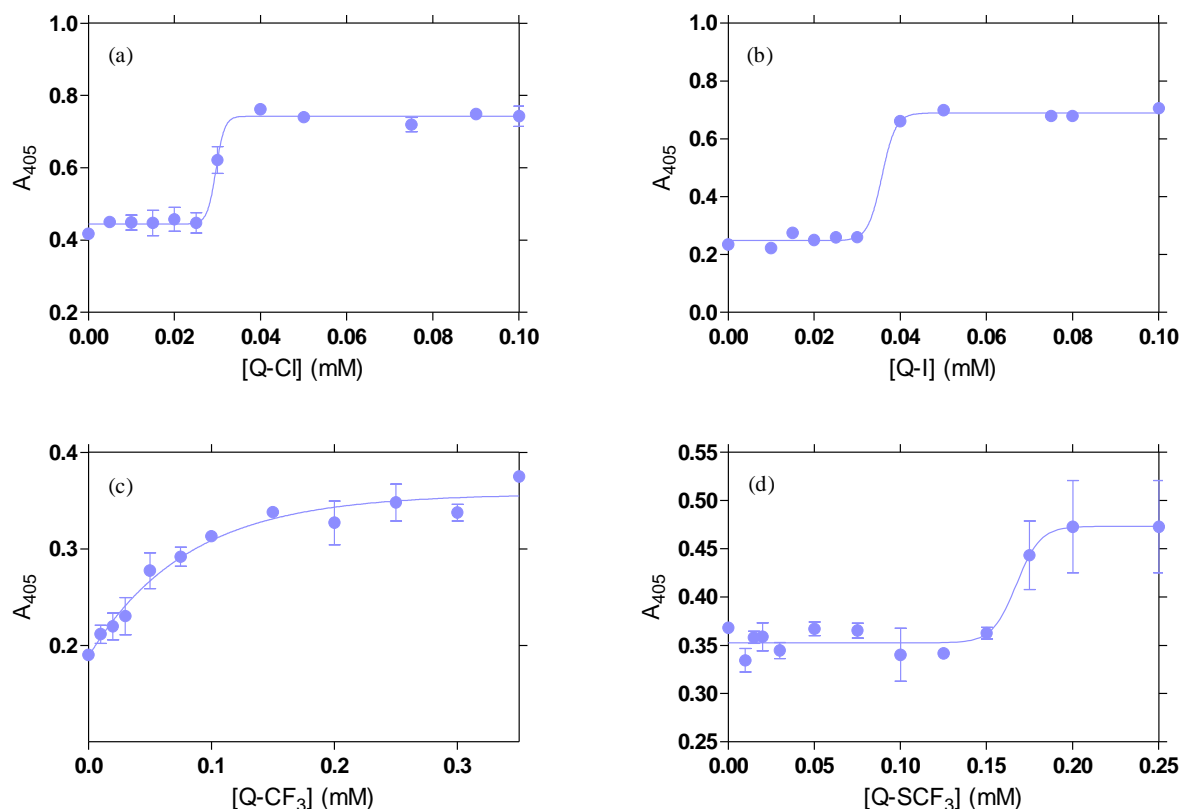
Figure 3.15 The inhibition of β-haematin formation by short-chain CQ analogue inhibitors at the lipid-water interface. Dose-response curves determined in activity studies after a four-hour incubation period as a function of increasing inhibitor concentration for the 4-aminoquinolines with (a) -Cl, (b) -I, (c) –CF$_3$ and (d) –SCF$_3$ substituents. The IC$_{50}$ value of each quinoline inhibitor is determined by fitting the data to either a sigmoidal (a, b and d) or a hyperbolic (c) function.

Both the BHIA$_{50}$, as well as the β-haematin inhibition ability determined spectroscopically (βHI) for each compound are reported in Table 3.7. The BHIA$_{50}$ values were previously-determined in an acetate buffer system,[158] while the βHI is indicated by a + for a β-haematin inhibitor and a – for a non- β-haematin inhibitor. According to their BHIA$_{50}$ values, these compounds appear to be moderately comparable in activity compared to CQ,[142] except Q-OMe, which is expected to be inactive. Unfortunately, the activity of Q-OMe could not be determined in the lipid-water interface system owing to the limited amount of material provided.

66

Table 3.6 Comparative IC_{50} values obtained for the inhibition of β-haematin formation by a series of chloroquine derivatives in the lipid-water interface system in 24-well plates and those determined previously in an acetate buffer system.[142,158]

Aminoquinolines	24-Well Plates (μM)[†]	βHI[Ŧ]	BHIA$_{50}$[‡]
Q-Cl	29.8 ± 0.7	+	2.2 ± 0.2
Q-I	35.7 ± 0.9	+	2.8 ± 0.2
Q-CF$_3$	55.5 ± 9.9	+	8.0 ± 2.0
Q-OMe	ND[‡]	-	>20
Q-SCF$_3$	167.3 ± 9.0	+	2.1 ± 0.3

[†]Error calculated as standard error of the mean (SEM), following at least two experimental repeats, each including triplicate data points, [‡]Not determined due to limited amount available, [Ŧ]Infrared determination of inhibition of β-haematin formation, [‡]BHIA$_{50}$ in equivalents of aminoquinoline relative to haematin to inhibit 50% conversion, [iii]

Interestingly, when plotting the observed IC_{50} values obtained in the lipid-water interface system for the combined set of quinoline inhibitors (antimalarials and aminoquinolines) against their BHIA$_{50}$ counterparts,[142,158] no obvious correlation is observed (Figure 3.16). The Q-SCF$_3$ analogue (circled in purple), which was found to be a relatively active β-haematin inhibitor in the acetate system, is readily identified as inactive when comparing its activity in the lipid-water system. Since the two different *in vitro* systems mediate β-haematin formation in different manners, it is likely that compounds may display different activity results. The observation does, however, suggest that the lipid-mediated system may be a better model for activity determination than the acetate model, since it is biologically more relevant than that of the acetate model. As mentioned before in section 1.4.3.1, the acetate method also displays a completely different crystallization behaviour compared to the lipid system, suggesting that the lack of correlation is perhaps somewhat unsurprising. Owing to the limited amount of activity data available for the 4-aminoquinoline compounds, no additional correlations could be further investigated between the β-haematin inhibitory activity values, determined in the current lipid-mediated system and other *in-vitro* assay systems (the NP40-detergent mediated system for example).
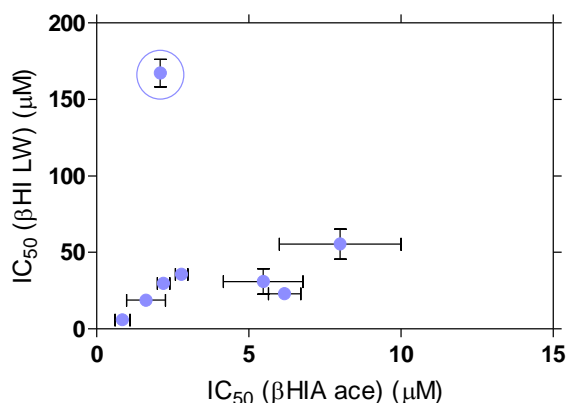
Figure 3.16 The correlation between the observed IC_{50} values, obtained after 4 hours in the 24-well plate assay, compared to previously determined BHIA$_{50}$ values in an acetate medium assay. [142,158]

3.3.2.2 Short-chain CQ Analogue Kinetics Studies

The kinetics studies were also extended from the known antimalarial drugs to investigate the effect of other quinoline-based β-haematin inhibitors. This study is the first to investigate the effect of other quinoline-based inhibitors on the lipid-mediated formation of β-haematin. Full kinetics profiles were collected for the formation of β-haematin in the presence of Q-Cl, Q-I, Q-CF$_3$, Q-OMe and Q-SCF$_3$. Taking into account the proposed theoretical kinetic model, which is based on the premise that adsorption of an inhibitor onto the growing crystal face of β-haematin is important, it is possible to explain the effect of each inhibitor on the formation of β-haematin, and to determine their equilibrium adsorption constants, K_{ads}, which is essentially the main aim in this section. The procedure outlined in section 3.2.1.6 was followed for kinetics data analysis.

A comprehensive kinetics profile for each short-chain CQ analogue inhibitor is presented below, which includes the plot of the inverse of z_{obs} as a function of increasing drug concentration, fitted to Equation 1.4 (Figure 3.17, left panel), as well as the plot of the percentage β-haematin formed over time, fitted to the theoretical kinetic model (Equation 3.1), (Figure 3.17, right panel). A table summarizing the calculated values for each antimalarial drug is also provided (Table 3.7).

Given that Q-Cl showed the greatest β-haematin inhibitory activity of the short-chain CQ analogues in the lipid-water system (IC$_{50}$ = 29.8 µM, which is equivalent to 0.0298 mM), a concentration range of 0.01 to 0.10 mM was considered. The same or higher concentration ranges were thus considered for the other quinoline inhibitors which are less active than Q-Cl.
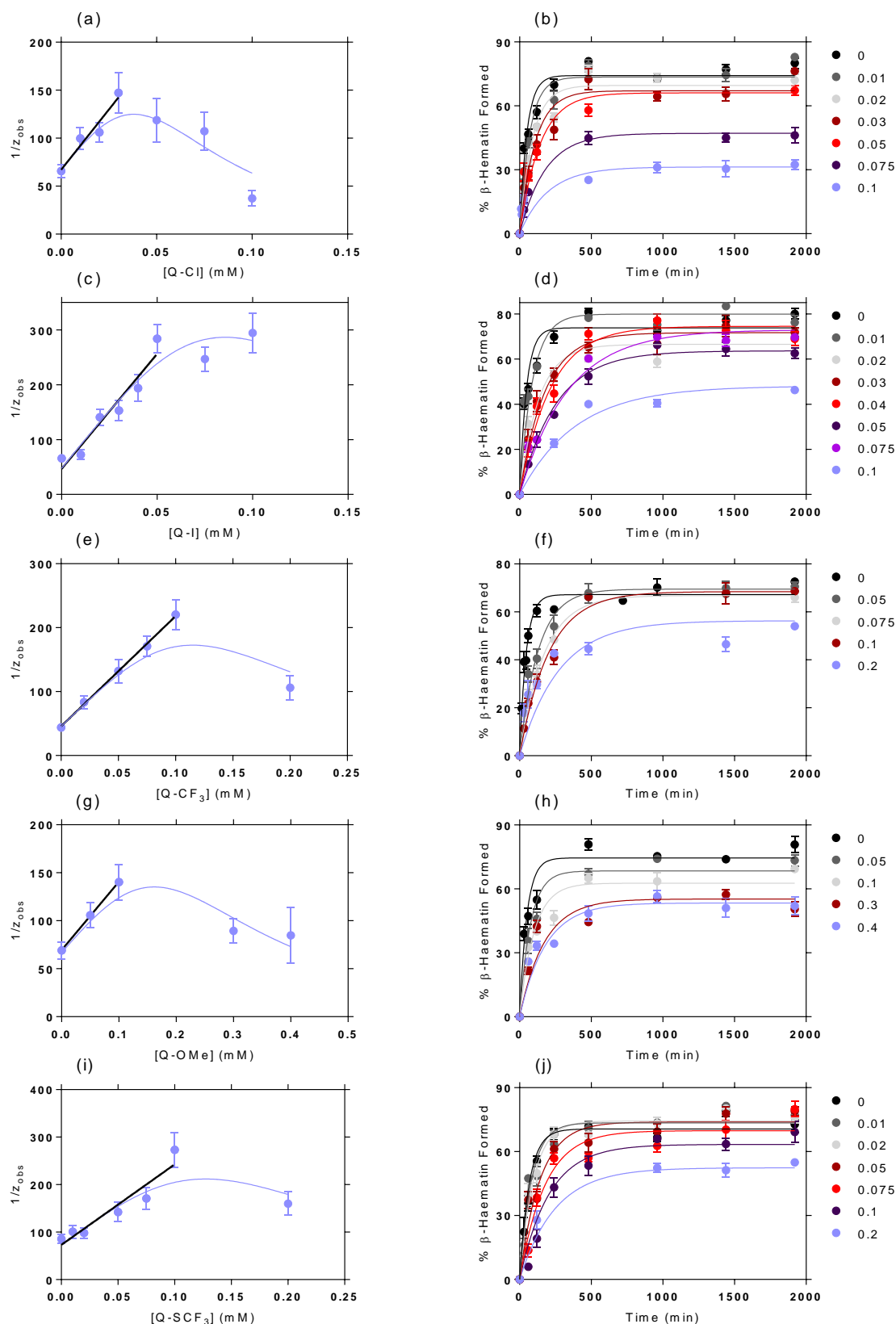
Figure 3.17 Kinetics of β-haematin formation in the presence of short-chain CQ analogues. Left panel (a, c, e, g, i): a plot of the inverse of the rate constant, z_{obs}, as a function of increasing inhibitor concentration, yields a linear correlation (black line) at low concentrations from which the K_{ads} and z values were computed from the slope and y-intercept values. The best fit of the experimental data to Equation 1.4 is shown in purple. Right panel (b, d, f, h, j): kinetic traces fitted to Equation 3.1 observed in the absence and presence of increasing inhibitor concentrations.

The linear correlation (black line) and the best fit of the experimental data to Equation 1.4 (purple curve) shown in the left panel of Figure 4.17 (a, c, e, g and i), correspond to good r^2 values (0.94, 0.93, 0.99, 0.99 and 0.90) and (0.78, 0.91, 083, 0.79 and 0.77), respectively, for each of the short-chain CQ analogue inhibitor. The kinetic traces fitted to Equation 3.1 in the right panel of Figure 3.17 (b, d, f, h and j) also correspond to good r^2 values for each inhibitor at each respective concentration. The r^2 values for these traces are between 0.61-0.93, 0.89-0.95, 0.65-0.96, 0.84-0.93 and 0.88-0.93 for Q-Cl, -I, -CF$_3$, -OMe and –SCF$_3$, respectively.

Table 3.7 The best fit values to the theoretical kinetic model for β-haematin formation in the presence of 4-aminoquinoline β-haematin inhibitors, Q-Cl, Q-I, Q-CF$_3$, Q-OMe and Q-SCF$_3$ in 24-well plates.[†]

4-Amino-quinolines	Slope (min.mM^{-1})	Intercept (min)	z (min^{-1})	k_2	K_{ads} (mM^{-1})	Log K_{ads} (K^{-1})
Q-Cl	2510 ± 455	67.1 ± 8.52	0.015 ± 0.002	0.090	37.4 ± 8.29	4.57 ± 0.35
Q-I	4192 ± 572	46.8 ± 17.3	0.021 ± 0.008	0.045	89.6 ± 35.4	4.95 ± 0.63
Q-CF$_3$	1724 ± 43.6	45.6 ± 2.65	0.022 ± 0.001	0.027	37.8 ± 2.39	4.58 ± 0.10
Q-OMe	712.5 ± 11.8	69.4 ± 0.76	0.014 ± 0.001	0.010	10.3 ± 0.20	4.01 ± 0.03
Q-SCF$_3$	1695 ± 277	73.0 ± 15.4	0.014 ± 0.003	0.035	23.2 ± 6.20	4.37 ± 0.43

[†]Error calculated as standard error of the mean (SEM), following at least two experimental repeats, each including triplicate data points.

As per antimalarial drugs, it is observed that the rate of β-haematin formation in the absence of an inhibitor, z, is the same for all short-chain chloroquine analogues. The value of z in all five cases is approximately 0.02 min^{-1}, which corresponds to the quinoline antimalarial drugs. The value of the rate constant of the proposed competing precipitation process, k_2, as mentioned previously, could take on a wide range of values, however, the reported values above were chosen in order to generate good fits to the theoretical model for each inhibitor, respectively. For the short-chain chloroquine analogues, k_2 varied between values of 0.01 and 0.09 for each compound, which falls into the broad range of k_2 values of 0.004 and 0.450 determined for the antimalarial drugs. There is, however, no specific relationship observed between the k_2 and respective K_{ads} values. Important relationships are observed between the K_{ads} values of these quinoline compounds and the antimalarial drugs and their respective IC$_{50}$ values determined in the previous sections. These relationships are discussed in the following section.

3.4 Combining Quinoline-based β-Haematin Inhibitors

After investigating the inhibition of β-haematin formation in the lipid-water interface system, it was important to consider all the quinoline-based β-haematin inhibitors, including both the antimalarial- and 4-aminoquinoline compounds, together. To establish whether the behaviour of these compounds conform to the hypothesis that the β-haematin inhibitory activity of a compound is related to its strength of adsorption to the growing β-haematin crystal, their respective IC_{50} and K_{ads} values were correlated to each other.

The observed K_{ads} values were compared to the IC_{50} values determined for each compound in the current study and this yielded a significant linear correlation, with an r^2 value of 0.78 (Figure 3.18 (a)). The data points for MQ (indicated by an open circle) and Q-OMe have not been included the correlation; MQ is the only compound which was introduced differently into the system and owing to limited material, no IC_{50} value could be determined for the latter. There is indeed a direct relationship between the respective K_{ads} and IC_{50} values determined in the biomimetic lipid-mediated system, suggesting that the proposed adsorption of an inhibitor to growing β-haematin crystals might possibly be related to the mechanism of inhibition of β-haematin formation.

Subsequently, the K_{ads} values were compared to the biological activity reported against the D10 CQS parasite strain for each compound,[158] which also yielded a linear correlation (r^2 value of 0.67) (Figure 3.18 (b)). There is a significant agreement between the biological- and experimental data, further suggesting that adsorption might indeed play a critical role in the biological mechanism of action by quinoline inhibitors.
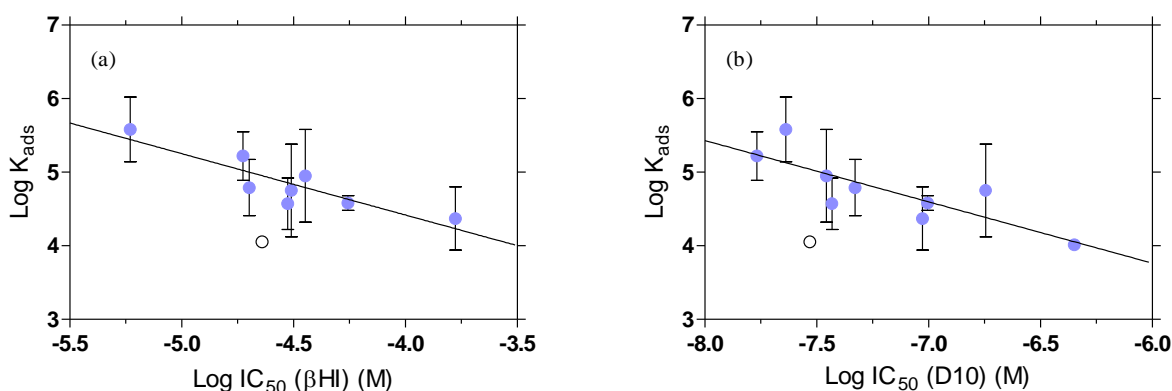
Figure 3.18 Important correlations observed for quinoline-based β-haematin inhibitors. The linear correlations between the observed K_{ads} values and (a) the IC_{50} values determined in the lipid-water system (24-well plates) and (b) previously determined biological activities against the CQS D10 parasite strain for both sets of quinoline inhibitors (antimalarials and 4-aminoquinolines).[158,160] The r^2 values are 0.78 and 0.67, respectively. In both cases the data point for MQ (open circle) has been omitted from the linear correlation.

3.5 Discussion

The main focus of this part of the study was to investigate the interaction between quinoline-based β-haematin inhibitors, and Fe(III)PPIX, resulting in the inhibition of β-haematin formation. The first important objective was to optimize the previously-used modified Phiβ assay. This work built on from preliminary studies reported in our laboratory,[40] which created a fundamental basis in understanding the behaviour of antimalarial drugs on the formation of β-haematin. In order to develop a higher-throughput assay, the same known antimalarial drugs were systematically incorporated into the lipid-mediated system, adjusting different variables in the process. The main advantage of the optimized assay is the faster turnaround time per individual compound investigated in the lipid-mediated system. Previously, it took weeks or months to conduct a detailed kinetics study for a single β-haematin inhibitor, hence the effect of only four compounds on the formation of β-haematin had been investigated prior to the current study in this system.[40]

It has previously been shown by Hoang *et al*.[74] that an increase in the surface area of a vessel in which β-haematin formation is performed results in a decrease in the overall percentage yield of β-haematin with little to no change in the rate of formation. This study evidently suggested that the surface area of a vessel plays a major role in the percentage yield of β-haematin formation. Interestingly, in the current study, the same amount of β-haematin is formed, but over a longer period of time, when changing the experimental vessel from 15 mL Greiner Falcon centrifuge tubes to 24-well plates. The diameter of the two vessels is, however, the same, accounting for the same amount of β-haematin formed. The observed ten-fold decrease in the rate of β-haematin formation in the absence of an inhibitor could be accounted for following an investigation of the effect of different solvent concentrations in the system. A higher lipid-Fe(III)PPIX to buffer ratio is present in the end volume of each well in a 24-well plate compared to the ratio in each Falcon tube, resulting in higher organic solvent (acetone: methanol) concentrations. Based on the proposed evolution of a lipid emulsion during solvent mixing rather than the formation of a distinct lipid-water interface,[74] it is plausible that the rate of diffusion of acetone and methanol, the solvents in which the lipid and Fe(III)PPIX are introduced into the system, is slower in each well compared to a faster rate of diffusion in each tube. This in return will have an effect on the rate at which the lipid-water interface forms in the system, and hence will influence the rate of β-haematin formation. By increasing the incubation period, the maximum yield of β-haematin could still be attained.

In order to probe the relative β-haematin inhibitory activity of each antimalarial drug, independent drug activity studies were carried out with AQ, CQ, MQ, QD and QN in the newly-optimized lipid-mediated system. When comparing the data obtained from the optimized assay to the previously-used lipid-mediated assay, the IC_{50} values are in good agreement with one another (Figure 3.8 (a)).[40] The observed trend in drug activity is the same, with AQ being the most active β-haematin inhibitor, followed by CQ, QD and QN, respectively. The 4-aminoquinoline antimalarial drugs are more active β-haematin inhibitors in the lipid-water interface system than the quinoline methanol antimalarial drugs. Subsequently, the β-haematin inhibitory activity of each drug

was also compared against previously-determined drug activities obtained from two different *in vitro* assays. The Phiβ acetate assay was one of the first higher-throughput assays developed to investigate the formation of β-haematin and the inhibition thereof.[145] There is no correlation between the IC_{50} values determined in the current lipid-mediated system and the IC_{50} values, determined as drug equivalents, in the acetate medium (Figure 3.8 (b)). A significant correlation is, however, observed when comparing the relative IC_{50} values to the drug activities determined in the NP40-detergent mediated assay, which is a lipid environment mimic assay (Figure 3.8 (c)). These observations suggest that a lipid-mediated environment is more relevant for investigating the inhibition of β-haematin formation than previously-used acetate medium assays. Furthermore, a good correlation is also observed between the IC_{50} values obtained from the current system and previously-determined activities against the 3D7 CQS parasite strain.[147] Overall, taking the correlations in Figures 3.8 and 3.9 into account, the data are indicative that the newly-optimized assay, incorporating in the lipid-water interface in 24-well plates, is indeed a valid system in which to investigate drug activity

As the theoretical model predicts, the dose-response behaviour from the respective kinetics profiles generates hyperbolic dose-response curves at shorter incubation times, and sigmoidal dose-response curves at longer incubation times (Figure 1.28). In the current study, however, both dose-response curves are observed for the experimental inhibition data for IC_{50} determination at a four-hour incubation period for the quinoline β-haematin inhibitors (antimalarial drugs and short-chain chloroquine analogues). AQ, CQ, MQ, Q-Cl, Q-I and Q-SCF$_3$ produce sigmoidal dose-response curves, while QD, QN and Q-CF$_3$ gives rise to a hyperbolic function. According to the theoretical model, a hyperbolic dose-response curve is indicative of a measurement having been made while the formation of β-haematin is still underway. On the other hand, the model predicts a sigmoidal dose-response curve when the incubation time is sufficiently long such that the formation of β-haematin has reached its maximum. Given the decreased rate of β-haematin formation in the 24-well plates, a longer incubation time (four hours) was chosen compared to the earlier studies (30 minutes). In both cases, the choice of incubation time was not informed by any particular experiment, and alternative incubation times could have been chosen. What is important, however, is that incubation time was fixed for the activity studies, allowing comparisons to be made and conclusions drawn based on the variable in the system, namely the different inhibitors.

An independent time study shows that there is a non-linear relationship between the IC_{50} values and increasing incubation time for CQ and QD (Figure 3.10). It is apparent that shorter incubation times have a more prominent effect on the IC_{50} value of a specific drug, while little further change is observed at longer incubation times. This is an important observation which was made in the previous study as well, suggesting the importance of taking incubation times into consideration when investigating β-haematin inhibitors.[40] The incubation time at which activity studies were investigated in the current study was chosen arbitrarily as four hours, compared to 30 minutes, which was also chosen arbitrarily in the previous study. The fact that the absolute magnitude of the IC_{50} value for a particular drug is marginally different in the two studies may be due in part to the fact that measurements were not made at the same incubation time. The increase in incubation time in the current study was, however, decided upon owing to the ten-fold decrease observed in the rate of β-

haemamtin formation. It is important to note that since the IC_{50} value of a compound is related to incubation time, a different IC_{50} would be expected when a different incubation time is chosen. This would have an impact on the overall correlations which are made with the calculated IC_{50} values in the lipid-mediated system and may improve the r^2 values of these correlations overall. However, with the current incubation time of four hours, the observed correlations still suggest that the lipid-mediated system is a suitable mimic of the *in vivo* environment.

No significant relationship is observed for the quinoline β-haematin inhibitors (antimalarial drugs and short-chain chloroquine analogues) when correlating their respective IC_{50} values obtained in the current lipid-mediated system to the β-haematin inhibitory activity in an acetate medium system (determined as inhibitor equivalents).[158] The inhibitory activity for Q-SCF$_3$ was determined to be better than Q-Cl in the acetate system,[158] however, it appears to be five time less active than the 7-chloro substituted short-chain 4-aminoquinoline in the lipid-mediated system. The other three inhibitors were found to have similar activities relative to each other when comparing the two systems; Q-Cl being more active than Q-I and Q-CF$_3$, respectively. This observation further supports the suggestion that the acetate medium, or any other non-biological medium, as a system of β-haematin formation and inhibition thereof is unfavourable and investigating β-haematin inhibitory activities in more biologically-relevant systems, such as the lipid-mediated systems, is more effective and sensible. Biologically-relevant systems are in closer comparison to the environment in the neutral lipid bodies within the digestive vacuole, in which haemozoin formation occurs *in vivo*. The fact that false positives may occur in the acetate system and not in the lipid system, indicates that the latter produces more reliable results.

In this part of the current study, the effect of quinoline-based β-haematin inhibitors on the formation of β-haematin was investigated at the lipid-water interface. Compared to the previous kinetics studies,[40] similar observations were recorded with regards to overall β-haematin inhibition. A decrease in the rate of β-haematin formation is observed as the inhibitor concentration is systematically increased, while a decrease in the percentage yield of the β-haematin formed is evident when introducing very high concentrations of inhibitor. This observation is made throughout the study for the antimalarial drugs and the 4-aminoquinoline analogues, suggesting that both sets of quinoline-based inhibitors behave similarly in the inhibition of β-haematin formation, even though the decrease in the yield of β-haematin formation is not noticeable for all the inhibitors. It is considered that the quinoline-based inhibitors act by decreasing the rate of β-haematin formation at low concentrations which are biologically relevant, rather than inhibiting the β-haematin formation completely. It has been proposed that the decrease in the rate of β-haematin formation may be accounted for by the noncovalent adsorption of the inhibitors to the growing crystal surface of β-haematin,[39] while the decrease in β-haematin yield at high inhibitor concentration, may be accounted for by the irreversible precipitation of Fe(III)PPIX as an inhibitor complex.[40] It is known that β-haematin inhibitory compounds are able to associate with free Fe(III)PPIX in solution by means of coordination or π-stacking. Such complexation would prevent its incorporation into β-haematin,[117,118] which would therefore result in a decrease in the final yield of β-haematin formed.

The observed rate constant of β-haematin formation in the absence of an inhibitor (z), was determined from the plots of the inverse of z_{obs} as a function of increasing inhibitor concentration, in each case. The value in all cases for the quinoline-based inhibitors was found to be approximately 0.02 min^{-1}. This observation is consistent with what is expected, since z is independent of an inhibitor under similar system conditions. The K_{ads} values were also successfully extracted from these plots for each quinoline-based inhibitor, while the experimental kinetics data recorded for each inhibitor conform to the proposed theoretical kinetic model used to probe the behaviour of each inhibitor in the lipid-mediated system. For the best fit to the model, the K_{ads} and z values were constrained to the values attained from the linear regression analysis. Accurate values for k_2, the rate constant for the proposed competing process that results in the precipitation of haematin, were not investigated in the current study, since this process is still poorly understood. The k_2 values were thus allowed to refine freely in order to generate the best fit of the experimental data to the model. The k_2 value can generally accommodate a range of values and is the only parameter that was adjusted to generate good r^2 fits. In the current study, k_2 was varied in a broad range between 0.003 and 0.155 for the antimalarial drugs, while a range of values between 0.01 and 0.09 was considered for the 4-aminoquinoline inhibitors. It is, however, important to be able to determine the k_2 values independently for each individual group of inhibitors, and this is recommended for future studies to improve our understanding of the system and the interplay between different processes involving Fe(III)PPIX.

Good linear correlations are observed between the observed K_{ads} values and the β-haematin inhibitory activity values for the antimalarial drugs determined in the current lipid-mediated system, as well as against different biological CQS NF54, 3D7 and D10 parasite strains (Figure 3.13). These correlations suggest that the β-haematin inhibitory activity of each compound is related to its strength of adsorption, which corresponds to the main hypothesis of β-haematin inhibition. However, having only four data points in hand, the correlations are not significant. In order to draw a meaningful conclusion about a possible activity-adsorption relationship, these drugs were viewed together with a set of short-chain CQ analogues.

A significant linear correlation with an r^2 value of 0.78 (P value < 0.01) is observed between the adsorption constants (K_{ads}) and the β-haematin inhibitory activities (IC$_{50}$) obtained for the quinoline-based β-haematin inhibitors (Figure 3.18 (a)). For AQ, the most active compound tested in the lipid-mediated system, the large adsorption constant of $K_{ads} = 384 \pm 105$ mM^{-1} is inversely related to its low IC$_{50}$ value, 5.9 ± 0.3 µM. Similarly, but on the other end of the scale, the least active inhibitor, Q-SCF$_3$ (IC$_{50}$ value of 167 ± 9.0 µM) adsorbs sixteen times weaker, $K_{ads} = 23.2 \pm 6.20$ mM^{-1}. According to the significant relationship observed, it is proposed that the strength at which the quinoline-based inhibitors might adsorb to the surface of β-haematin crystals, inhibiting further growth, is associated with its β-haematin inhibitory activity, at least in the lipid-water interface system.

Notably, a significant linear correlation with an r^2 value of 0.67 is also observed between the K_{ads} values and previously-determined biological activity against the CQS D10 parasite strain (Figure 3.18 (b)). It is important to notice that the data points are well spread out along the linear line, suggesting that the correlation is not in any way a result of points assembling together or the weighting of one particular data point on either side of

the line. The adsorption-activity correlation is evident and correlating this to the observations made in the lipid-mediated system, it further suggests that the biological mechanism of haemozoin inhibition by quinoline-based inhibitors, might also be *via* adsorption. The somewhat less-impressive value of r^2 may be a consequence of several other factors that contribute in the biological system, for example a compounds rate of metabolism and rate of accumulation in the digestive vacuole.

The kinetics β-haematin formation in the presence of the 4-aminoquinoline- and quinoline methanol antimalarial drugs, as well as the short-chain CQ analogue inhibitors, all conform to the proposed theoretical kinetic model, which was developed in an attempt to explain the effect of each inhibitor on the formation of β-haematin in the lipid-mediated system. The results reported in this chapter strongly support the hypothesis of inhibitor adsorption to the β-haematin crystal surface, as the mode of action, at least in the case of quinoline-containing inhibitors.

3.6 Conclusion

The previously modified Phiβ assay, used to investigate the inhibition of β-haematin formation in the lipid-water interface system, was successfully optimized in this study. The assay was developed by primarily introducing 24- and 96-well plates, as well recording multiple UV-visible measurements simultaneously. The assay was validated as biologically-relevant by investigating the β-haematin inhibitory activity of clinically-relevant antimalarial drugs. The newly-optimized assay reproduced results similar to what has previously been recorded, however, in a faster turnaround time per compound, which led to kinetics studies investigating β-haematin formation in the presence of these antimalarial drugs. The set of quinoline-based inhibitors was increased by introducing a series of short-chain CQ analogues into the system, which had not been investigated in this manner to date. Based on the results reported in this chapter, an increase in a quinoline-based inhibitor concentration results in a decrease in the rate of β-haematin formation. This was observed at low concentrations, while a decrease in the yield of β-haematin formation was observed when introducing higher doses of each inhibitor. The kinetics data observed for the non-clinically relevant quinoline-based inhibitors, provide great insight into understanding β-haematin inhibition, in adding to what has been reported to date in this regard. Overall, the results reported in this chapter suggest that there might be a direct relationship between the β-haematin inhibitory activity of a compound and its strength of adsorption to the growing face of β-haematin crystals.

Chapter 4. The Effect of Non-Quinoline Inhibitors on the Formation of β-Haematin at the Lipid-Water Interface

4.1 Introduction

Owing to the increase in parasite resistance to previously successful quinoline-based antimalarial drugs, such as CQ, the development of novel chemotherapeutic agents is of high imporatnce.[161] This is well known to date and has been a great motivation behind understanding the mechanism of antimalarial drug action to improve rational drug design to overcome quinoline resistance. The kinetics results obtained for the inhibition of β-haematin formation by quinoline-based β-haematin inhibitors, reported in the previous chapter and based on previous studies,[40] has provided significant insight regarding the possible mechanism of action of an inhibitor on the formation of β-haematin crystals. Based on these results, a complimentary study has been carried out in order to investigate the effect of non-quinoline-based β-haematin inhibitors on the formation of β-haematin. This is the first study carried out in order to investigate the effect of benzamide non-quinoline β-haematin inhibitors in the biologically-relevant lipid-water interface system, using monopalmitoyl-*rac*-glycerol (MPG) to mediate the formation of β-haematin. Introducing these compounds into the system and comparing their effect on the kinetics of β-haematin formation relative to the quinoline-based β-haematin inhibitors extends the set of compounds for which the theoretical kinetic model developed previously, may be applied. For each compound, activity and kinetics experiments have been carried out.

This chapter provides a detailed discussion of the experimental methods followed and results found, regarding both the activity- and kinetics studies for a series of benzamide β-haematin inhibitors.

4.2 Extending the System to Non-quinoline β-Haematin Inhibitors

Having extended the inhibition studies by introducing other quinoline-based inhibitors into the lipid-water interface system, it was then considered important to investigate additional β-haematin inhibitors, particularly those containing non-quinoline scaffolds. The non-quinoline inhibitors investigated in this section were a series benzamide scaffolds varying in substituents on the main aromatic ring, and have been chosen since they were readily available from our collaborators and appeared to be active β-haematin inhibitors. Their molecular structures have been presented previously in Figure 1.30 (b).

4.2.1   Experimental Methods

4.2.1.1 Introducing Non-quinoline β-haematin Inhibitors into the Aqueous Citrate Buffer

The non-quinoline β-haematin inhibitors are completely different in their molecular structure and properties compared to the quinoline-based inhibitors, which greatly affects their solubility in the aqueous system. Alternative mixed aqueous-organic solvent systems were initially considered promising, however, these systems complicated the rates and yields of β-haematin formed. Previous investigations have shown that while pH does have a significant effect on the yield of β-haematin, lowering the pH of the aqueous buffer such that $3.0 < \text{pH} < 4.8$ would incur only marginal decreases in yield.[74] The benzamide compounds were completely dissolved in the aqueous citrate buffer by moderately heating the solution and lowering the pH to 3.0. The more acidic environment ensured complete protonation and hence solubilisation of each compound.

Stock solutions of citric acid monohydrate buffer (50.0 mM, pH 3.0), including the appropriate mass of the non-quinoline (Table 4.1), were prepared similarly as described in section 3.2.1.1

Table 4.1 Quantities of benzamide non-quinoline compounds required to prepare a 100.0 mL[†] stock in 50.0 mM citrate buffer, pH 3.0.

Non-quinolines	Molecular Mass (g.mol⁻¹)	Concentration (mM)	Mass (mg)
nQ-KW16	316.35	0.15	4.8
nQ-KW17	374.17	0.05	1.9
nQ-KW23	361.35	0.10	3.6
nQ-KW31	319.32	0.50	16.0
nQ-KW32	374.44	0.10	3.7
nQ-KW33	348.36	0.10	3.5

[†] The volume can be adjusted according to the amount needed for a specific experiment and according to the actual amount available of each compound.

4.2.1.2 Non-Quinoline Activity Studies

Studies were carried out to determine the IC_{50} value for each non-quinoline compound in the lipid-water interface system. In these experiments, the incubation time was fixed, while the concentration of the β-haematin inhibitor was varied.

The procedure described in section 3.2.1.2 was followed to investigate the activity of the non-quinoline compounds, however, due to limited quantities of each compound provided, triplicate studies could not be repeated three times for all of the compounds as before.

4.2.1.3 Non-Quinoline Kinetics Studies

Kinetics studies were carried out in order to determine the K_{ads} value for each non-quinoline compound in the lipid water interface system. In these experiments, the incubation time, as well as the concentration of each β-haematin inhibitor, were varied in order to obtain a full profile for each compound.

The procedure described in section 3.2.1.5 was followed to investigate the kinetics of β-haematin formation in the presence of the non-quinoline compounds, however, due to limited quantities of each product provided, triplicate studies could not be repeated three times for all of the compounds.

4.2.2   Results

4.2.2.1 Solubilising Non-Quinoline β-Haematin Inhibitors

Owing to the poor solubility of the non-quinoline compounds in the aqueous buffer system (pH 4.8), it was necessary to optimize the solvent environment of the assay further to accommodate these compounds in the system. Two benzamide compounds, nQ-KW23 and nQ-KW32, were used in solubility tests to investigate their behaviour in different solvent systems.

Initially, attempts were made to dissolve the compounds in the 1:9 acetone: methanol solution and introduce them into the system in a similar manner as MQ. However, after a short incubation period, the compounds precipitated out of the buffer solution. Owing to the greater hydrophobicity of non-quinoline compounds, an alternative option was to dissolve the compounds in organic solvents. Compounds were dissolved in either DMSO or acetonitrile (ACN) and added to the aqueous citrate buffer in varying ratios (20:80, 30:70, 40:60, 50:50, 60:40). Multiple solubility tests, which included and excluded the inhibitor, were investigated at room temperature after an hour, and at 37 °C after 15 hours, respectively, to investigate the solubility of the buffer and the compounds in these solutions. Interestingly, the two compounds behaved similarly (Table 4.2). The only solutions in which the compounds did not precipitate out after 15 hours, was the 40:60, 50:50 and 60:40 ACN: buffer solutions. To investigate the effects of the change in solvent compositions on β-haematin inhibition, free base CQ (CQ_{fb}) was employed as a standard. CQ_{fb} was dissolved in the solvent containing the

lowest quantity of organic solvent (40:60) and its ability to inhibit β-haematin was evaluated. The results were, however, irreproducible and were inconsistent with the findings obtained in the absence of ACN. Alternatively, a different approach was required.

Table 4.2 Solubility tests using nQ-KW23 and nQ-KQ32. Investigating different organic solvent: buffer ratios as possible solvent systems for non-quinoline compounds.

	DMSO: Buffer				ACN: Buffer			
	At room Temp, 1h		At 37 °C, 15 h		At room Temp, 1h		At 37 °C, 15 h	
	W/o inhib.	W inhib.	W/o inhib.	W inhib.	W/o inhib.	W inhib.	W/o inhib.	W inhib.
20:80	✓	x	✓	x	✓	x	✓	x
30:70	✓	x	✓	x	✓	x	✓	x
40:60	✓	x	✓	x	✓	✓	✓	✓
50:50	✓	✓	✓	x	✓	✓	✓	✓
60:40	✓	✓	x	x	✓	✓	✓	✓

Control samples without (W/o) an inhibitor (inhib) were also included to monitor the effect of possible buffer precipitation out of solution. W: with. ✓: Soluble. x: Insoluble

Subsequently, it was considered that a change in the pH of the aqueous citrate buffer may improve the solubility of the benzamide compounds. This hypothesis was made on the basis of the computed pKa values which indicated that the compounds would be cationic at pH values lower than 3.[162] Upon heating and decreasing the pH to 3.0, acidifying the aqueous environment, the benzamide compounds were able to solubilise more readily in the aqueous system. Owing to previous pH-dependence studies of β-haematin formation at the lipid-water interface,[74] kinetics studies in the absence of an inhibitor were carried out in order to investigate the effect of the lowering in the pH on the formation of β-haematin. Under these conditions, the yield of β-haematin in the absence of an inhibitor was found to be the same as in the original approach (pH 4.8). Interestingly, however, a further decrease in the rate of β-haematin formation was observed, with the rate decreasing from 0.02 ± 0.001 min^{-1} to 0.01 ± 0.001 min^{-1} (Figure 4.1)
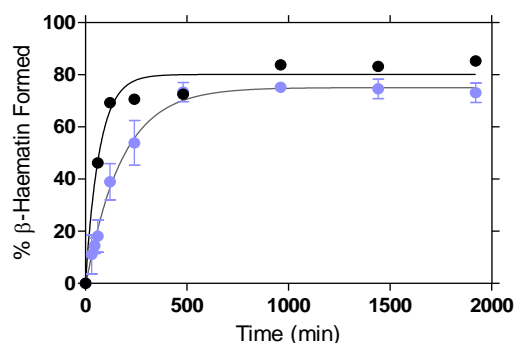
Figure 4.2 The effect of pH on the kinetics of β-haematin formation (in the absence of an inhibitor) in the lipid-water interface system. Curves for pH 4.8 (●) and pH 3.0 (●) were obtained. The observed rate constants are 0.02 ± 0.001 min^{-1} and 0.01 ± 0.001 min^{-1}, respectively.

4.2.2.2 Non-Quinoline Activity Studies

Similarly to the quinoline-based inhibitors, inhibitor activity studies were performed independently of the kinetics studies to determine the IC_{50} value for each non-quinoline compound (section 3.2.1.2). The dose-response curves for the inhibition of β-haematin formation by the benzamide β-haematin inhibitors are shown in Figure 4.2.
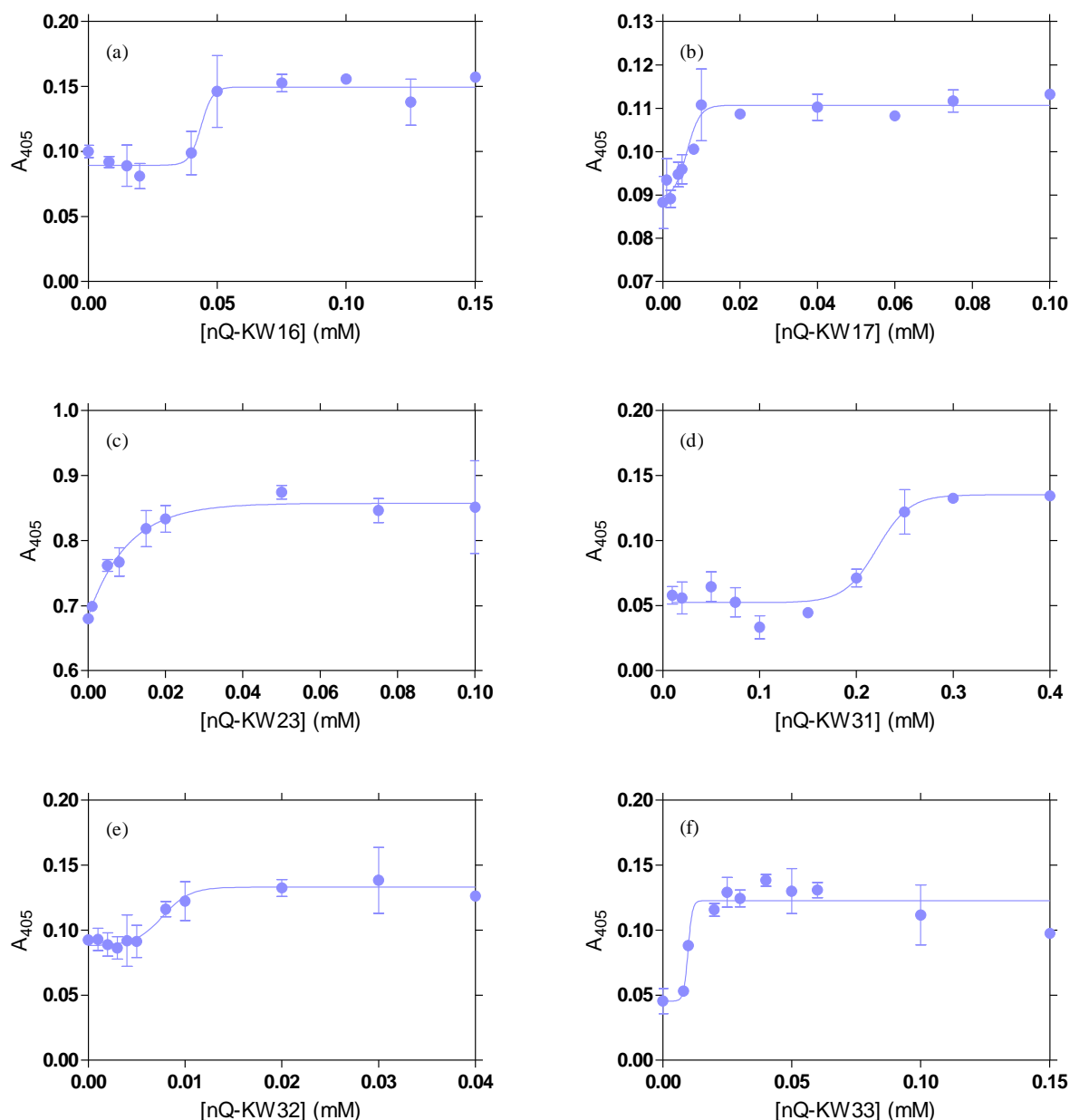
Figure 4.2 The inhibition of β-haematin formation by non-quinoline inhibitors at the lipid-water interface. Dose-response curves were determined in activity studies after a four-hour incubation period as a function of increasing inhibitor concentration for the benzamides (a) nQ-KW16, (b) nQ-KW17, (c) nQ-KW23, (d) nQ-KW31, (e) nQ-KW32 and (f) nQ-KW33. The IC_{50} value of each non-quinoline inhibitor is determined by fitting the data either to a sigmoidal (a, b, d, e and f) or a hyperbolic (c) function.

The observed IC_{50} values for each inhibitor (Table 4.3) were determined by fitting the data either to a sigmoidal or a hyperbolic function. Five of the benzamide compounds, namely nQ-KW16, -KW17, -KW31, -KW32 and –KW33, yielded a good sigmoidal fit with r^2 values of 0.65, 0.69, 0.71, 0.66 and 0.76, respectively, while the data obtained for nQ-KW23 fit to a hyperbolic function with an r^2 value of 0.64. In all six cases, an increase in the absorbance at 405 nm is observed as a function of increasing inhibitor concentration. As before, an increase in the concentration of an inhibitor is expected to inhibit the conversion of free Fe(III)PPIX into β-haematin, and hence an increase in the concentration of free Fe(III)PPIX, measured as the bis-pyridyl complex, is observed.

Table 4.3 IC_{50} values obtained for the inhibition of β-haematin formation by non-quinoline compounds in the lipid-water interface system and those determined previously in NP40 and against the NF54 strain.[163]

Non-Quinolines	24-Well Plates (µM)	NP40-detergent (µM)	Bio. Activity NF54 (µM)
nQ-KW16	43.8 ± 4.9	506.9 ± 32.6	9.09 ± 3.94
nQ-KW17	6.2 ± 1.4	9.05 ± 0.69	0.57 ± 0.14
nQ-KW23	7.0 ± 2.7	6.99 ± 0.23	1.35 ± 0.15
nQ-KW31	221 ± 16	260.3 ± 7.2	313 ± ND
nQ-KW32	7.7 ± 0.9	13.25 ± 0.70	1.61 ± 0.16
nQ-KW33	9.8 ± 0.6	22.18 ± 1.44	3.04 ± 0.46

Error calculated as standard error of the mean (SEM), following at least two experimental repeats, each including triplicate data points.

The IC_{50} values were compared to the activities previously-determined *in vitro* in the NP40 detergent-mediated assay,[163] in order to further validate the newly-optimized lipid assay. A linear correlation with an r^2 value of 0.96 was obtained (Figure 4.3), however, the correlation excludes the IC_{50} data for nQ-KW16 (circled in purple). This compound appeared to be extremely inactive in the NP40 system, however, owing to its moderate biological activity, it was selected for testing in the lipid-water interface system where it was also observed to be moderately active.
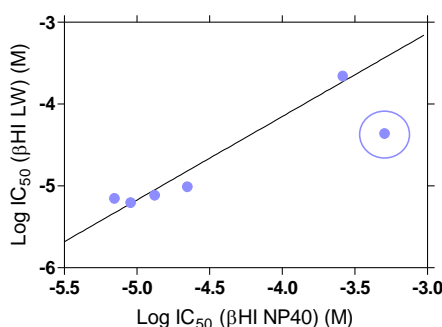
Figure 4.3 Investigating the inhibition of β-haematin formation by non-quinoline inhibitors in the lipid-mediated system. The correlation between the observed IC_{50} values compared to previously determined IC_{50} values in the NP40 detergent-mediated assay[163] (the trend excludes the IC_{50} data for nQ-KW16). $r^2 = 0.96$.

The biological activity of each compound against the NF54 parasite strain was determined by our collaborators who provided the benzamide compounds for this study.[163] When comparing the observed IC_{50} values obtained in the lipid-water interface system to these biological values, a significant linear correlation is evident with an r^2 value of 0.95 (Figure 4.4). There is a good agreement between the experimental and biological activity of these compounds, validating the lipid-water interface system, using 24-well plates, even further for investigating inhibitors other than quinoline-based compounds.
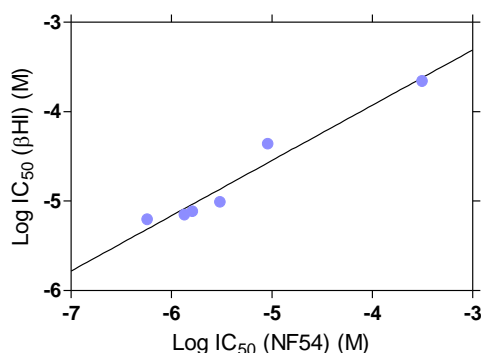
Figure 4.4 Investigating the inhibition of β-haematin formation by non-quinoline inhibitors in the lipid-mediated system. A linear correlation is observed between the observed IC_{50} values and the biological activity against a CQS parasite strain, NF54[163] with an r^2 value of 0.95.

4.2.2.3 Non-quinoline Kinetics Studies

This study is the first to investigate the effect of non-quinoline inhibitors on the lipid-mediated formation of β-haematin. Full kinetics profiles were collected for the formation of β-haematin in the presence of nQ-KW16, nQ-KW17, nQ-KW23, nQ-KW31, nQ-KW32 and nQ-KW33. Taking into account the proposed theoretical kinetic model, which is based on the premise that adsorption of an inhibitor onto the growing crystal face of β-haematin is important, it was possible to determine the equilibrium adsorption constants, K_{ads}, as well as the rate of β-haematin formation in the absence of an inhibitor, z, for each benzamide compound. The procedure outlined in section 3.2.1.6 was followed for the analysis of all kinetics data of each compound.

A comprehensive kinetics profile for each non-quinoline inhibitor is presented below, which includes the plot of the inverse of z_{obs} as a function of increasing drug concentration, fitted to Equation 1.4 (Figure 4.5, left panel), as well as the plot of the percentage β-haematin formed over time, fitted to Equation 3.1 (Figures 4.5, right panel). A table summarizing the calculated values for each compound is also provided (Tables 4.4).

Compound nQ-KW16 was shown to be the least active of the benzamides in the lipid-water system (IC_{50} = 43.8 μM, which is equivalent to 0.0438 mM), and a concentration range of 0.01 to 0.15 mM was considered. Lower concentration ranges were considered for the remaining non-quinoline inhibitors, which are more active than nQ-KW16.
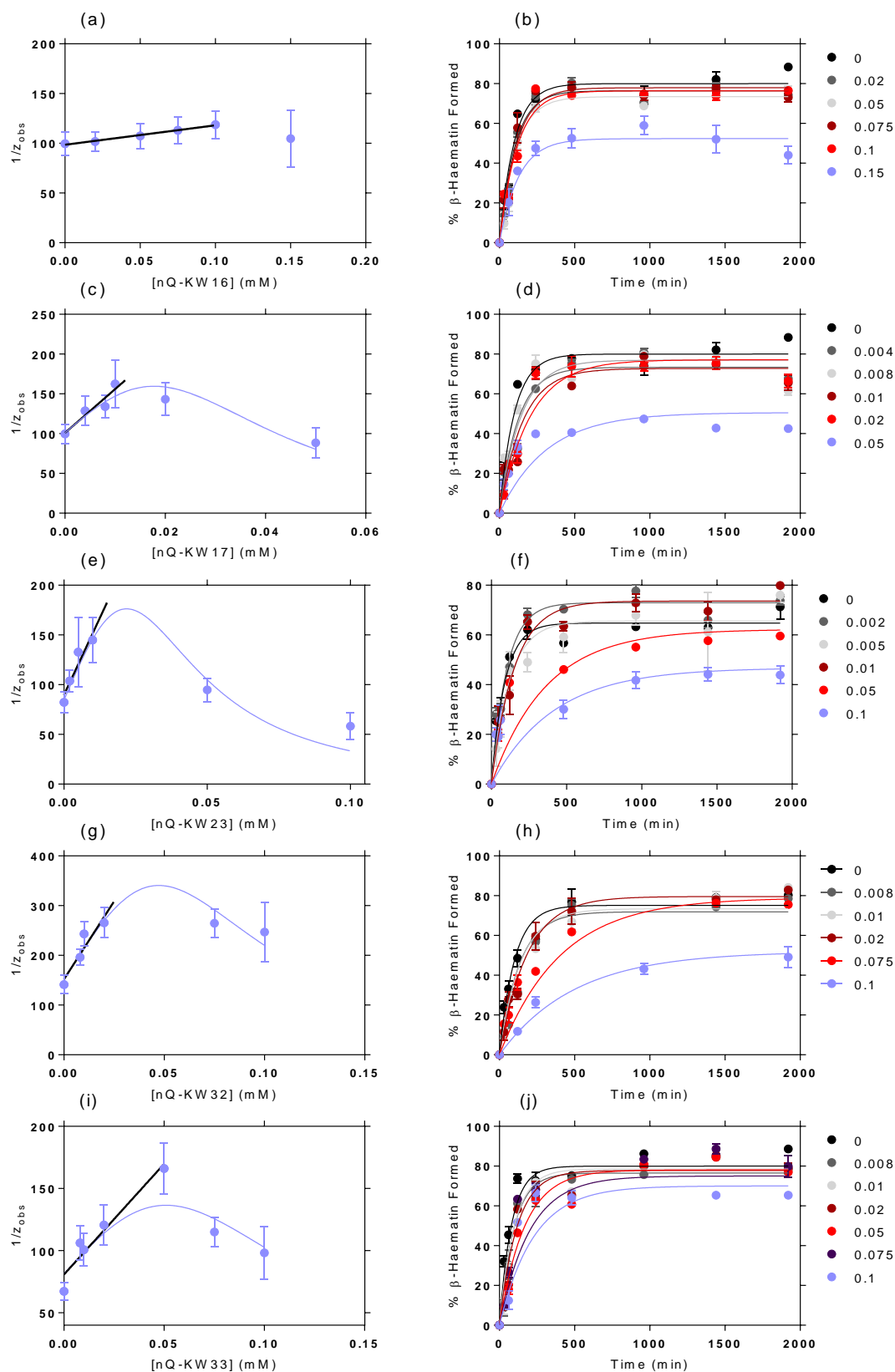
Figure 4.5 Kinetics of β-haematin formation in the presence of non-quinoline inhibitors. Left panel (a, c, e, g, i): a plot of the inverse of the rate constant, z_{obs}, as a function of increasing inhibitor concentration, yields a linear correlation (black line) at low concentrations from which the K_{ads} and z values were computed from the slope and y-intercept values. The best fit of the experimental data to Equation 1.4 is shown in purple. Right panel (b, d, f, h, j): kinetic traces fitted to Equation 3.1 observed in the absence and presence of increasing inhibitor concentrations.

The linear correlation (black line) and the best fit of the experimental data to Equation 1.4 (purple curve) shown in the left panel of Figure 4.5 (a, c, e, g and i), correspond to good r^2 values (0.99, 0.90, 0.90, 0.88 and 0.93) and (ND, 0.84, 0.80, 0.79 and 0.74), respectively, for each of the non-quinoline inhibitors. The experimental data for nQ-KW16 (in a) was not fit to Equation 1.4 owing to insufficient amount of data points. The kinetic traces fitted to Equation 3.1 in the right panel of Figure 4.5 (b, d, f, h and j) also correspond to good r^2 values for each inhibitor at each respective concentration. The r^2 values for these traces are between 0.87-0.97, 0.60-0.95, 0.42-0.95, 0.89-0.94 and 0.78-0.95 for nQ-KW16, -17, -23, 32 and -33, respectively.

Table 4.4 The best fit values to the theoretical kinetic model for β-haematin formation in the presence of benzamide β-haematin inhibitors, nQ-KW16, nQ-KW17, nQ-KW23, nQ-KW32 and Q-KW33 in 24-well plates.[†]

Non-quinolines	Slope (min.mM^{-1})	Intercept (min)	z (min^{-1})	k_2	K_{ads} (mM^{-1})	Log K_{ads} (M^{-1})
nQ-KW16	195.2 ± 12.0	98.5 ± 0.7	0.010 ± 0.001	0.0015	1.98 ± 0.12	3.30 ± 0.10
nQ-KW17	5507 ± 1294	100.9 ± 8.7	0.010 ± 0.001	0.2000	54.6 ± 13.7	4.74 ± 0.40
nQ-KW23	6179 ± 1488	89.7 ± 8.5	0.011 ± 0.001	0.1000	68.9 ± 17.8	4.84 ± 0.41
nQ-KW32	6275 ± 1649	152.0 ± 19.6	0.010 ± 0.001	0.0055	41.3 ± 12.1	4.62 ± 0.47
nQ-KW33	1782 ± 275	80.8 ± 6.8	0.012 ± 0.001	0.0300	22.1 ± 3.9	4.34 ± 0.28

[†]Error calculated as standard error of the mean (SEM), following at least two experimental repeats, each including triplicate data points.

As was the case for the quinoline-based β-haematin inhibitors, it was observed that the rate of β-haematin formation in the absence of an inhibitor, z, was the same for all non-quinoline compounds. The value of z in all five cases is approximately 0.01 min^{-1}, which interestingly is lower than that of the quinoline-based compounds, however, this observation is due to the lower pH (3.0) of the aqueous buffer used in this section of the studies, compared to the quinoline inhibitors. The value of the rate constant for the proposed competing precipitation process, k_2, as mentioned previously, could take on a wide range of values, however, the reported values above were chosen in order to generate good fits to the theoretical model for each inhibitor, respectively. For the non-quinoline compounds, k_2 varied between values of 0.0015 and 0.20. There is no significant relationship observed between the k_2 and K_{ads} values of the non-quinoline compounds. Important relationships are observed between the K_{ads} values of the non-quinoline compounds and their respective IC$_{50}$ values determined in the previous section, as well as interesting relationships with the quinoline inhibitors. These relationships are discussed in the following two sections.

4.2.3 Relationships between Drug Activity and Strength of Adsorption

After performing both activity- and kinetic studies with the benzamide non-quinoline inhibitors at the lipid-water interface, the relationship between the observed IC_{50} and K_{ads} values was investigated. A linear correlation, with an r^2 value of 0.98 was obtained (Figure 4.6 (a)), which strongly suggests that the strength of inhibitor adsorption to the growing β-haematin crystal is directly related to its inhibition activity in this biomimetic system. This relationship supports the proposed hypothesis that the more active a compound, the stronger it will adsorb to the β-haematin crystal face.

The K_{ads} values were also correlated with the biological activity data reported against the NF54 parasite strain,[163] which yielded a linear regression, with an r^2 value of 0.82 (Figure 4.6 (b)). This correlation indicates a good agreement between the biological and experimental data. Both of these correlations are significant with a P value smaller than 0.05. These correlations are in agreement with those observed for the quinoline-based inhibitors, suggesting that all three groups of inhibitors investigated in this project might conform to the same mechanism of action when inhibiting the formation of β-haematin *in vitro*. This in turn might be related to the biological mechanism for haemozoin inhibition. In the following section the correlations between all three sets of compounds are discussed.
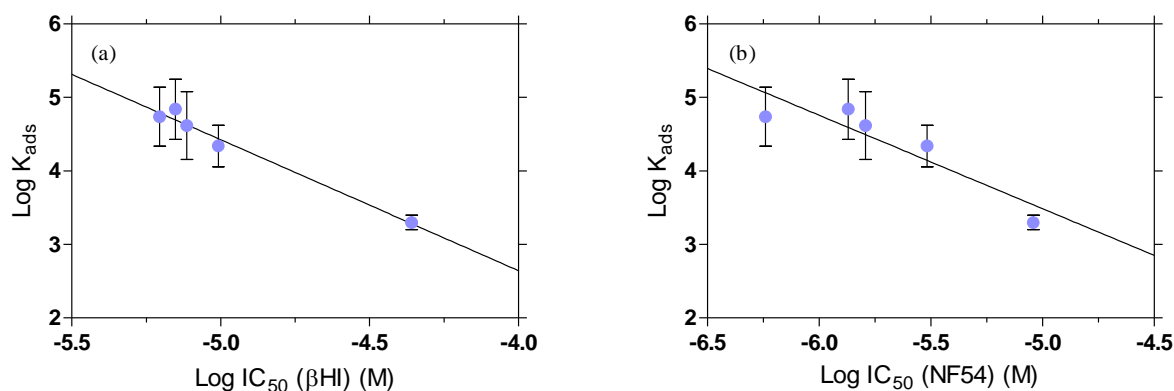
Figure 4.6 Important correlations observed for non-quinoline β-haematin inhibitors. The linear correlations between the observed K_{ads} values and (a) the IC_{50} values determined in the lipid-water system and (b) the biological IC_{50} values previously-determined against the NF54 parasite strain.[163] The r^2 values are 0.98 and 0.82, respectively, with $P < 0.05$ in both cases.

4.3 Combining Quinoline- and Non-quinoline-based β-Haematin Inhibitors

In an attempt to address the question whether a single mechanism of action exists for β-haematin inhibitors, the data for non-quinoline inhibitors were combined with the results obtained for the quinoline inhibitors in the previous chapter. A direct relationship between the respective K_{ads} and IC_{50} values determined in the lipid-mediated system for each individual set of inhibitors (Figure 4.7 (a)) was obtained. Significant linear correlations, with r^2 values of 0.78 and 0.98, are observed between the K_{ads} values and the IC_{50} values obtained in the lipid-water interface system for the quinoline and non-quinoline inhibitors, respectively. Interestingly, however, it is observed that the data for the two families fall on separate lines. Furthermore, some of the quinoline and non-quinoline inhibitors are observed to have nearly identical IC_{50} values, yet distinctly different K_{ads} values. This suggests that certain non-quinoline compounds may be equally active with regards to their β-haematin inhibitor activity, yet adsorb to a lesser extent to the crystal surfaces than some quinoline compounds. This observation suggest that these two classes of compounds may behave differently after all.

Subsequently, the K_{ads} value for each compound was compared with the corresponding biological activities reported against the NF54 parasite strain.[160,163] Considering the quinoline antimalarial and non-quinoline inhibitors separately, two linear correlations were obtained with r^2 values of 0.68 and 0.82, respectively (Figure 4.7 (b)). A significant linear correlation is also obtained, however, when considering both classes of compounds as a single group ($r^2 = 0.68$, $P < 0.05$) (Figure 4.7 (b)). The short-chain chloroquine analogues could not be included in the correlation as they were not tested against the NF54 strain.
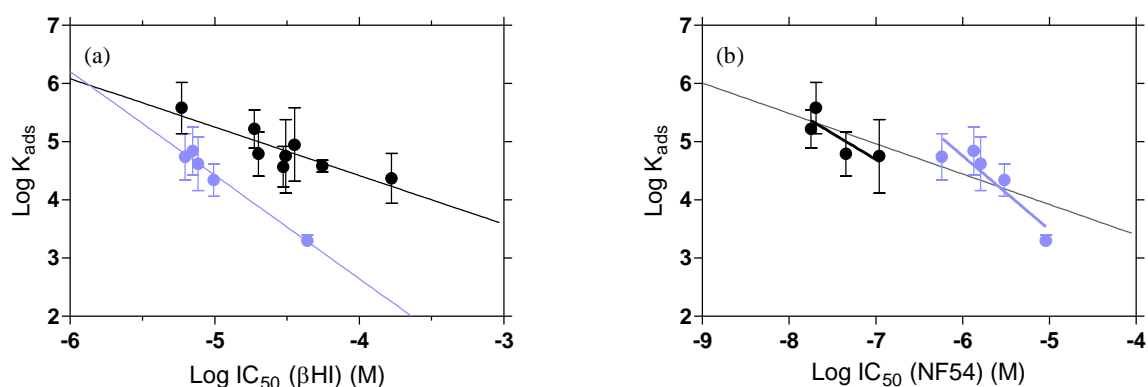
Figure 4.7 Important correlations observed between quinoline and non-quinoline inhibitors. (a) The linear correlations between the K_{ads} and the IC_{50} values obtained in the lipid-water system for the quinoline- (●) and non-quinoline inhibitors (●), with r^2 values of 0.79 and 0.98, respectively. (b) The linear correlations between the obtained K_{ads} values and the biological activity previously-determined against the NF54 parasite strain[160,163] for the antimalarial (●) and non-quinoline inhibitors (●), with r^2 values of 0.61 and 0.81, respectively.

When the antimalarial drugs and the non-quinoline inhibitors are considered as one group, no significant correlation is observed between the β-haematin inhibitory activities and the NF54 biological activities for these compounds (Figure 4.8). A relationship can, however, be observed when the two groups of compounds are investigated separately.
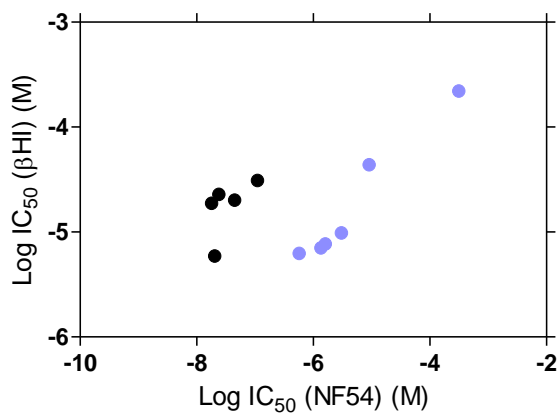
Figure 4.8 No correlation is observed between the IC_{50} values obtained in the lipid-water interface system and the NF54 biological activities[160,163] for the antimalarial drugs (●) and the non-quinoline inhibitors (●), when they are considered as a group of compounds.

4.4 Discussion

The aim of the work presented in this chapter is directly related to that of the work reported in the previous chapter, namely to investigate the inhibition of β-haematin formation, however, by introducing non-quinoline inhibitors into the lipid-water interface system. The introduction of other β-haematin inhibitors, which are structurally different to those possessing a quinoline moiety, into the system was considered, since parasite resistance to known quinoline-based antimalarial drugs has increased in recent years.[161] Chemically-distinct compounds possessing the same mode of action are attractive as new antimalarial drug candidates and are thus investigated in this study. This is the first study carried out in order to investigate the effects of benzamide inhibitors on the kinetics of β-haematin formation in the lipid-mediated system.

Owing to their poor solubility in aqueous medium, the newly-optimized assay was further modified to facilitate the incorporation of the benzamide non-quinoline compounds into the aqueous citrate buffer system. To readily solubilise the compounds in the aqueous solvent, the pH was lowered to 3. Hoang *et al.*[74] has previously determined the pH dependence of β-haematin formation in the lipid-water interface system and recorded a bell-shaped curve, indicating maximum β-haematin production between pH 3 and 4. This aided the decision to lower the pH, since optimal β-haematin formation was still expected, and subsequently confirmed, in the biomimetic system.

In order to probe their relative β-haematin inhibitory activities, independent activity studies were carried out with a series of benzamide β-haematin inhibitors in the newly-optimized system. Again, as previously noted for the quinoline inhibitors, some of the inhibitors conform to a sigmoidal dose-response curve, while others conform to a hyperbolic dose-response curve. In this case, only one benzamide compound, nQ-KW23, fits to a hyperbolic function, suggesting that a four-hour incubation time may simply be too short of a time for nQ-KW23 to inhibit β-haematin formation, compared to the other compounds for which a four-hour incubation time may be enough or too long.

A significant relationship is observed between the IC_{50} values obtained in the current lipid-water interface system and the NP40 detergent-mediated system (Figure 4.3), justifying the relevance of lipid-mediated systems, which are biologically more relevant in which to investigate β-haematin inhibition. The obtained IC_{50} values show a good correlation to what has previously been reported against the CQS NF54 parasite strain (Figure 4.4). This indicates that the lipid-mediated assay is an efficient system in which inhibitor activity can be determined. The relative β-haematin inhibitory activity of each compound is similar in the three systems (lipid-water, NP40 and biological); it was found that nQ-KW17 is the most active inhibitor, while nQ-KW31 is the least active inhibitor in the series. An IC_{50} value of 221 ± 16 µM was obtained for nQ-KW31 within the lipid-water interface system, indicating the inactive nature of this compound as a β-haematin inhibitor. This is in agreement to what has been reported for nQ-KW31 against the CQS NF54 parasite strain and in the NP40 detergent-mediated system. Interestingly, the IC_{50} value obtained for nQ-KW16 is not in agreement with what was previously obtained in the NP40 detergent-mediated system. It was found that the inhibitor is moderately

active in the lipid-mediated system, however, it was reported to be completely inactive in the NP-40 detergent-mediated system. This suggests that the lipid-mediated system is ultimately a better biomimetic system, when comparing the activity to what has been obtained against the NF54 parasite strain.

Furthermore, kinetics studies were carried out in the lipid-mediated system in order to investigate the effect of each non-quinoline compound on the formation of β-haematin. A decrease in the rate of β-haematin formation is observed as the inhibitor concentration was systematically increased. This observation may be accounted for by the reversible adsorption process of the inhibitor to the surface of β-haematin crystals, decreasing the rate of formation, rather than inhibiting it completely. A noticeable decrease in the yield of β-haematin formation is observed at high inhibitor concentrations for nQ-KW16, nQ-KW23 and nQ-KW32. The noticeable decrease in the yield of β-haematin is not observed for the other inhibitors, suggesting that a higher inhibitor concentration might be required in order for the proposed precipitation of the inhibitor-haematin complex to become evident. The observed decrease in the percentage yield of β-haematin formation may be accounted for by a Fe(III)PPIX-inhibitor complex forming in solution.[117,118] This may suggest that the inhibitors which show this noticeable decrease in the yield may form precipitation complexes with the free haematin more rapidly than other inhibitors. Upon fitting the inverse of the observed rate constants as a function of increasing inhibitor concentration, the respective K_{ads} and z values are determined for each inhibitor. The rate constant in the absence of an inhibitor is identical for all the non-quinoline inhibitors, with z values equal to ≈ 0.01 min^{-1}, which is feasible, since z is independent of the inhibitor under similar system conditions. The rate constant is, however, lower in the pH 3 aqueous citrate buffer compared to the pH 4.8 buffer system, in which the quinoline-based inhibitors were investigated

The experimental kinetics data recorded in this study conform to the proposed theoretical kinetic model, suggesting that the model is valid for inhibitors other than only quinoline-based inhibitors. Similar to the quinoline inhibitors, the K_{ads} and z values were determined from the linear regression analysis, and used for the best fit to the model. Accurate values for k_2, the rate constant for the competing process that results in the precipitation of haematin, were not investigated in the current study, since this process is still poorly understood. The k_2 values were thus allowed to refine freely to generate the best fit of the experimental data to the model. The k_2 value can generally accommodate a range of values and is the only parameter that was allowed to vary in order to generate good r^2 fits. In the current study, k_2 was varied in a broad range between 0.0015 and 0.20 for the benzamide non-quinoline inhibitors.

A significant linear correlation, with an r^2 value of 0.98 (P value < 0.01) is observed between the adsorption constants (K_{ads}) and the β-haematin inhibitory activities (IC$_{50}$) obtained for the non-quinoline β-haematin inhibitors (Figure 4.6 (a)). It was found that nQ-KW23 has the largest K_{ads} value of the all the non-quinoline inhibitors, however, it was expected that nQ-KW17, the most active inhibitor, to have the largest adsorption constant. These respective K_{ads} values are close to each other in magnitude (68.9 ± 17.8 compared to 54.6 ± 13.7 mM^{-1}), however, the log K_{ads} values only deviate by 0.1 log units from each other, resulting in the good linear correlation. nQ-KW16, which was found to be the least active benzamide inhibitor in the lipid-mediated system, obtaining an IC$_{50}$ value seven times larger than that of nQ-KW17, was found to have the weakest

91

adsorption constant, $K_{ads} = 1.98 \pm 0.12$ mM^{-1}. Similar to the quinoline inhibitors, this significant correlation suggests that the strength at which this group of non-quinoline inhibitors may adsorb to the surface of β-haematin crystals, inhibiting further growth, is associated with its β-haematin inhibitory activity, in the lipid-water interface system.

Another significant linear correlation, with an r^2 value of 0.82 (P value < 0.04) is observed when considering the relationship between the K_{ads} values obtained from the lipid-mediated system and previously-determined biological β-haematin inhibitory activities reported against the CQS NF54 parasite strain. Subsequently, the adsorption-activity correlation for this group of non-quinoline compounds is evident and correlating this to the observations made in the lipid-mediated system, it further suggests that the biological mechanism of haemozoin inhibition by non-quinoline-based inhibitors, might also be *via* adsorption.

Irrespective of the individual correlation observed between the K_{ads} and the IC$_{50}$ values of each set of quinoline- and non-quinoline-based β-haematin inhibitors, it is important to consider the two groups of β-haematin inhibitors together. Figure 4.7 shows two plots in which the following correlations were investigated: the K_{ads} and IC$_{50}$ values obtained in the lipid-mediated system for both sets of quinoline-and non-quinoline-based inhibitors (a) and the K_{ads} values obtained in the lipid-mediated system against the biological CQS NF54 parasite strain for the antimalarial drugs and non-quinoline-based inhibitors (b). The IC$_{50}$ values obtained in the lipid-mediated system against the biological CQS NF54 parasite strain for the antimalarial drugs and non-quinoline-based inhibitors Figure 4.8.

Even though the linear trends for each individual set of inhibitors are good, an important observation is made regarding the β-haematin inhibition mechanism of action by these compounds. Three fundamentally important observations are; firstly, there is indeed a significant correlation between the obtained K_{ads} values and the biological activities determined against the CQS NF54 parasite strain, when considering the antimalarial drugs and non-quinoline-based inhibitors together (Figure 4.7 (b), r^2 value of 0.68). This suggests that the inhibitor concentration required to inhibit haemozoin formation by 50%, is dependent on the specific strength of adsorption of a specific inhibitor to a haemozoin crystal surface. Secondly, when considering the plot of the observed IC$_{50}$ values against the biological activities determined against the CQS NF54 parasite strain for the same group of inhibitors, the antimalarial drugs and non-quinoline-based inhibitors, no correlation is observed (Figure 4.8) There is, however, separate correlations for the two individual inhibitor families, however, the data points are completely random when they are considered together. These observations are contradictory towards each other, since both the β-haematin inhibitory activity and the K_{ads} values were determined in the same biologically relevant, lipid-mediated system. Thirdly, it is interesting to notice that there are compounds which have virtually the same β-haematin inhibitory activity, however, their respective K_{ads} values differ greatly from each other (Figure 4.7 (a)). As an example, AQ and nQ-KW17 both possess similar log IC$_{50}$ values; -5.23 and -5.21, respectively, however, their K_{ads} values differ more than seven-fold; 384 ± 105 mM^{-1} and 54.6 ± 13.7 mM^{-1}, respectively. Similarly, the K_{ads} value for Q-I is nearly forty-five-fold larger than that of nQ-KW16, however, they were found to have similar β-haematin inhibitory activity. There are consequently inhibitors that adsorb stronger than others, however, their relative β-haematin inhibitory activity is the same.

These observations raise further questions in understanding β-haematin inhibiting compounds and their mode of action by which they inhibit β-haematin formation, since these compounds appear to behave differently when they are compared together as a group of β-haematin inhibitors.

When considering the main kinetic model, Equation 1.2, which explains the effect of an inhibitor on the formation of β-haematin,[40] it is evident that there are two factors, namely K_{ads} and k_2, that may contribute to individual inhibitors possessing the same IC_{50} value. In an attempt to rationalize the interplay between these two factors, arbitrary values were chosen initially for z, K_{ads} and k_2 in the kinetic model. A series of curves are obtained for the percentage β-haematin formation as a function of time (Figure 4.9 (a)). The decrease in the rate and overall yield of β-haematin formation are observed as previously described; the decrease in rate being accounted for by the adsorption of an inhibitor to the β-haematin crystal surface and the decrease in the yield being attributed to the proposed irreversible precipitation of a Fe(III)PPIX-inhibitor complex. When the IC_{50} value for β-haematin inhibition is measured, essentially the expected percentage inhibition of β-haematin at a specific time point as a function of drug concentration is investigated. It is possible therefore to predict a dose-response curve from the kinetics profile by examining expected yields at a particular time point, as a function of drug concentration. The dose-response curve obtained from the original set of kinetics traces at a specific time point yields a specific IC_{50} value (Figure 4.9 (b)).

However, by increasing the arbitrary value for K_{ads} ten-fold, and keeping z and k_2 constant, another series of curves are obtained (Figure 4.9 (c)). It is evident that the rate of β-haematin formation slows down more dramatically with increasing inhibitor concentration. Likewise, a dose-response curve obtained from the set of curves, at a specific time point, as a result of increasing K_{ads}, thus also yields a specific IC_{50} value (Figure 4.9 (d)). If K_{ads} is increased ten-fold, however, less of the inhibitor is needed to inhibit β-haematin formation by 50% and the IC_{50} value is expected to be lower. Indeed this is the case if the two theoretical data sets are compared with one another.

By increasing the original arbitrary value of k_2 five thousand-fold, hence rapid precipitation of the Fe(III)PPIX-inhibitor complex, and keeping the original values for z and K_{ads} constant, another series of curves, different from the original, are obtained (Figure 4.9 (e)). A more distinct decrease in the overall yield of β-haematin formation is observed after each addition of inhibitor concentration. Measuring the IC_{50} value at the same time point, a predicted dose-response curve is obtained (Figure 4.9 (f)). In both cases (Figure 4.9 (d) and Figure 4.9 (f)), β-haematin formation is inhibited by at least 50% after the fourth addition of the inhibitor.

Another interesting observation is made when the dose-response curves obtained after increasing K_{ads} and k_2, respectively, are compared to the original. The slight sigmoidal-shaped dose-response curve changes in shape to a less sigmoidal function, and rather fits a hyperbolic function. This suggests that the incubation time may not be exclusively responsible for the shape of the respective dose-response curves, however, this, along with the rate of precipitation, k_2, should be investigated further.
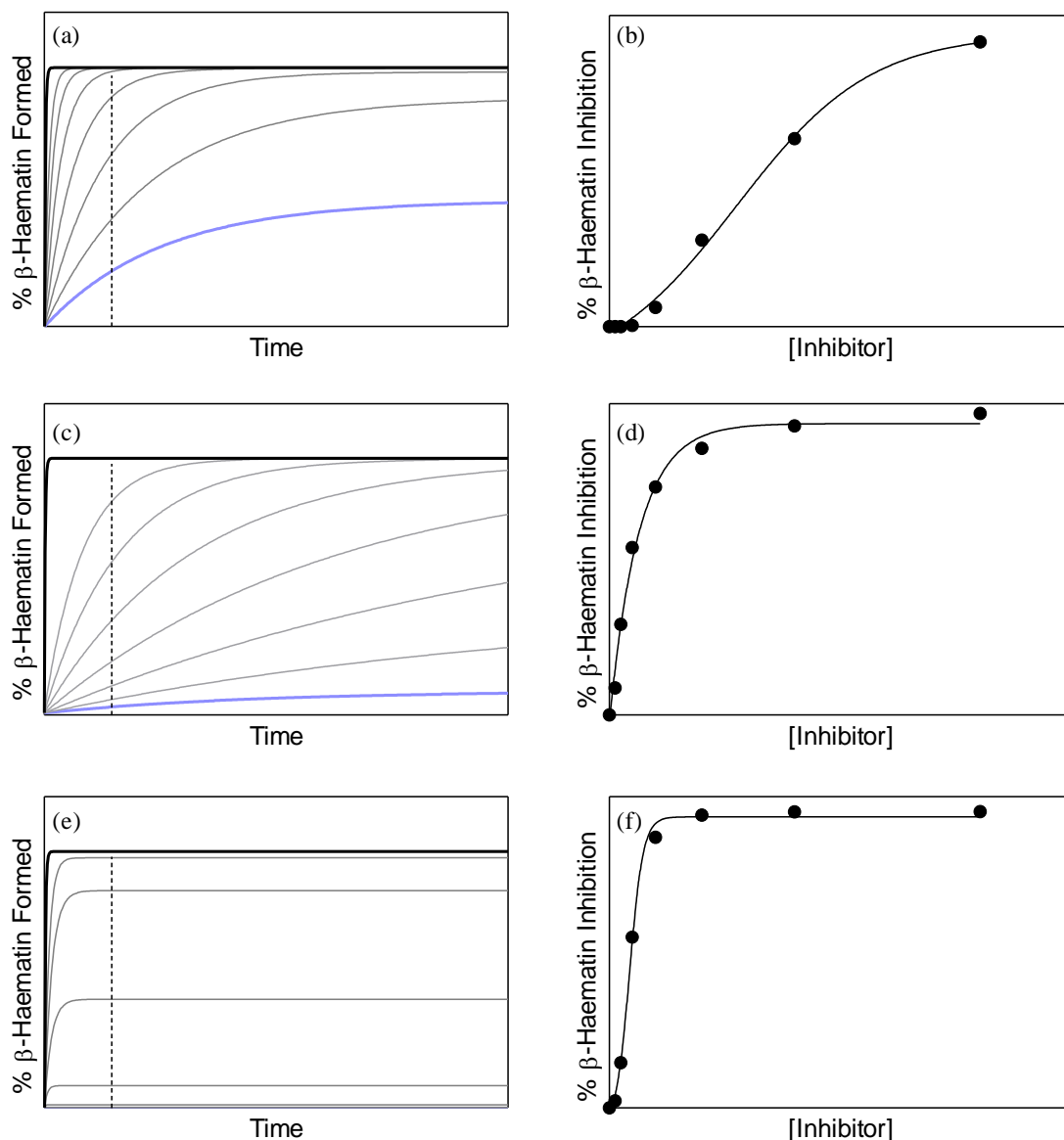
Figure 4.9 The kinetic behaviour of β-haematin formation explained by the theoretical model (Equation 1.2). Left panel: percentage β-haematin formed over time. Arbitrary values for z, K_{ads} and k_2 yields a series of curves (a). By increasing K_{ads} ten-fold, a rapid decrease in the rate of formation can be observed (c) and by increasing k_2 five thousand fold, compared to the original arbitrary value, a significant decrease in the β-haematin formation is observed in the series of curves (e). Right panel: dose-response curves. The IC$_{50}$ values in all three cases are obtained from the predicted dose-response curves (b, d and f), by slicing through the curves in (a), (c) and (e) at a specific time point (broken lines).

An extremely important realisation is evident when plotting the percentage β-haematin inhibition against the log of the inhibitor concentration in each of the above cases and overlaying the resultant dose-response curves. In the one case the value of K_{ads} was increased (black curve), while in the other, the value of k_2 was increased (purple curve), however, the same IC$_{50}$ value is obtained in both cases (Figure 4.10). The broken line indicates the actual IC$_{50}$ value at β-haematin inhibition by 50%, and it is evident from the two points overlaying each other, that these IC$_{50}$ values are in close proximity to each other.

94
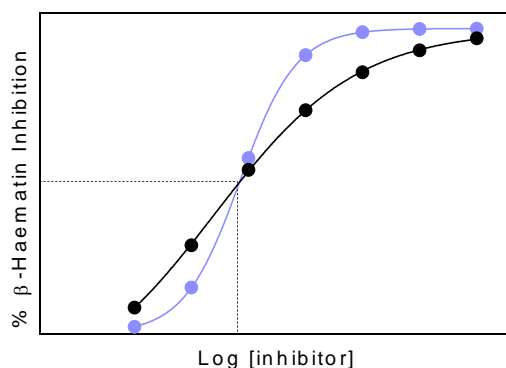
Figure 4.10 Overlapping the dose-response curves obtained in both cases with increasing K_{ads} (●) and increasing k_2 (●), respectively, yields virtually the same IC_{50} values.

There are thus two reasons that account for individual inhibitors possessing the same IC_{50} values; either via strong inhibitor adsorption (K_{ads}) or rapid precipitation of the Fe(III)PPIX-inhibitor complex (k_2). This is possibly the rationale behind the observations which were made in the study regarding certain inhibitors that adsorb stronger than others with the same β-haematin inhibitory activity in the lipid-mediated system. The individual two factors, K_{ads} and k_2, are in turn determined by sub-factors, which are dependent on individual inhibitor families. K_{ads} is dependent on the extent of adsorption of an inhibitor onto the fastest growing face of the β-haematin crystal, which is currently being investigated computationally in order to better understand structure-activity relationships of β-haematin inhibitors. As mentioned previously in this study, the process of precipitation of a haematin-inhibitor complex is still poorly understood and requires further investigation.

Based on our knowledge from this aqueous system and method of β-haematin inhibition, it is considered that the extent of the solubility of an inhibitor may greatly contribute to the rate of the precipitation complex forming between Fe(III)PPIX and the respective inhibitor. It is thus crucial to investigate this further and will be discussed in more detail in Chapter 6.

4.5 Conclusion

The current, newly-optimized assay was further developed in order to investigate a wider set of β-haematin inhibiting compounds. Non-quinoline compounds of the benzamide series were introduced into the lipid-water interface system, by decreasing the pH of the aqueous buffer to 3. The inhibitory activity, as well as the effects on the kinetics of β-haematin formation, of these compounds was successfully investigated in the lipid-mediated system. A decrease in the rate of β-haematin formation in the absence of an inhibitor, compared to the rate in the pH 4.8 aqueous buffer system, was observed. Based on the results reported in this chapter, a similar observation to that of the quinoline-based inhibitors was made; an increase in the benzamide inhibitor concentration resulted in a decrease in the rate of β-haematin formation at low concentrations, while a decrease in the yield of β-haematin formation was observed when introducing higher doses of each inhibitor. The kinetics results are in agreement to what is predicted by the theoretical kinetic model and also suggest that β-haematin inhibitory activity may be related to the strength of adsorption of an inhibitor to the growing face of a β-haematin crystal. By introducing the non-quinoline compounds into the lipid-mediated system, and fitting the experimental kinetic data to the proposed kinetic model, provides further insight into understanding the β-haematin inhibition process. The validity of the model has been extended, since a set of both non-clinically related quinoline- and non-quinoline-based inhibitors has been introduced into the system. The results reported in this chapter further introduced thought-provoking information, which concerns quinoline and non-quinoline β-haematin inhibitors possessing virtually the same β-haematin inhibitory activity, however, appearing to adsorb stronger than one another. According to the theoretical kinetic model, it is evident that the IC_{50} values are dependent on both K_{ads} and k_2. A further understanding in the competing precipitation process of the inhibitor-Fe(III)PPIX complex is required to account for the behaviour of different β-haematin inhibitors. Additional kinetics studies, including different series of non-quinoline β-haematin inhibitors are also required to further extend the biological-relevant system of β-haematin inhibition. It is also important to investigate the adsorption of inhibitors to β-haematin independently, since kinetics alone cannot account for the proposed mechanism of action in β-haematin inhibition.

Chapter 5. Independent Adsorption Studies

5.1 Introduction

The results reported in the previous two chapters have provided considerable insight into understanding the possible mechanism of action of the inhibition of β-haematin formation, however, kinetics alone cannot account for this proposed chemical inhibition process occurring. These findings warranted further investigation, in which evidence for adsorption of inhibitors to β-haematin was independently confirmed. Direct adsorption studies have previously been investigated in our laboratory using two known antimalarial drugs, CQ and QD.[152] These studies were, however, time-consuming and were carried out as preliminary studies with little optimization. This motivated a more detailed investigation into the direct adsorption to the surface of pre-formed β-haematin crystals by known antimalarial drugs, AQ, CQ, QD and QN, and a short-chain CQ analogue, Q-CF$_3$. The method in which the direct adsorption studies are performed was optimized in order to investigate a greater number of inhibitors in a shorter period of time. By calculating the proposed amount of inhibitor adsorbed to the β-haematin crystals using Beer's Law, and considering the Langmuir Isotherm, which explains monolayer coverage of an adsorbent to a solid surface, the relative strength of adsorption of an inhibitor to β-haematin crystals, K, was determined for each compound respectively. This is the first detailed study to investigate the direct adsorption of four antimalarial drugs and a short-chain CQ analogue to the surface of β-haematin crystals, enabling one to obtain an actual adsorption value.

5.2 Experimental Methods

The methods in this section describe how the aqueous citrate buffer solution was prepared in order to investigate the adsorption of 4-aminoquinoline and quinoline methanol antimalarial drugs, as well as a short-chain CQ analogue, directly to pre-formed β-haematin crystals. The direct adsorption of CQ, AQ, QD, QN and Q-CF$_3$ was investigated, respectively.

5.2.1   β-Haematin Synthesis

5.2.1.1 Preparation of β-Haematin at the Lipid-Water Interface

Four Scott Duran crystallising dishes (internal diameter of 9 cm), containing 50.0 mL of the 50.0 mM sodium citrate buffer (section 2.5.1), and covered with tin foil, were pre-incubated in a water bath set at 37 °C for 30 minutes, during which time the lipid and Fe(III)PPIX solutions were freshly prepared. Solutions containing 1.0 mL of the lipid and 0.50 mL of the Fe(III)PPIX stock solutions (section 2.5.4 and 2.5.5) were premixed in a 2.0 mL Eppendorf tube, using micro pipettes. The 1.5 mL aliquots of lipid-Fe(III)PPIX solution were added dropwise to the pre-incubated buffer using a syringe with a needle diameter of 0.5 mm, yielding an interface between hydrophobic and hydrophilic regions after solvent mixing. Following an incubation period of 30 minutes, the contents of all four glass vessels were agitated to release the product into the bulk aqueous medium. The total volume (~206.0 mL) was distributed equally into 15 mL Falcon Greiner centrifuge tubes which were then centrifuged at 4000 rpm for 10 minutes. The supernatant was removed from the pellet, and discarded. The pellet was subsequently washed with 1.0 mL of the 5:45:50 (v/v) pyridine: aqueous buffer: acetone solution (section 2.5.9) to remove unreacted Fe(III)PPIX. The product was dried in a desiccator over phosphorus pentoxide for up to 52 hours before further analysis and use.[73]

5.2.1.2 Preparation of β-Haematin at the Pentanol-Water Interface

The same procedure as outlined in section 5.2.1.1 was followed to prepare β-haematin at the pentanol-water interface, however, as a lipid alternative, 10.0 mL of 1-pentanol were layered on top of the 50.0 mL aqueous buffer. Since the pentanol is not miscible with water, two layers form, to create the pentanol-water interface. The pentanol-water interface system is a model for the lipid system.[73] 1.0 mL of the Fe(III)PPIX solution was added dropwise to the pre-incubated pentanol-water interface system. Following the incubation period of 45 minutes, the solid material was collected by centrifugation and unreacted haematin was removed by washing the pellet with 1.0 mL of the 5:45:50 (v/v) pyridine: aqueous buffer: acetone solution. The remaining product was dried in a desiccator over phosphorus pentoxide for up to 52 hours before further analysis and use.[73]

5.2.2   Direct Adsorption Studies

Direct adsorption studies were carried out independently to the kinetics studies, to determine the extent to which a specific β-haematin inhibitor adsorbs to β-haematin. In contrast to the kinetics studies, these studies investigated the adsorption of inhibitors to pre-formed β-haematin crystals, rather than investigating the effect of the inhibitor on the real-time formation of β-haematin. In these experiments, the incubation time was fixed while the concentrations of all inhibitors were varied. A series of at least ten different inhibitor concentrations was prepared by diluting the inhibitor-containing stock solution with zero-drug citrate buffer (section 2.5.1) using calibrated micro-pipettes. These studies were conducted for four antimalarial drugs, AQ, CQ, QD and QN, as well as a short-chain CQ analogue, Q-CF$_3$.

All of the experiments were performed in 2.0 mL Eppendorf tubes, containing 1.0 mg of preformed β-haematin crystals (prepared from the pentanol-water interface, section 5.2.1.2). The β-haematin crystals were initially ground together to yield a homogenous sample of small crystallites and to increase the concentration of individual crystals over large clumps. Following the addition of 1.5 mL of inhibitor-containing citrate buffer (50 mM, pH 4.8) to each Eppendorf tube, the tubes were placed in a floating tray and allowed to incubate in an ultrasonic water bath at 37 °C, set on power level 2, for sixteen hours. Each concentration was measured in triplicate and a single control which excluded β-haematin was also included for each concentration. One experiment thus included 40 individual Eppendorf tubes (4 × 10) per compound.

Following the incubation period, a 200.0 mL aliquot of the supernatant was transferred to a clean 96-well plate and the UV-visible absorbance spectrum of each experiment was measured and compared to the initial spectrum before the incubation period. The proposed amount of inhibitor adsorbed to the β-haematin crystals was calculated from Beer's Law plots as described in section 5.3.2.2. By fitting the experimental data to the Langmuir Isotherm, using GraphPad, the adsorption constant, K, which is the relative strength of adsorption to the β-haematin crystals, could be determined for each inhibitor. The experimental procedure for direct adsorption studies is shown in Figure 5.1.
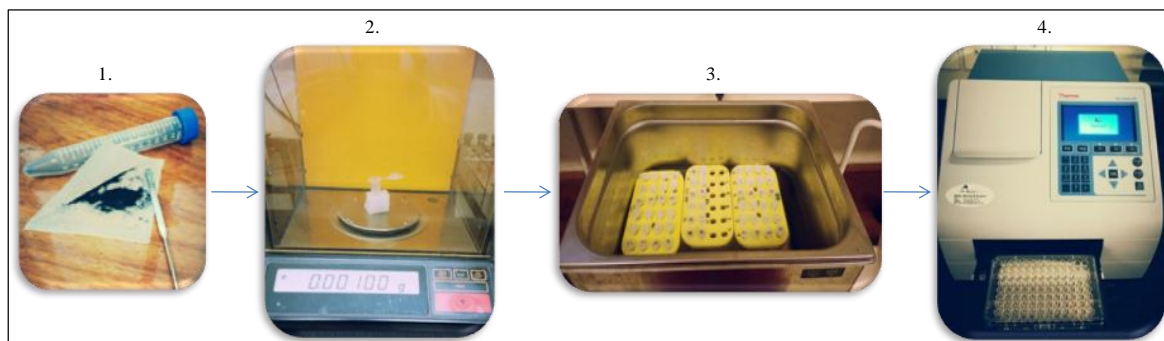
Figure 5.1 Flow diagram of the experimental procedure followed for performing direct adsorption studies. (1) Finely, ground β-haematin crystals were (2) weighed off as 1.0 mg samples in 2.0 mL Eppendorf tubes. (3) On adding different concentration inhibitor-containing citrate buffer solutions, the tubes were placed in floating trays and incubated in an ultrasonic water bath at 37 °C for sixteen hours. (4) Single wavelength readings, as well as UV-visible spectra, were measured for each inhibitor.

5.3 Results

5.3.1   Characterisation of β-Haematin Crystals

The formation of good quality β-haematin crystals is required in order to investigate the adsorption of quinoline inhibitors onto the crystal surface of β-haematin directly. β-haematin crystals can generally be recovered from the lipid-water and pentanol-water interface system, as well as from an acetate medium solution.[64] The direct adsorption studies were carried out using β-haematin crystals recovered from the pentanol-water interface system first, since crystals grown from this environment are of a better quality compared to the crystals grown in the lipid-water interface system. The formation of β-haematin was confirmed after the samples had been carefully characterised using attenuated total reflection infrared spectroscopy (ATR-IR), powder X-ray diffraction (PXRD) and scanning electron microscopy (SEM).

β-Haematin is comprised of cyclic dimers formed following the reciprocal coordination of the propionate group of each Fe(III)PPIX molecule coordinating to the metal centre of the neighbouring Fe(III)PPIX molecule.[37] The ATR-IR spectra for the β-haematin crystals recovered from the lipid-water interface system (Figure 5.2 (a)) and the pentanol-water interface system (Figure 5.2 (b)) are in good agreement with the literature.[35] The characteristic absorbance bands present at 1662 and 1205 cm^{-3} are assigned to the propionate C=O and C−O stretching frequencies, respectively.[35]
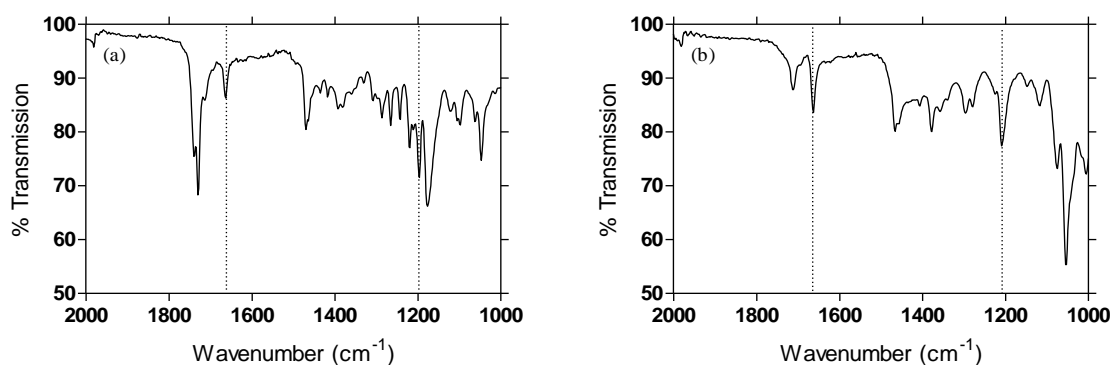
Figure 5.2 β-Haematin formation and characterization. ATR-IR spectra of β-haematin crystals recovered from the lipid-water (a) and pentanol-water (b) interface system. The peaks indicated with the dotted line at 1662 and 1205 cm^{-1} are characteristic of β-haematin, confirming the formation of the crystalline material.

The PXRD patterns of β-haematin crystals recovered from the lipid-water interface system (Figure 5.3 (a)) and the pentanol-water interface system (Figure 5.3 (b)) correspond to what has previously been observed in the literature,[73,150] again confirming the formation of β-haematin. Both the reflection peaks denoted as (100) and (131) are characteristic of β-haematin crystals. The sharpness of the peaks indicate a greater degree of crystallinity in the pentanol system.
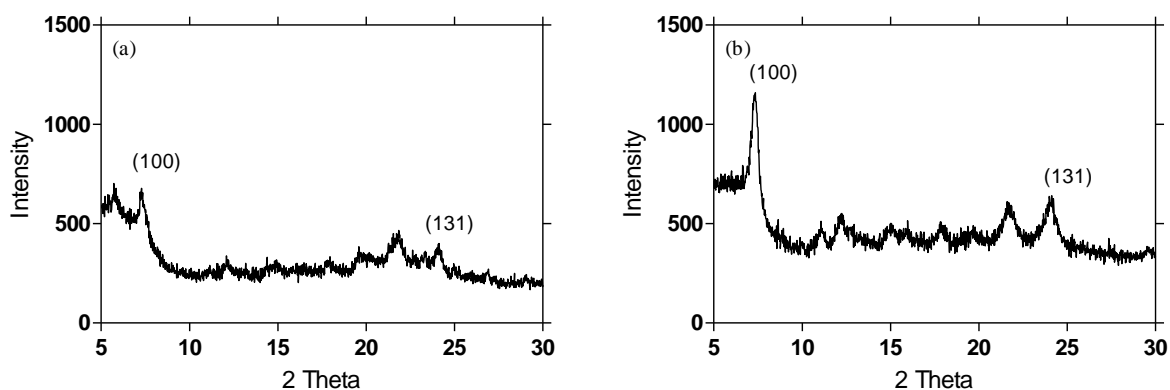
Figure 5.3 β-Haematin formation and characterization. Powder X-ray diffraction patterns of β-haematin recovered from the lipid-water (a) and pentanol-water (b) interface system. The two reflections at (100) and (131) are characteristic of the crystal planes in β-haematin.

The SEM micrographs are also characteristic of β-haematin formation.[58] The images represent the β-haematin crystals recovered from the lipid-water interface system (Figure 5.4 (a)) and the pentanol-water interface system (Figure 5.4 (b)). Multiple samples of β-haematin were recovered and collected for characterization. Good quality β-haematin crystals were further used in the direct adsorption studies.
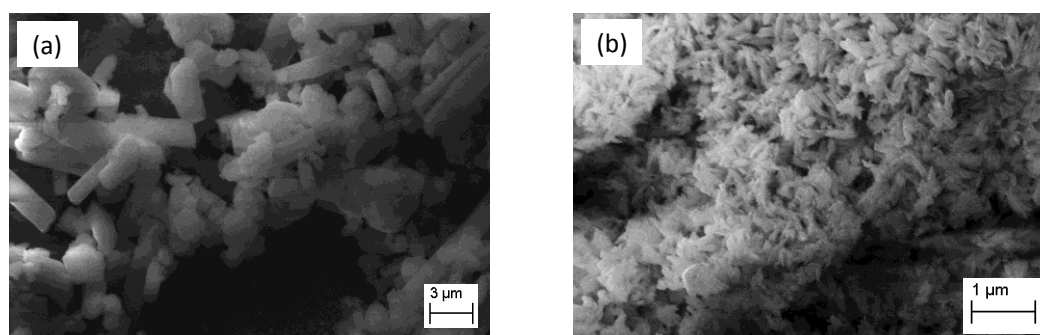
Figure 5.4 β-Haematin formation and characterization. Scanning electron micrographs of β-haematin recovered from the lipid-water (a) and pentanol-water (b) interface system.

5.3.2   Direct Adsorption Studies

The direct adsorption of CQ and QD to preformed β-haematin crystals has previously been investigated in our laboratory by monitoring the extent of depletion of the inhibitor from solution when in the presence of β-haematin crystals.[152] However, the experimental method was time-consuming, used less efficient absorbance measurement reading methods, and had a slow turnaround time per compound. This prompted the revisions and further optimizations carried out in the current study, which has allowed a greater number of compounds to be investigated.

5.3.2.1 Method of Optimization

When considering an experimental method for direct adsorption studies, the primary objective was to maintain conditions in line with those used in the activity and kinetics studies as far as possible. The temperature at which the direct adsorption studies were carried out was thus increased from room temperature (~25 °C) to 37 °C. To ensure homogeneity of the β-haematin weighed off into Eppendorf tubes, samples were ground together. The studies were also carried out in a heated ultrasonic water bath; in this way, it was assumed that crystallites would not clump together, thus ensuring maximal contact between the inhibitor in solution and the β-haematin crystal surfaces. The efficiency of measurement of each inhibitor concentration was improved by transferring a 200.0 µL aliquot of the supernatant from each tube to a 96-well plate and performing multiple absorbance readings simultaneously.

The optimization steps outlined above have resulted in considerable improvement compared to the previous method used to investigate the direct adsorption of inhibitors to preformed β-haematin crystals. All of the important differences and similarities between the previous and the new method are summarized in Table 5.1.

Table 5.1 A comparison between the previous and new experimental direct adsorption method.

Previous Method	Optimized Method
2.0 mL Eppendorf tubes	2.0 mL Eppendorf tubes
1.0 mg preformed β-haematin crystals	1.0 mg preformed β-haematin crystals
2.0 mL inhibitor-containing buffer solutions	1.5 mL inhibitor-containing buffer solutions
Room temperature	37 °C
Incubation period, 72 hours	Incubation period, 16 hours
Unshaken	Shaken continually in ultrasonic water bath
2.0 mL aliquot measurements in cuvette	0.2 mL aliquot measurements in 96-well plates

5.3.2.2 Recording Initial UV-visible Spectra

A full UV-visible spectrum was recorded from 200-600 nm for different concentrations of AQ, CQ, QD, QN and Q-CF$_3$ respectively, in order to determine the maximum absorbance wavelength of each inhibitor (Figure 5.5). The wavelengths selected for monitoring throughout the direct adsorption studies were 342, 344, 332, 344 and 341 nm, for AQ, CQ, QD, QN and Q-CF$_3$, respectively. After placing the preformed β-haematin crystals in a solution containing a particular concentration of an inhibitor, the absorbance reading of the supernatant at the relevant reference wavelength was measured after 16 hours (A_t) and compared to the initial absorbance (A_i) reading.
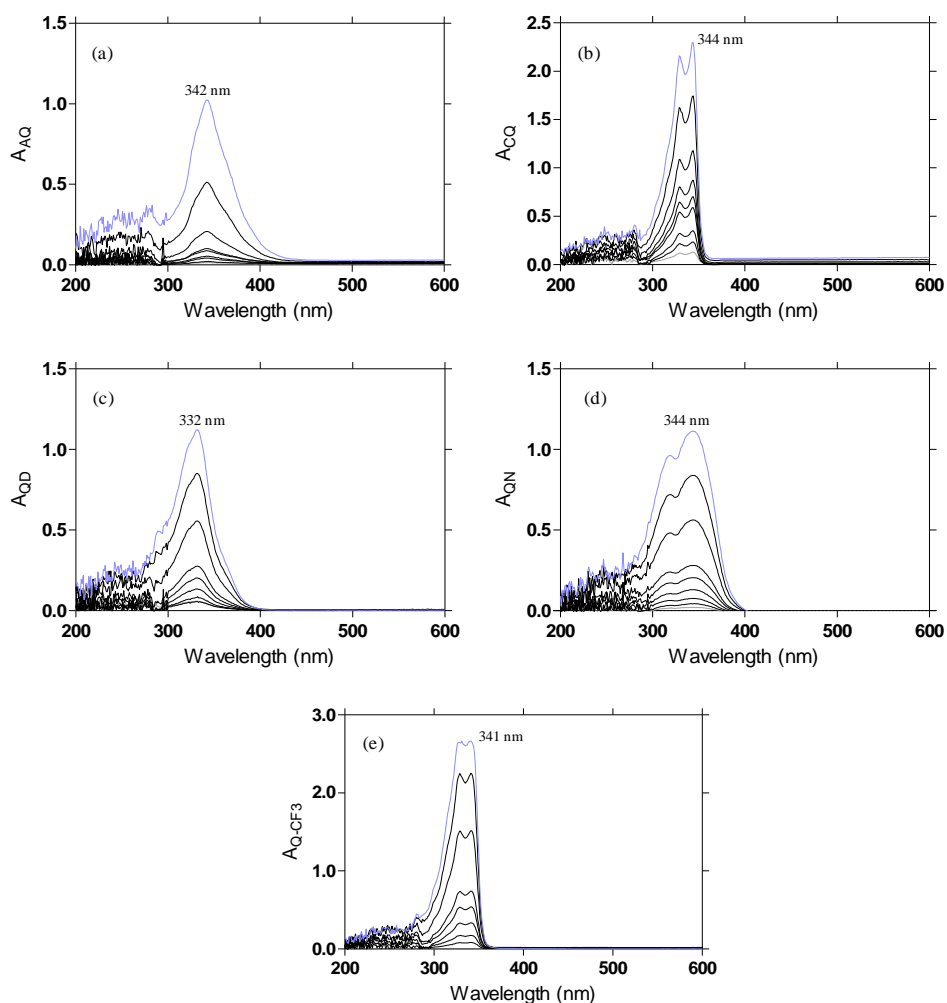
Figure 5.5. UV-visible spectra of antimalarial inhibitors dissolved in aqueous citrate buffer, pH 4.8. Maximum absorbance peaks are indicated for (a) AQ, (b) CQ, (c) QD, (d) QN and (e) Q-CF₃ in the absorbance range of 200-600 nm from initial low (●) to high (●) inhibitor concentrations.

5.3.2.3 Beer's Law Plots

The amount of each respective inhibitor, which remains in solution after a fraction of molecules have adsorbed onto the β-haematin crystals over a period of time, can be calculated by implementing Beer's Law equation. By definition, it is evident from the Beer's Law equation (Eq. 5.1) that the transmission of light through a solution is related to its concentration. In the relationship, A is the absorbance being measured of the material in solution, ε is the molar absorptivity, c is the concentration of the material in solution and l is the path length of light through the sample.[164]

$$A = \varepsilon c l \qquad \text{(Eq. 5.1)}$$

By plotting the initial measured absorbance, A_i, of each inhibitor as a function of increasing concentration, c, a linear correlation is observed (Figure 5.6, black lines), from which each specific inhibitor molar absorptivity,

ε, can be extracted from the slope value. The path length of the sample, l, which in this case is the depth of the well in a 96-well plate, was determined for each compound from a Beer's Law plot conducted in a 96-well plate (it is thus important to ensure exactly 200.0 µL aliquots are in each well). A decrease in absorbance of each inhibitor is observed when plotting the measured absorbance after 16 hours incubation time (A_t) as a function of increasing inhibitor concentration (Figure 5.6, purple lines). A more distinct decrease in absorbance is observed for AQ, CQ and Q-CF$_3$, compared to the small decrease in absorbance observed for QD and QN. An inhibitor control sample, excluding the β-haematin crystals, which was investigated under consistent experimental conditions, was also included and measured after 16 hours for each inhibitor concentration (Figure 5.6, grey lines). The absorbance values obtained for the control samples (A_c) were similar to the initial absorbance measurements, indicating no decrease in all cases, which strongly suggests that the observed decrease in absorbance observed after 16 hours (purple lines), can most likely be accounted for by inhibitor adsorption to the β-haematin crystals present in the solution.
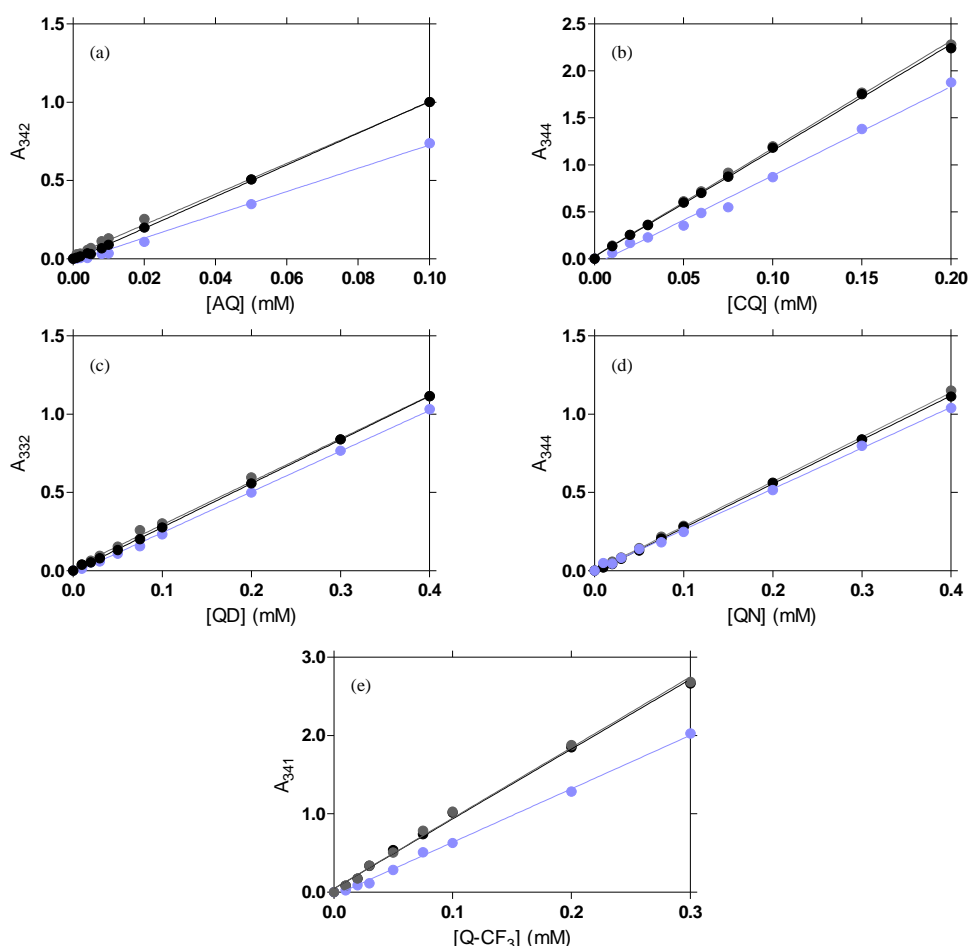
Figure 5.6 Direct adsorption studies in 50.0 mM citrate buffer, pH 4.8. Beer's Law plots of the maximum absorbance peak of (a) AQ, (b) CQ, (c) QD, (d) QN and (e) Q-CF$_3$, measured at 342, 344, 332, 344 and 341 nm, respectively, show a decrease in A_t after 16h (●), compared to A_i (●). An inhibitor control, excluding β-haematin, indicated no decrease in absorbance (●), which supports the hypothesis of inhibitor- β-haematin adsorption.

5.3.2.4 Explaining the Observed Direct Adsorption Behaviour using the Langmuir Isotherm

It is apparent from the Beer's Law plots in section 5.3.2.3 that a decrease in the inhibitor concentration in solution does indeed occur over a period of time for all compounds, when present together with β-haematin crystals in an aqueous citrate buffer solution. To further extract valuable information from the experimental data, the Langmuir Isotherm was again considered. In order to calculate the amount of inhibitor adsorbed to the β-haematin sample, the experimental data were fitted to equation 5.2, which is a mass-balance form of the Langmuir isotherm. [165, 166]

$$q_e = \frac{K \cdot Q_a^0 \cdot C_e}{1 + K \cdot C_e} \qquad \text{(Eq. 5.2)}$$

The Langmuir Isotherm is based on monolayer coverage and constant binding energy between a solid surface and adsorbent,[165] which is in this case β-haematin and the inhibiting inhibitor, respectively. In the above equation, q_e represents the mass of the adsorbed inhibitor per mass of β-haematin crystals at equilibrium, while C_e is the inhibitor concentration in solution when the amount of inhibitor adsorbed equals q_e, i.e. the inhibitor concentration after adsorption. Q_a^0 represents the maximum adsorption capacity (the amount of adsorption corresponding to monolayer coverage) and *K* is the adsorption constant, or the Langmuir constant, quantifying the relative strength of inhibitor adsorption onto the β-haematin crystals.

C_e values for each inhibitor concentration are calculated by substituting the absorbance values, measured after 16 hours, as well as the extracted ε values (determined from the slope as mentioned above), into Equation 5.1. (with $l = 1$). Values of q_e are calculated by subtracting C_e from the initial concentration, and converting it into the actual mass of inhibitor adsorbed per milligram of β-haematin.

The experimental data of q_e as a function of increasing C_e for each inhibitor are plotted in Figure 5.7. C_e is increasing owing to the initial increase in inhibitor concentrations. The experimental data conform to a non-linear fit of Equation 5.2 with r^2 values of 0.94, 0.91, 0.89, 0.91 and 0.93 for AQ, CQ, QD, QN and Q-CF$_3$ respectively. Default constraints were set for the *K* and Q_a^0 values to be greater than 0.

Subsequently, fitting the experimental data to Equation 5.2, yields *K* and Q_a^0 values for each inhibitor. These values are given in Table 5.2. The values of *K* are of most interest, since these values represent the proposed relative strength at which the inhibitor adsorbs to the β-haematin crystals.
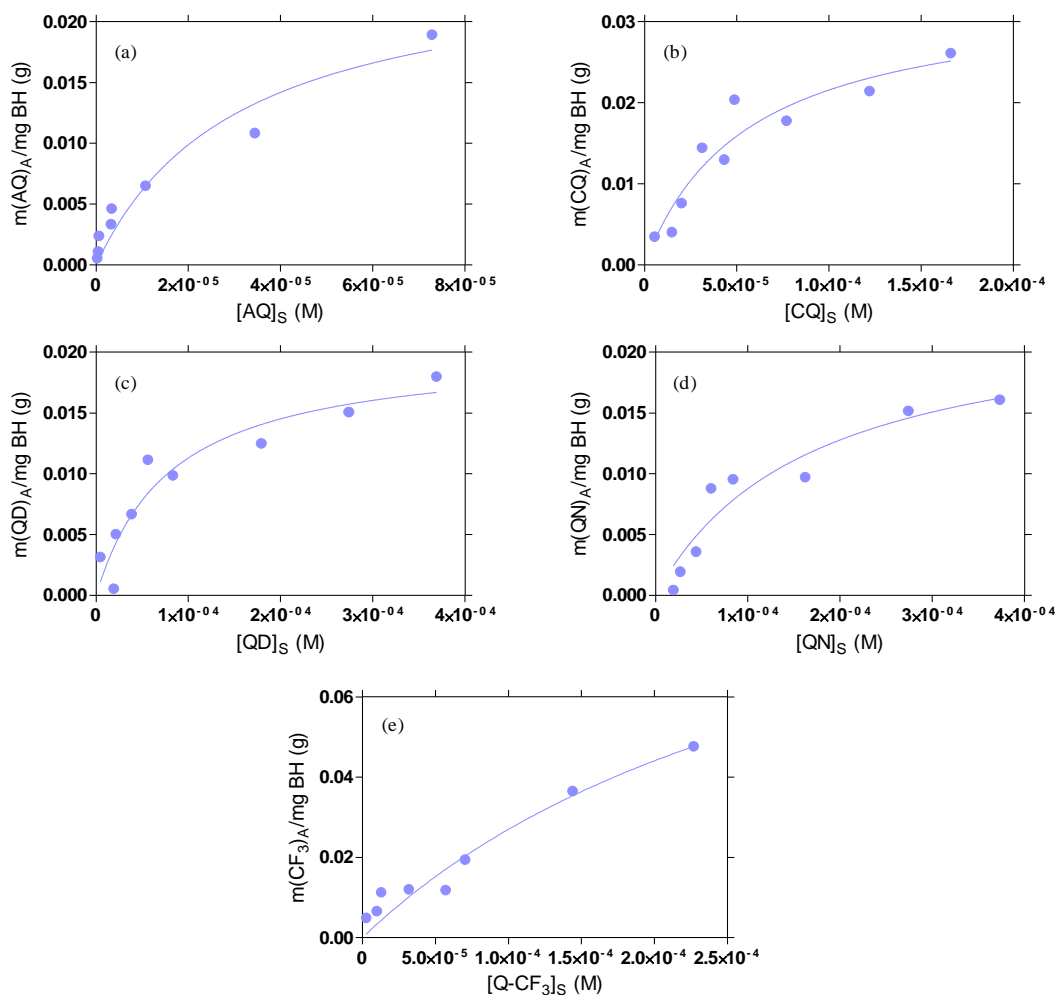
Figure 5.7 Direct adsorption studies in 50.0 mM citrate buffer, pH 4.8. The best fits of the mass of the inhibitor adsorbed per mg β-haematin crystals (m(inh)$_A$/mg BH), against the inhibitor concentration remaining in solution after adsorption ([inh]$_S$) to the Langmuir Isotherm for (a) AQ, (b) CQ, (c) QD, (d) QN and (e) Q-CF$_3$ yields the adsorption constant K. The r^2 values are 0.94, 0.91, 0.89, 0.91 and 0.93, respectively.

Table 5.2 Direct adsorption studies in 50.0 mM citrate buffer, pH 4.8. The K and Q_a^0 values were obtained from the best fits to the form of the Langmuir Isotherm Equation given by equation 5.1.

Antimalarial Inhibitor	K (mM^{-1})	Log K	Q_a^0
AQ	32294 ± 15756	4.51 ± 0.78	0.025 ± 0.005
CQ	17959 ± 6342	4.25 ± 0.56	0.034 ± 0.005
QD	12564 ± 4666	4.09 ± 0.59	0.020 ± 0.003
QN	5961 ± 2572	3.78 ± 0.69	0.024 ± 0.005
Q-CF$_3$	2881 ± 1916	3.46 ± ND	0.120 ± 0.055

5.3.2.5 Introducing Atovaquone as a Negative Control in Direct Adsorption Studies

The above reported results for the direct adsorption studies lend great insight into understanding the observed inhibitor depletion in solution in the presence of preformed β-haematin crystals. The assumption that an inhibitor adsorbs to the β-haematin crystal surface may, however, only be validated with additional experiments supporting these observations.

It was consequently considered to investigate the effect of a non-β-haematin inhibitor, namely atovaquone (AtQ, Figure 5.8), on the direct adsorption to β-haematin crystals. Since AtQ exhibits very weak or no β-haematin inhibitory activity,[140,149] no significant adsorption between AtQ and the β-haematin crystals, and hence no decrease in AtQ concentration over a period of time, was expected.
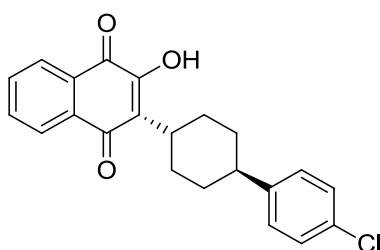
Figure 5.8 Structure of Atovaquone.

Owing to the insoluble nature of AtQ in the aqueous citrate buffer, the compound was alternatively dissolved in acetonitrile. The same procedure was then carried out in order to investigate the direct adsorption of AtQ. The Beer's Law plot (Figure 5.9 (a)) shows no decrease in the AtQ absorbance after 16 hours (purple curve), compared to the initial absorbance measurement (black curve) at 330 nm. A control sample, excluding the β-haematin crystals, which was investigated under similar experimental conditions, was included and measured after 16 hours (grey curve), and indicated no decrease in the absorbance values. These results are, however, not conclusive on their own, since the experimental environment in which the adsorption studies were carried out is somewhat different, owing to the inclusion of acetonitrile, from the biologically-relevant citrate buffer system.

Subsequently, the direct adsorption study of free base chloroquine (CQ$_{fb}$) was carried out in order to investigate the effect of the solvent and to validate the observations which were made for AtQ. The Beer's Law plot (Figure 5.9 (b)) shows a decrease in CQ$_{fb}$ absorbance after 16 hours (purple curve), compared to the initial absorbance measurement (black curve) at 330 nm. A control, excluding the β-haematin crystals was included and measured after 16 hours (grey curve), and indicated no decrease in the absorbance values.

These observations are similar to that observed for the antimalarial inhibitors, suggesting that the extent of CQ$_{fb}$ depletion can be accounted for the possible adsorption to the β-haematin crystal surfaces in acetonitrile, which in turn strongly supports the conclusion reached above that AtQ did not adsorb to the β-haematin

crystals. Subsequently, fitting the experimental data to Equation 5.2, yields the adsorption constant for CQ_{fb} from the best fir curve, with an r^2 value of 0.92 (Figure 5.9 (c)). A *log K* value of 4.43 ± 0.54 was obtained for CQ_{fb}, which is in good agreement to the adsorption value obtained for CQ in the citrate buffer system (4.25 ± 0.56).
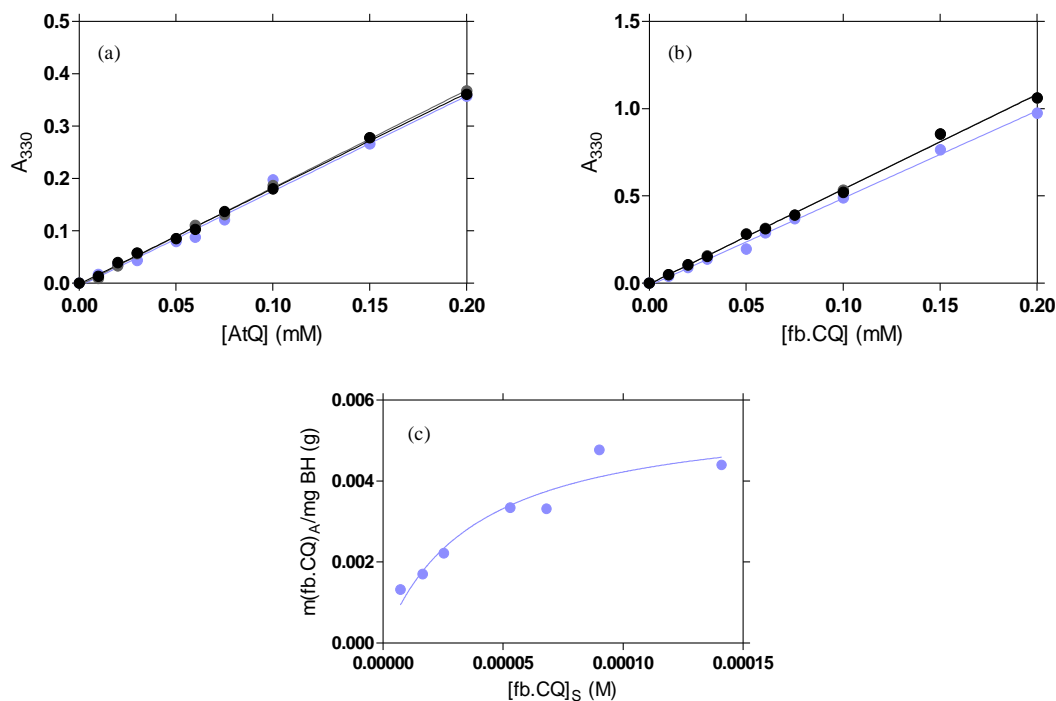
Figure 5.9 Direct adsorption studies in acetonitrile**.** Beer's Law plots of the maximum absorbance peak of (a) AtQ measured at 330 nm, shows no decrease in absorbance after 16h (●), compared to the initial absorbance (●), and (b) CQ_{fb} measured at 330 nm, shows a decrease in absorbance after 16h (●), compared to the initial absorbance (●). An inhibitor control, excluding β-haematin**,** indicated no decrease in absorbance for both AtQ and CQ_{fb} (●). (c) The best fits of the mass of the inhibitor adsorbed per mg β-haematin crystals, against the inhibitor concentration remaining in solution after adsorption, to the Langmuir Isotherm for CQ_{fb}, yields the adsorption constant K ($r^2 = 0.92$).

5.4 Combining the Kinetics Adsorption Studies to the Direct Adsorption Studies

The results obtained in the two different studies are compared below in order to evaluate if there is any significant correlation between the two independent methods of investigating the proposed adsorption of an inhibitor to β-haematin.

A correlation between the β-haematin inhibitory activity (IC_{50}) and relative strength of adsorption to preformed β-haematin crystals (K), yields a good linear relationship, with an r^2 value of 0.91 (Figure 5.10 (a)). Statistically this trend is significant, indicated by a P value smaller than 0.05.

Subsequently, a linear correlation between the relative strengths of adsorption, K_{ads} and K, determined in the kinetics and the direct adsorption studies, respectively, is observed, with an r^2 value of 0.84 (Figure 5.10 (b)). The good fit is significant, indicated by a P value smaller than 0.05, and suggests that the quinoline-based inhibitors do adsorb to the β-haematin crystal surface. In both cases AQ adsorbs the strongest to the β-haematin crystals, while Q-CF$_3$ adsorbs the weakest, which is in agreement with their respective β-haematin inhibitory activity. The difference in the absolute values of K determined in the two methods is approximately one log unit. This may be due to the fact that in kinetics, the adsorption is expected at the fastest growing face to bring about real-time inhibition of β-haematin formation. In the case of the direct adsorption experiments, the β-haematin is preformed and thus adsorption does not result in inhibition; in this case, it is also possible that the inhibitors may have adsorbed to other crystal faces, thus accounting for the overall weaker interaction on the primary face (indicated by smaller values of K).
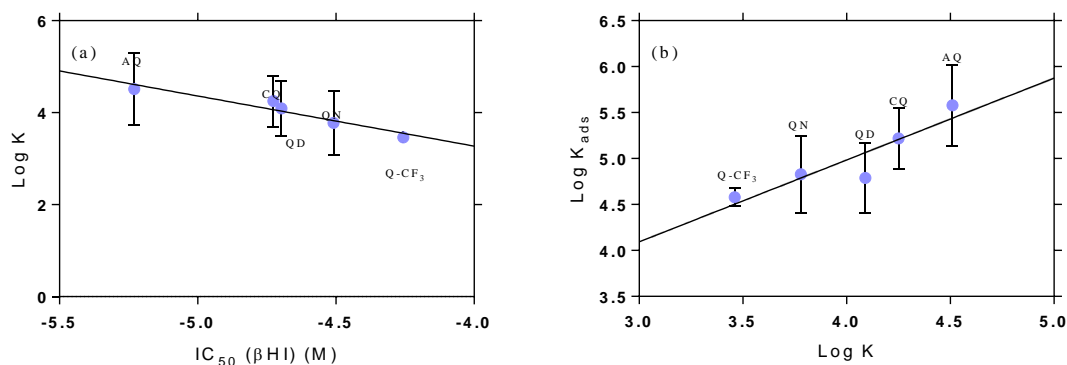
Figure 5.10 Direct adsorption studies compared to inhibitor activity and kinetics studies carried out in 50.0 mM citrate buffer, pH 4.8. Linear correlations between (a) the observed K values, determined in the current study, against the IC_{50} values, determined in the previous inhibitor activity studies and (b) the observed K_{ads} values, determined in the kinetic studies, against the K value, determined in the direct adsorption studies, are observed for the quinoline-based inhibitors. The r^2 values are 0.91 and 0.84, respectively.

5.5 Discussion

The focus of this chapter has been to independently investigate the proposed adsorption by quinoline-based inhibitors to preformed β-haematin crystals. β-Haematin crystals were successfully synthesized in a pentanol-water interface system, since this method of preparation yields larger amounts of good quality crystals, compared to the lipid-mediated system, and is frequently used as a lipid alternative system for β-haematin formation.[73] The β-haematin crystals were successfully characterized using infrared spectroscopy, powder X-ray diffraction and scanning electron microscopy. Only good quality, homogenous β-haematin samples were used in the direct adsorption studies.

Direct adsorption studies have previously been carried out in order to establish whether there is any interaction between an inhibitor and the surface of preformed β-haematin crystals. The method of investigation has, however, been optimized in the current study, which now has a faster turnaround time per compound, is biologically more relevant and measures multiple absorbance readings simultaneously.

The direct adsorption of four clinically known antimalarial drugs, AQ, CQ, QD and QN, as well as a short-chain CQ analogue, Q-CF$_3$, was investigated in an aqueous citrate buffer, over 16 hours at 37 °C. A decrease in absorbance is observed for all the quinoline inhibitors at their respective maximum absorbance wavelengths (Figure 5.6). Interestingly, a greater decrease in absorbance is observed for the two 4-aminoquinoline antimalarials, AQ and CQ, compared to the decrease in absorbance observed for the two quinoline methanol antimalarials, QD and QN. These observations suggest that more AQ and CQ have interacted with the β-haematin crystals than the quinoline methanol antimalarial drugs, resulting in a greater decrease in absorbance, which is in agreement with the activity results reported in Chapter 3, since it has been observed that AQ and CQ are more active β-haematin inhibitors than QD and QN. Higher doses of QD and QN are most likely required to induce a larger decrease in absorbance.

The extent of depletion of each inhibitor in solution may be accounted for by a β-haematin-inhibitor interaction occurring. Since no free Fe(III)PPIX is present in the solution, the interaction is not expected to be the irreversible precipitation reaction of a Fe(III)PPIX-inhibitor complex. Rather therefore, the only possible interaction that may be occurring is direct adsorption of the inhibitor to the β-haematin crystal surface. A control sample, which included only the inhibitor-containing buffer, did not indicate a decrease in absorbance, which in return supports the above statement.

Subsequently, the mass of the inhibitor adsorbed per mg β-haematin crystals as a function of the inhibitor concentration remaining in solution after adsorption, was fit to the Langmuir Isotherm. Non-linear curves (Figure 5.7) were obtained, from which the adsorption constant, K, was determined for each quinoline inhibitor. A decrease in the strength of direct adsorption is observed, K decreasing from AQ to Q-CF$_3$; AQ>CQ>QD>QN> Q-CF$_3$. AQ may possibly adsorb the strongest to the preformed β-haematin crystals, and Q-CF$_3$ the weakest.

Direct adsorption studies for AtQ indicated no decrease in absorbance, suggesting that no interaction to the β-haematin crystals occurred, which was expected since AtQ is not a β-haematin inhibitor.[140,149] Direct adsorption studies for CQ_{fb} were, however, carried out in order to validate the observations that were made in the acetonitrile environment. A decrease in the concentration of CQ_{fb}, similar to the quinoline inhibitors, is observed, suggesting that the extent of CQ_{fb} depletion in acetonitrile may also be accounted for by the direct adsorption to the surface of the preformed β-haematin crystals. This in turn provides support for the case that AtQ did not adsorb to the β-haematin crystals. A log K value of 4.43 ± 0.54 for CQ_{fb} corresponds well to the log K value obtained in the buffer system (4.25 ± 0.56). Regardless of the two different environments in which the direct adsorption studies were carried out, the observations that AtQ does not show a decrease in absorbance, while CQ_{fb} does, suggest that a decrease in inhibitor concentration (as evidence by a decrease in absorbance) in the presence of performed β-haematin crystals, is most likely owing to a inhibitor- β-haematin adsorption interaction.

Furthermore, the adsorption constants, K, determined in the independent investigation compared to the β-haematin inhibitory activity obtained in Chapter 3, show a linear correlation between the quinoline inhibitors (Figure 5.10 (a)). The correlation suggests that more active inhibitors, like AQ, adsorb more strongly to the β-haematin crystals than less active inhibitors, such as Q-CF$_3$. This is in agreement to the overall hypothesis that the strength of adsorption of an inhibitor to β-haematin may be related to its relative β-haematin inhibition activity.

Subsequently, a direct correlation is observed between the adsorption constants, K_{ads}, which were determined in the kinetics studies, and the adsorption constants, K, which were determined in the direct adsorption studies (Figure 5.10 (b)). The linear correlation suggests that the strength of adsorption determined theoretically in the kinetics studies are related to their relative strength of adsorption independently. The absolute values differ in orders of magnitudes, however, the same trend in adsorption strength is observed for the quinoline-based inhibitors. Using preformed β-haematin crystals in the direct adsorption studies is not the same as inhibiting β-haematin crystal growth as a dynamic process. The direct adsorption of an inhibitor to the β-haematin crystals is furthermore also not face-specific in this case, since inhibitors can adsorb to multiple faces of the preformed β-haematin crystal. Unpublished computational data by one of our co-workers suggests that interactions at the second fastest growing face may also take place, while the kinetics model is based on the fastest growing face only. The absence of the lipid solution in the citrate buffer system, compared to the kinetics lipid-water interface system, may possibly have an effect on the extent at which the quinoline inhibitors interact with the β-haematin crystals.

Overall, the most probable inhibitor-β-haematin interaction is considered to be adsorption; however, this still cannot be completely confirmed based on the current results alone. Additional studies, investigating the face or faces to which adsorption may be occurring, are required to explain the observations reported in this chapter. This is currently being investigated computationally, however, independent experimental results would also be required to completely understand the mode of inhibitor-β-haematin interaction.

5.6 Conclusion

The previous method in which the direct adsorption of an inhibitor to the surface of β-haematin crystals was investigated, has been optimized in the current study. The direct adsorption studies were expanded by investigating four clinically known antimalarial drugs, as well as a short-chain CQ analogue. The decrease in absorbance for a range of concentrations over a period of time may be accounted for by the possible absorption of the inhibitor to the surface of the preformed β-haematin crystals present in the aqueous system. This assumption is valid since a control sample, excluding β-haematin crystals, indicated no decrease in absorbance when investigated under the similar experimental conditions. By fitting the mass of the inhibitor adsorbed per mg β-haematin, against the inhibitor concentration which remains in solution after adsorption to the Langmuir Isotherm, the relative strength of inhibitor adsorption to β-haematin crystals, K, was obtained. The K values determined in the current study are in agreement to the β-haematin inhibitory activity, as well as the K_{ads} values obtained for each inhibitor from the kinetics studies carried out in the lipid system (Chapter 3). The direct adsorption studies are, however, not sufficient enough to draw a definite conclusion on the exact inhibition mechanism of action, since this experimental method does not provide adequate information on the site of inhibitor adsorption. Even though the β-haematin crystal face to which adsorption occurs can be predicted and investigated computationally, this should ideally be probed experimentally.

Chapter 6. Overall Conclusion and Future Work

6.1 Overall Conclusion

The main aim of this research project, underpinned by the hypothesis that the β-haematin inhibitory activity of a compound is related to its strength of adsorption to free surface binding sites on the fastest growing face of the crystalline material, was to investigate the effect of diverse β-haematin inhibitors on the kinetics of β-haematin formation using a lipid-mediated system.

This aim was achieved by firstly developing a new, improved-throughput lipid-mediated assay in which to investigate the inhibition of β-haematin formation. A previously-used Phiβ assay[40] was optimized by introducing 24-well plates and was successfully validated as a means of assaying drug activity by introducing clinically-relevant antimalarial drugs, namely chloroquine, amodiaquine, quinidine, quinine and mefloquine into the system. Having developed this more efficient lipophilic assay, it has been possible throughout this project to extend the data set to include short-chain chloroquine analogues, as well as a series of benzamide non-quinoline β-haematin inhibitors.

β-Haematin inhibitory activity was investigated for the first time in this way under biologically-relevant conditions (pH4.8, 37 °C). The experimentally-determined IC_{50} values for all of the compounds show good correlation with biological activity determined against various chloroquine-sensitive parasite strains, namely 3D7, D10 and NF54. Furthermore, the investigation of the kinetics on β-haematin formation at the lipid-water interface in the presence of antimalarial drugs, short-chain CQ analogues, as well as the benzamide non-quinolines, shows that an increase in inhibitor concentration results in a decrease in the rate of β-haematin formation. This was observed at low concentrations, while a decrease in the yield of β-haematin formation was observed when introducing higher doses of each inhibitor. The exponential kinetics results are similar to what has previously been recorded,[40] and can be explained by a theoretical kinetic model, previously developed in our group.[40] Importantly, consistent β-haematin formation rate constants in the absence of an inhibitor were observed in the biologically-relevant environment, however, the rate was slightly faster in the pH 4.8 buffer solution, compared to pH 3.0.

The experimental data strongly support a mechanism of inhibitor action *via* adsorption to the surface of β-haematin crystals by both sets of quinoline- and non-quinoline inhibitors, and it is proposed that the equilibrium between adsorbed and desorbed inhibitor is responsible for the decrease in the rate of β-haematin formation. The decrease in the yield of β-haematin at high concentrations may be accounted for by the proposed irreversible precipitation of an inhibitor-Fe(III)PPIX complex. The interaction between each individual inhibitor and the crystal surface was measured (K_{ads}) and found to correlate well with its β-haematin inhibitory

activity determined in the lipid-mediated system, as well as the biological activity determined against D10 and NF54 chloroquine-sensitive parasite strains, for quinoline- and non-quinoline-based inhibitors, respectively.

An important observation made during this study is that various quinoline- and non-quinoline β-haematin inhibitors can have the same β-haematin IC_{50} value, yet quite different K_{ads} values. Using the theoretical kinetic model it has become evident that both K_{ads} and k_2 have a direct effect on the IC_{50} value of a respective inhibitor. It would seem that the interplay between the two parameters determines the overall activity of a family of compounds. The formation of inhibitor-haem complexes did not, however, form part of this project, so that independent studies regarding k_2 are required urgently to improve our understanding of the different processes involving Fe(III)PPIX.

Since kinetics alone cannot account for the proposed mechanism of β-haematin inhibition, independent studies were carried out to investigate the relative strength by which an inhibitor is able to adsorb to the surface of preformed β-haematin crystals. The interaction between the inhibitor and the preformed β-haematin was measured (K) and was found correlate well with the inhibitory activity and K_{ads} values determined in the kinetics experiments.

Overall, this research project provides important insight into the possible mode of β-haematin inhibition by quinoline- and importantly, non-quinoline-based inhibitors. Indeed, adsorption (K_{ads}) is an important process and was observed to correlate to both β-haematin and biological activities of the compounds investigated. If the interactions that aid the adsorption of compounds to surface binding sites are identified, the insight will be invaluable in the rational design of novel haemozoin inhibitors.

6.2 Future Work

The results of the work presented in Chapter 3 and 4 regarding the investigation of the kinetics of β-haematin formation in the presence of a variety of inhibitors at the lipid-water interface provide a great deal of insight into the possible mode of action of these inhibitors, however, the following future studies are proposed to further our understanding:

1. To investigate a wider range of non-quinoline β-haematin inhibitors and determine their effects on the kinetics of β-haematin formation in order to demonstrate the validity of the theoretical kinetic model further.
2. To use fluorescence microscopy in conjunction with the β-haematin inhibition studies; by tagging an inhibitor with a fluorescent marker, it may be possible to visualise the adsorbed inhibitor on the surface of β-haematin crystals. This may contribute definitive insight into the mechanism of action of the inhibitors.

Subsequent to the kinetics of β-haematin formation, which mainly focus on the equilibrium adsorption constant of an inhibitor, K_{ads}, in this study, it is evident from the results presented in Chapter 4 that a better understanding of the proposed competing precipitation of an inhibitor-Fe(III)PPIX complex is required, and future studies in this regard are suggested as follows:

3. To investigate k_2 independently, in order to truly understand how the rate of precipitation of an inhibitor and free Fe(III)PPIX in solution plays a role in the formation of an inhibitor-haem complex, which in turn may have an effect on β-haematin formation. The solubility of inhibitor-Fe(III)PPIX complexes in aqueous pyridine is of high importance and differential solubility of β-haematin inhibitors may provide significant insight in this regard. This data will improve the overall understanding of the system and of the relationship between different processes involving Fe(III)PPIX.

The results presented in Chapter 5 further support the hypothesis that β-haematin inhibition is brought about by direct adsorption of an inhibitor to preformed β-haematin crystal surfaces, however, subsequent experimental proof is still required to further support this phenomenon independently. Future studies in this regard include:

4. Infrared and/or solid-state UV-vis spectroscopic analyses and characterization of β-haematin crystals after leaving samples exposed to an aqueous inhibitor solution, in order to probe the presence of an inhibitor adsorbed to the preformed β-haematin crystal surface.

Chapter 7: References

1   World Health Organisation, 2014.

2   F. E. G. Cox, *Clin. Microbiol. Rev.*, 2002, **15**, 595–612.

3   F. E. G. Cox, *Parasit. Vectors*, 2010, **3**, 5.

4   G. Harrison, *Mosquitoes, malaria and man.*, John Murray, London, United Kingdom, 1978.

5   G. M. Lancisi, *De noxiis paludum effuvius eorumque remediis*, Salvioni, J M: Rome, 1717.

6   A. Laveran, *Bull Mém Soc Méd Hôpitaux Paris*, 1881, **17**, 158–164.

7   A. Laveran, *Trait. des Fiévres Palustres avec la Descr. des Microbes du Palud. Paris Doin*, 1884.

8   A. F. A. King, *Pop Sci*, 1883, **23**, 644–658.

9   P. Manson, *J Linn Soc*, 1878, **14**, 304–311.

10   R. Ross, *Memoirs With a Full Account of the Great Malaria Problem and Its Solution*, 1923, vol. 13.

11   B. Grassi, *Atti dei. Linncei. Mem.*, 1901, **3**, 229–505.

12   K. Kirk, *Physiol. Rev.*, 2001, **81**, 495–537.

13   R. Carter and K. N. Mendis, *Clin. Microbiol. Rev.*, 2002, **15**, 564–594.

14   E. Ashley, R. McGready, S. Proux and F. Nosten, *Travel Med. Infect. Dis.*, 2006, **4**, 159–173.

15   L. H. Bannister, J. M. Hopkins, R. E. Fowler, S. Krishna and G. H. Mitchell, *Parasitol. Today*, 2000, **16**, 427–433.

16   Y. Michalakis and F. Renaud, *Nature*, 2009, **462**, 298–300.

17   K. K. Eggleson, K. L. Duffin and D. E. Goldberg, *J. Biol. Chem.*, 1999, **274**, 32411–32417.

18   M. Krugliak, J. Zhang and H. Ginsburg, *Mol. Biochem. Parasitol.*, 2002, **119**, 249–256.

19   R. Hayward, K. J. Saliba and K. Kirk, *J. Cell Sci.*, 2006, **119**, 1016–1025.

20   S. E. Francis, I. Y. Gluzman, A. Oksman, A. Knickerbocker, R. Mueller, M. L. Bryant, D. R. Sherman, D. G. Russell and D. E. Goldberg, *EMBO J.*, 1994, **13**, 306–317.

21   I. Y. Gluzman, S. E. Francis, A. Oksman, C. E. Smith, K. L. Duffin and D. E. Goldberg, *J. Clin. Invest.*, 1994, **93**, 1602–1608.

22   S. E. Francis, I. Y. Gluzman, A. Oksman, D. E. Goldberg and D. Banerjee, *Mol. Biochem. Parasitol.*, 1996, **83**, 189–200.

23   P. J. Rosenthal, J. H. McKerrow, M. Aikawa, H. Nagasawa and J. H. Leech, *J. Clin. Invest.*, 1988, **82**, 1560–1566.

24   L. M. B. Ursos and P. D. Roepe, *Med. Res. Rev.*, 2002, **22**, 465–491.

25   T. J. Egan, J. M. Combrinck, J. Egan, G. R. Hearne, H. M. Marques, S. Ntenteni, B. T. Sewell, P. J. Smith, D. Taylor, D. A. van Schalkwyk and J. C. Walden, *Biochem. J.*, 2002, **365**, 343–347.

26   T. J. Egan, *Mol. Biochem. Parasitol.*, 2008, **157**, 127–136.

27   P. L. Olliaro and Y. Yuthavong, *Pharmacol. Ther.*, 1999, **81**, 91–110.

28   M. F. Oliveira, J. C. P. D'Avila, C. R. Torres, P. L. Oliveira, A. J. Tempone, F. D. Rumjanek, C. M. S. Braga, J. R. Silva, M. Dansa-Petretski, M. A. Oliveira, W. De Souza and S. T. Ferreira, *Mol. Biochem. Parasitol.*, 2000, **111**, 217–221.

29   M. M. Chen, L. Shi and D. J. Sullivan, *Mol. Biochem. Parasitol.*, 2001, **113**, 1–8.

30   J. M. Pisciotta, E. L. Ponder, B. Fried and D. Sullivan, *Int. J. Parasitol.*, 2005, **35**, 1037–1042.

31   H. Meckel, *Zeitschr f Psychiatr. IV*, 1847, 198–226.

32   R. Virchow, *Arch. fur Pathol. Anat.*, 1849, **2**, 587–598.

33   W. H. Brown, *J. Exp. Med.*, 1911, **13**, 290–299.

34   C. D. Fitch and P. Kanjananggulpan, *J. Biol. Chem.*, 1987, **262**, 15552–15555.

35   A. F. Slater, W. J. Swiggard, B. R. Orton, W. D. Flitter, D. E. Goldberg, A. Cerami and G. B. Henderson, *Proc. Natl. Acad. Sci. U. S. A.*, 1991, **88**, 325–329.

36   D. S. Bohle, R. E. Dinnebier, S. K. Madsen and P. W. Stephens, *J. Biol. Chem.*, 1997, **272**, 713–716.

37   S. Pagola, P. W. Stephens, D. S. Bohle, A. D. Kosar and S. K. Madsen, *Nature*, 2000, **404**, 307–310.

38   A. Hamsik, *Z. Physiol. Chem.*, 1936, **190**.

39   R. Buller, M. L. Peterson, Ö. Almarsson and L. Leiserowitz, *Cryst. Growth Des.*, 2002, **2**, 553–562.

40   J. Gildenhuys, T. le Roex, T. J. Egan and K. A. de Villiers, *J. Am. Chem. Soc.*, 2013, **135**, 1037–1047.

41   E. Hempelmann and T. J. Egan, *Trends Parasitol.*, 2002, **18**, 11.

42   D. J. Sullivan, I. Y. Gluzman and D. E. Goldberg, *Science*, 1996, **271**, 219–222.

43   C. Y. H. Choi, J. F. Cerda, C. Hsiu-An, G. T. Babcock and M. A. Marletta, *Biochemistry*, 1999, **38**, 16916–16924.

44   A. Lynn, S. Chandra, P. Malhotra and V. S. Chauhan, *FEBS Lett.*, 1999, **459**, 267–271.

45   J. Ziegler, R. T. Chang, D. W. Wright, V. Pennsyl, R. V September, V. Re, M. Recei and V. January, 1999, 2395–2400.

46   V. Papalexis, M. A. Siomos, N. Campanale, X. G. Guo, G. Kocak, M. Foley and L. Tilley, *Mol. Biochem. Parasitol.*, 2001, **115**, 77–86.

47   T. Akompong, M. Kadekoppala, T. Harrison, A. Oksman, D. E. Goldberg, H. Fujioka, B. U. Samuel, D. Sullivan and K. Haldar, *J. Biol. Chem.*, 2002, **277**, 28923–28933.

48   G. S. Noland, N. Briones and D. J. Sullivan, *Mol. Biochem. Parasitol.*, 2003, **130**, 91–99.

49   D. J. Sullivan, *Int. J. Parasitol.*, 2002, **32**, 1645–1653.

50   M. Chugh, V. Sundararaman, S. Kumar, V. S. Reddy, W. A. Siddiqui, K. D. Stuart and P. Malhotra, *PNAS*, 2013, **110**, 5392–5397.

51   A. Dorn, R. Stoffel, H. Matile, A. Bubendorf and R. G. Ridley, *Nature*, 1995, **374**, 269–271.

52   K. Bendrat, B. J. Berger and A. Cerami, *Nature*, 1995, **378**, 138–139.

53   A. Dorn, S. R. Vippagunta, H. Matile, C. Jaquet, J. L. Vennerstrom and R. G. Ridley, *Biochem. Pharmacol.*, 1998, **55**, 727–736.

54   C. D. Fitch, G. Z. Cai, Y. F. Chen and J. D. Shoemaker, *Biochim. Biophys. Acta - Mol. Basis Dis.*, 1999, **1454**, 31–37.

55   K. E. Jackson, N. Klonis, D. J. P. Ferguson, A. Adisa, C. Dogovski and L. Tilley, *Mol. Microbiol.*, 2004, **54**, 109–122.

56   I. Coppens and O. Vielemeyer, *Int. J. Parasitol.*, 2005, **35**, 597–615.

57   J. M. Pisciotta, I. Coppens, A. K. Tripathi, P. F. Scholl, J. Shuman, S. Bajad, V. Shulaev and D. J. Sullivan, *Biochem. J.*, 2007, **402**, 197–204.

58   M. F. Oliveira, S. W. Kycia, A. Gomez, A. J. Kosar, D. S. Bohle, E. Hempelmann, D. Menezes, M. A. Vannier-Santos, P. L. Oliveira and S. T. Ferreira, *FEBS Lett.*, 2005, **579**, 6010–6016.

59   T. J. Egan, D. C. Ross and P. A. Adams, *FEBS Lett.*, 1994, **352**, 54–57.

60   N. Basilico, D. Monti, P. Olliaro and D. Taramelli, *FEBS Lett.*, 1997, **409**, 297–299.

61   N. Basilico, E. Pagani, D. Monti, P. Olliaro and D. Taramelli, *J. Antimicrob. Chemother.*, 1998, **42**, 55–60.

62   D. S. Bohle, *Biochem. Biophys. Res. Commun.*, 1993, **193**, 504–508.

63   P. A. Adams, T. J. Egan, D. C. Ross†, J. Silver and P. J. Marsh, *Biochem. J.*, 1996, **27**, 25–27.

64   T. J. Egan, W. W. Mavuso and K. K. Ncokazi, *Biochemistry*, 2001, **40**, 204–213.

65   M. J. Avrami, *J. Chem. Phys.*, 1939, **7**, 1103–1112.

66   M. J. Avrami, *J. Chem. Phys.*, 1940, 8, 212–224.

67   T. J. Egan and M. G. Tshivhase, *Dalton Trans.*, 2006, 5024–5032.

68   M. D. Carter, V. V Phelan, R. D. Sandlin, B. O. Bachmann and D. W. Wright, *Comb. Chem. High Throughput Screen.*, 2010, **13**, 285–292.

69   R. D. Sandlin, M. D. Carter, P. J. Lee, J. M. Auschwitz, S. E. Leed, J. D. Johnson and D. W. Wright, *Antimicrob. Agents Chemother.*, 2011, **55**, 3363–3369.

70   R. D. Sandlin, K. Y. Fong, K. J. Wicht, H. M. Carrell, T. J. Egan and D. W. Wright, *Int. J. Parasitol. Drugs Drug Resist.*, 2014, **4**, 316–325.

71   N. T. Huy, A. Maeda, D. T. Uyen, D. T. X. Trang, M. Sasai, T. Shiono, T. Oida, S. Harada and K. Kamei, *Acta Trop.*, 2007, **101**, 130–138.

72   R. Stiebler, A. N. Hoang, T. J. Egan, D. W. Wright and M. F. Oliveira, *PLoS One*, 2010, **5**, 1–10.

73   T. J. Egan, J. Y. J. Chen, K. A. de Villiers, T. E. Mabotha, K. J. Naidoo, K. K. Ncokazi, S. J. Langford, D. McNaughton, S. Pandiancherri and B. R. Wood, *FEBS Lett.*, 2006, **580**, 5105–5110.

74   A. N. Hoang, K. K. Ncokazi, K. A. de Villiers, D. W. Wright and T. J. Egan, *Dalton Trans.*, 2010, **39**, 1235–1244.

75   M. A. Ketchum, K. N. Olafson, E. V. Petrova, J. D. Rimer and P. G. Vekilov, *J. Chem. Phys.*, 2013, **139**.

76   P. G. Vekilov, J. D. Rimer, K. N. Olafson and M. A. Ketchum, *CrystEngComm*, 2015.

77   N. T. Huy, Y. Shima, A. Maeda, T. T. Men, K. Hirayama, A. Hirase, A. Miyazawa and K. Kamei, *PLoS One*, 2013, **8**, 1–7.

78   J. Shack and W. M. Clarke, *J. Biol. Chem.*, 1947, **171**, 143–187.

79   H. Davies, *J. Biol. Chem.*, 1938, **135**, 597–622.

80   S. B. Brown, P. Jones and I. R. Lantzke, *Nature*, 1969, **223**, 960–961.

81   B. S. B. Brown, T. C. Dean and P. Jones, 1970, 733–739.

82   K. A. de Villiers, C. H. Kaschula, T. J. Egan and H. M. Marques, *J. Biol. Inorg. Chem.*, 2007, **12**, 101–117.

83   D. H. O'Keeffe, C. H. Barlow, G. A. Smythe, W. H. Fuchsman, T. H. Moss, H. R. Lilienthal and W. S. Caughey, *Bioinorg. Chem.*, 1975, **5**, 125–147.

84   D. L. Budd, G. N. La Mar, K. C. Langry, K. M. Smith and R. Nayyir-Mazhir, *J. Am. Chem. Soc.*, 1979, **101**, 6091.

85   D. F. Koenig, *Acta Crystallogr*, 1965, **18**, 663–673.

86   B. Cheng, M. K. Safo, R. D. Orosz, C. A. Reed, P. G. Debrunner and W. R. Scheidt, 1994, **33**, 1319–1324.

87   C. Asher, K. A. de Villiers and T. J. Egan, *Inorg. Chem.*, 2009, **48**, 7994–8003.

88   K. A. de Villiers, H. M. Marques and T. J. Egan, *J. Inorg. Biochem.*, 2008, **102**, 1660–1667.

89   K. A. de Villiers, M. Osipova, T. E. Mabotha, I. Solomonov, Y. Feldman, K. Kjaer, I. Weissbuch, T. J. Egan and L. Leiserowitz, *Cryst. Growth Des.*, 2009, **9**, 626–632.

90   K. J. Saliba, P. I. Folb and P. J. Smith, *Biochem. Pharmacol.*, 1998, **56**, 313–320.

91   A. F. Slater, *Pharmacol. Ther.*, 1993, **57**, 203–35.

92   A. Yayon, Z. I. Cabantchik and H. Ginsburg, *EMBO J.*, 1984, **3**, 2695–2700.

93   C. P. Sanchez, W. D. Stein and M. Lanzer, *Trends Parasitol.*, 2007, **23**, 332–339.

94   S. R. Meshnick and M. J. Dobson, *The history of anti-malarial drugs.*, Humana Press Inc., Totowa, NJ, 2001, vol. 6.

95   D. C. Smith, *J. Hist. Med. Allied Sci.*, 1976, **31**, 343–367.

96   P. F. Russell, *Man's mastery of malaria*, Oxford University Press, London, 1955.

97   G. Gramiccia, *The life of Charles Ledger (1818-1905),* London: Macmillan, 1988.

98   M. Foley and L. Tilley, *Pharmacol. Ther.*, 1998, **79**, 55–87.

99   D. Greenwood, *J. Antimicrob. Chemother.*, 1995, **36**, 857–872.

100   C. Ohnmacht and A. Patel, *J. Med. Chem.*, 1971, **14**, 926–928.

101   T. R. Sweeney, *Drugs with quinine-like action In. Antimalarial drugs II. Current antimalarials and new drug developments*, Springer-Verlag, Berlin, Heidelberg, 1984.

102   C. M. Trenholme, R. L. Williams, R. E. Desjardins, H. Frischer, P. E. Carson, K. H. Rieckmann and C. J. Canfield, *Science (80-.).*, 1975, **190**, 792–794.

103   K. J. Palmer, S. M. Holliday and R. N. Brogden, *Drugs*, 1993, **45**, 430–475.

104   M. Foley and L. Tilley, *Int. J. Parasitol.*, 1997, **27**, 231–240.

105   D. J. Krogstad, I. Y. Gluzman, D. E. Kyle, a M. Oduola, S. K. Martin, W. K. Milhous and P. H. Schlesinger, *Science*, 1987, **238**, 1283–1285.

106   D. A. Fidock, T. Nomura, A. K. Talley, R. A. Cooper, S. M. Dzekunov, M. T. Ferdig, L. M. B. Ursos, A. S. Sidhu, B. Naudé, K. W. Deitsh, X. Z. Su, J. C. Wootton, P. D. Roepe and T. E. Wellems, *Mol Cell.*, 2000, **6**, 861–871.

107   A. F. Cowman, K. S, D. Galatis and J. G. Culvenor, *J. Cell Biol.*, 1991, **113**, 1033–1042.

108   T. E. Wellems, a Walker-Jonah and L. J. Panton, *Proc. Natl. Acad. Sci. U. S. A.*, 1991, **88**, 3382–3386.

109   A. F. Cowman, D. Galatis and J. K. Thompson, *Proc. Natl. Acad. Sci. U. S. A.*, 1994, **91**, 1143–1147.

110   M. T. Ferdig, R. a. Cooper, J. Mu, B. Deng, D. a. Joy, X. Z. Su and T. E. Wellems, *Mol. Microbiol.*, 2004, **52**, 985–997.

111   I. Petersen, S. J. Gabryszewski, G. L. Johnston, S. K. Dhingra, A. Ecker, R. E. Lewis, M. J. de Almeida, J. Straimer, P. H. Henrich, E. Palatulan, D. J. Johnson, O. Coburn-Flynn, C. Sanchez, A. M. Lehane, M. Lanzer and D. a. Fidock, *Mol. Microbiol.*, 2015, **97**, n/a–n/a.

112   A. Ecker, A. M. Lehane, J. Clain and D. a. Fidock, *Trends Parasitol.*, 2012, **28**, 504–514.

113   A. Dorn, S. R. Vippagunta, H. Matile, C. Jaquet, J. L. Vennerstrom and R. G. Ridley, *Biochem. Pharmacol.*, 1998, **55**, 727–736.

114   D. J. Sullivan, I. Y. Gluzman, D. G. Russell and D. E. Goldberg, *Proc. Natl. Acad. Sci. U. S. A.*, 1996, **93**, 11865–11870.

115   A. F. Slater and A. Cerami, *Nature*, 1992, **355**, 167–169.

116   S. N. Cohen, K. O. Phifer and K. L. Yielding, *Nature*, 1964, **202**, 805–806.

117   A. C. Chou, R. Chevli and C. D. Fitch, *Biochemistry*, 1980, **19**, 1543–1549.

118   T. J. Egan, *J. Inorg. Biochem.*, 2006, **100**, 916–926.

119   H. M. Marques, O. Q. Munro and M. L. Crawcour, *Inorganica Chim. Acta*, 1992, **196**, 221–229.

120   H. M. Marques, *Inorganica Chim. Acta*, 1991, **190**, 291–295.

121   J. L. Hoard, M. J. Hamor and W. S. Caughey, *J. Am. Chem. Soc.*, 1965, **87**, 2312–2319.

122   C. Lecomte, D. L. Chadwick, P. Coppens and E. D. Stevens, 1983, 2982–2992.

123   M. R. Johnson, W. K. Seok, W. Ma, C. Slebodnick, K. M. Wilcoxen and J. A. Ibers, *J. Org. Chem.*, 1996, **61**, 3298–3303.

124   L. B. Casabianca, D. An, J. K. Natarajan, J. N. Alumasa, P. D. Roepe, C. Wolf and A. C. De Dios, 2008, **47**, 6077–6081.

125   L. B. Casabianca, J. B. Kallgren, J. K. Natarajan, J. N. Alumasa, P. D. Roepe, C. Wolf and A. C. De Dios, *J. Inorg. Biochem.*, 2009, **103**, 745–748.

126   K. A. de Villiers, J. Gildenhuys and T. le Roex, *ACS Chem. Biol*, 2012, **7**, 666–671.

127   J. K. Gildenhuys, C. J. Sammy, R. Muller, V. Streltsov, T. le Roex, D. Kuter and K. A. de Villiers, *Dalt. Trans.*, 2015, **In Press**, 9–12.

128   A. C. de Dios, R. Tycko, L. M. B. Ursos and P. D. Roepe, *J. Phys. Chem. A*, 2003, **107**, 5821–5825.

129   A. Leed, K. Dubay, L. M. B. Ursos, D. Sears, A. C. De Dios and P. D. Roepe, *Biochemistry*, 2002, **41**, 10245–10255.

130   J. K. Natarajan, J. N. Alumasa, K. Yearick, K. A. Ekoue-kovi, L. B. Casabianca, A. C. De Dios, C. Wolf and P. D. Roepe, *J. Med. Chem*, 2008, **51**, 3466–3479.

131   K. F. Schwedhelm, M. Horstmann, J. H. Faber, Y. Reichert, M. Buchner, G. Bringmann and C. Faber, *Open Spectrosc. J.*, 2008, **2**, 10–18.

132   G. T. Webster, D. Mcnaughton and B. R. Wood, *J. Phys. Chem. B*, 2009, **113**, 6910–6916.

133   S. Moreau, B. Perly, C. Chachaty and C. Deleuze, *Biochim. Biophys. Acta*, 1985, **840**, 107–116.

134   A. M. D. S. D. Acharige and M. Durrant, *Transit. Met Chem*, 2014, **39**, 721–726.

135   D. Kuter, V. Streltsov, N. Davydova, G. A. Venter, K. J. Naidoo and T. J. Egan, *J. Inorg. Biochem.*, 2015.

136   D. Kuter, S. J. Benjamin and T. J. Egan, *J. Inorg. Biochem.*, 2014, **133**, 40–49.

137   E. L. Dodd and D. S. Bohle, *Chem. Commun.*, 2014, **50**, 13765–13768.

138   M. S. Walczak, K. Lawniczak-Jablonska, A. Wolska, A. Sienkiewicz, L. Suarez, A. J. Kosar and D. S. Bohle, *J. Phys. Chem. B*, 2011, **115**, 1145–1150.

139   M. S. Walczak, K. Lawniczak-Jablonska, A. Wolska, M. Sikora, A. Sienkiewicz, L. Suarez, A. J. Kosar, M.-J. Bellemare and D. S. Bohle, *J. Phys. Chem. B*, 2011, **115**, 4419–4426.

140   N. Basilico, E. Pagani, D. Monti, P. Olliaro and D. Taramelli, *J. Antimicrob. Chemother.*, 1998, **42**, 55–60.

141   R. Baelmans, E. Deharo, G. Bourdy, V. Munoz, C. Quenevo, M. Sauvain and H. Ginsburg, *J. Ethnopharmacol.*, 2000, **73**, 271–275.

142   S. Parapini, N. Basilico, E. Pasini, T. J. Egan, P. Olliaro, D. Taramelli and D. Monti, *Exp. Parasitol.*, 2000, **96**, 249–256.

143   J. Ziegler, L. Pasierb, K. a. Cole and D. W. Wright, *J. Inorg. Biochem.*, 2003, **96**, 478–486.

144   M. Kalkanidis, N. Klonis, L. Tilley and L. W. Deady, *Biochem. Pharmacol.*, 2002, **63**, 833–842.

145   K. K. Ncokazi and T. J. Egan, *Anal. Biochem.*, 2005, **338**, 306–319.

146   K. A. Cole, J. Ziegler, C. A. Evans and D. W. Wright, *J. Inorg. Biochem.*, 2000, **78**, 109–115.

147   S. R. Hawley, P. G. Bray, M. Mungthin, J. D. Atkinson, P. M. O'Neill and S. a. Ward, *Antimicrob. Agents Chemother.*, 1998, **42**, 682–686.

148   E. Deharo, R. N. García, P. Oporto, a. Gimenez, M. Sauvain, V. Jullian and H. Ginsburg, *Exp. Parasitol.*, 2002, **100**, 252–256.

149   C. R. Chong and D. J. Sullivan, *Biochem. Pharmacol.*, 2003, **66**, 2201–2212.

150   T. J. Egan and K. K. Ncokazi, *J. Inorg. Biochem.*, 2005, **99**, 1532–1539.

151   R. F. Pasternack, B. Munda, A. Bickford, E. J. Gibbs and L. M. Scolaro, *J. Inorg. Biochem.*, 2010, **104**, 1119–1124.

152   J. Gildenhuys, Stellenbosch University: PhD Thesis, 2013.

153   I. Solomonov, M. Osipova, Y. Feldman, C. Baehtz, K. Kjaer, I. K. Robinson, G. T. Webster, D. McNaughton, B. R. Wood, I. Weissbuch and L. Leiserowitz, *J. Am. Chem. Soc.*, 2007, **129** , 2615–2627.

154   K. A. de Villiers, M. Osipova, T. E. Mabotha, I. Solomonov, Y. Feldman, K. Kjaer, I. Weissbuch, T. J. Egan and L. Leiserowitz, *Cryst. Growth Des.*, 2009, **9**, 626–632.

155   D. S. Bohle, A. D. Kosar and P. W. Stephens, *Acta Crystallogr. Sect. D Biol. Crystallogr.*, 2002, **58**, 1752–1756.

156   I. Solomonov, M. Osipova, Y. Feldman, C. Baehtz, K. Kjaer, I. K. Robinson, G. T. Webster, D. McNaughton, B. R. Wood, I. Weissbuch and L. Leiserowitz, *J. Am. Chem. Soc.*, 2007, **129** , 2615–2627.

157   T. E. Wellems and C. V Plowe, *J. Infect. Dis.*, 2001, **184**, 770–776.

158   C. H. Kaschula, T. J. Egan, R. Hunter, N. Basilico, S. Parapini, D. Taramelli, E. Pasini and D. Monti, *J. Med. Chem.*, 2002, **45**, 3531–3539.

159   R. Muller, *Personal Communication*, 2015.

160   J. M. Combrinck, *Personal Communication*, 2015.

161   P. G. Kremsner and S. Krishna, *Lancet*, 2004, **364**, 285–294.

162   MarvinSketch, 5.5.1.0, ChemAxon Ltd., Budapest, 2011.

163   K. J. Wicht, *Personal Communication*, 2015.

164   D. A. Skoog, D. M. West, F. J. Holler and S. R. Crouch, *Fundamentals of Analytical Chemistry*, Thomson Brooks/Cole, 2004.

165   I. Langmuir, *J. Am. Chem. Soc.*, 1916, **38**, 2221–2295.

166   R. Tseng, F. Wu and R. Juang, *Carbon.,* 2002, **41**, 487-495.